Instabilities, anomalous transport, and nonlinear structures in partially and fully magnetized plasmas.

A Thesis Submitted to the

College of Graduate and Postdoctoral Studies

in Partial Fulfillment of the Requirements

for the degree of Doctor of Philosophy

in the Department of Physics and Engineering Physics

University of Saskatchewan

Saskatoon

By

Oleksandr Koshkarov

Permission to Use

In presenting this thesis in partial fulfilment of the requirements for a Postgraduate degree from the University of Saskatchewan, I agree that the Libraries of this University may make it freely available for inspection. I further agree that permission for copying of this thesis in any manner, in whole or in part, for scholarly purposes may be granted by the professor or professors who supervised my thesis work or, in their absence, by the Head of the Department or the Dean of the College in which my thesis work was done. It is understood that any copying or publication or use of this thesis or parts thereof for financial gain shall not be allowed without my written permission. It is also understood that due recognition shall be given to me and to the University of Saskatchewan in any scholarly use which may be made of any material in my thesis.

Requests for permission to copy or to make other use of material in this thesis in whole or part should be addressed to:

Head of the Department of Physics and Engineering Physics

Rm 163

116 Science Place

University of Saskatchewan

Saskatoon

Saskatchewan

Canada

S7N 5E2

Abstract

Plasmas behavior, to a large extent, is determined by collective phenomena such as waves. Wave excitation, turbulence, and formation of quasi-coherent nonlinear structures are defining features of nonlinear multi-scale plasma dynamics. In this thesis, instabilities, anomalous transport, and structures in partially and fully magnetized plasmas were studied with a combination of analytical and numerical tools. The phenomena studied in this thesis are of interest for many applications, e.g., plasma reactors for material processing, electric propulsion, magnetic plasma confinement, and space plasma physics. Large equilibrium flows of ions and electrons exist in many devices with partially magnetized plasmas in crossed electric and magnetic fields. Such flows result in various instabilities and turbulence that produce anomalous electron transport across the magnetic field. We present first principle, self-consistent, nonlinear fluid simulations that predict the level of anomalous current generally consistent with experimental data. We also show that drift waves in partially magnetized plasmas (which we called Hall drift waves), destabilized by the electron drift along with density gradients, tend to form (via inverse energy cascade) shear flows similar to zonal flows in fully magnetized plasmas. These flows become unstable due to a secondary instability (similar to Kelvin–Helmholtz instability) and produce large-scale quasi-stationary vortices. Then, it was shown that in nonlinear regimes, the axial mode instability due to electron and ion flows (along the electric field) forms large-amplitude cnoidal type waves. At the same time, the strong electric field produced by axial modes affects Hall drift waves stability and provides a feedback mechanism on density gradient driven turbulence, creating a complex picture of interacting anomalous transport, zonal flows, vortices, and streamers. In the case where axial modes are destabilized by boundary effects, the nonlinear dynamics result in a new nonlinear equilibrium or standing oscillating waves. The formation of shear flows (zonal flows) was also studied in the framework of the Hasegawa-Mima equation and it was established that zonal flows can saturate due to nonlinear self-interactions. Lastly, a novel approach for high-fidelity numerical simulations of multi-scale nonlinear plasma dynamics is developed which is illustrated with the example of an unmagnetized plasma.

Acknowledgements

CONTENTS

LIST OF TABLES

LIST OF FIGURES

Chapter 1

Introduction

1.1 Motivation and thesis outline

Plasma is the most common state of visible matter in our universe. Therefore, understanding of plasma physics is necessary to answer fundamental questions about the nature of the universe. Plasma physics is addressing numerous practical applications as well as fundamental problems such as wave turbulence. As a collective medium, plasma behavior is dominated by wave dynamics, and turbulence still remains a great unsolved problem of classical physics with many far-reaching practical implications.

Plasma dynamics is characterized by many different parameters with large disparity of temporal and spatial scales. In most cases, some kind of reduction and multi-scale expansions are necessary to solve the problem. The purpose of this thesis is to analyze several nonlinear plasma phenomena of great interest for fundamental plasma physics and practical applications such as electric propulsion and material processing. These will be treated with a combination of theoretical and numerical techniques, and plasma models of different complexity will be used. In relatively simple models, a pure analytical method will be used. A complete kinetic description will require fully numerical treatment. An intermediate approach will also be used where analytical tools are combined with numerical simulations.

The study will begin with nonlinear wave-wave interactions of drift waves, which are fundamental in plasmas with an inhomogeneous density and a strong magnetic field (e.g., tokamak). As will be shown in Chapter 2, their nonlinear interactions transfer energy into large-scale modes called zonal flows. This fundamental plasma process is the inverse energy cascade. The standard theory of modulational instability will be extended to include the effects of nonlinear self-saturation of zonal flows.

In Chapter 3, we will investigate a similar nonlinear process — the inverse energy cascade due to nonlinear interaction of density gradient driven waves in partially magnetized plasmas. In this text, we call them Hall drift waves by analogy with density gradient driven waves in fully magnetized plasmas (i.e., drift waves). The nonlinear interaction of Hall drift waves may be responsible for anomalously high electron conductivity (mobility) across the magnetic field in a Hall thruster. This anomalous mobility produces large axial current and reduces Hall thruster efficiency. It also excites large-amplitude axial waves: their nonlinear dynamics is studied in Chapters 4, 5. The full system with Hall drift and axial waves is considered in Chapter 6. Throughout Chapters 3-6, the reduced fluid model proposed in [115] is used to describe waves in Hall thruster and a combination of analytical and numerical tools are employed to study it.

Finally, in Chapter 7, the classical beam-plasma interaction problem is considered to illustrate a new numerical method for solving the full kinetic equation. The standard numerical method for the kinetic equation is particle-in-cell (PIC). Unfortunately, it is ill-suited for turbulent and chaotic problems (e.g., drift wave turbulence) because of a large particle noise. Therefore, the new proposed numerical method overcomes this problem by combining PIC with a highly accurate spectral method. The pure spectral method is a good choice for turbulent problems, but the particle distribution function may have a complicated shape causing poor convergence in case of collisionless plasmas. The new hybrid method avoids this problem by using particles to discretize complicated parts of the distribution function.

The content of this thesis is based on several manuscripts that have been published already and/or submitted or in preparation for publication. The chapters that are based on published manuscripts have preface sections describing how the chapter fits into the overall theme of the thesis and the rest of such chapters is reproduced verbatim.

1.2   What is a plasma

Plasma is a gaseous state of matter where some atoms have lost one or more electrons. As an example, one can consider the possible states of matter (for example water H_2O) shown in Figure 1.1 on the temperature (T) line. At low temperatures, water is a solid and all

molecules are bounded into a crystal. At higher temperatures[1] ($T > 0°$ C ≈ 0.024 eV), thermal energy overcomes the bonding energy between molecules in the crystal lattice and ice melts, becoming a liquid. If the temperature is raised further ($T > 100°$ C ≈ 0.032 eV), the water transitions into a molecular gas state. At temperatures around $T \sim 1$ eV, water molecules dissociate into atoms and the gas becomes atomic, so we can no longer call the considered gas water. The next transition happens when the temperature approaches an ionization energy (e.g., for Oxygen and Hydrogen atoms it is around 13.6 eV). At this point, a significant fraction of atoms are ionized, and the matter is said to be in a plasma state.
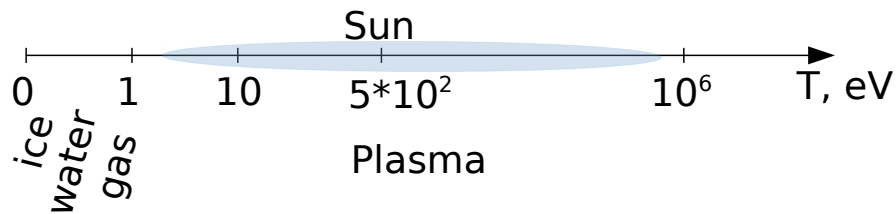
Figure 1.1: Illustration of different water states on the temperature line (not to scale) and its transition into plasma state.

A plasma is an ionized gas, which usually consists of several different species that control its dynamics, e.g., free electrons, ions (i.e., ionized atoms), and neutrals (i.e., not ionized atoms). Therefore, the definition of temperature as an ensemble average of kinetic energy, $3T/2 = \langle mv^2/2 \rangle$, should be generalized for different species, beginning with the distinction between electron temperature (T_e), ions temperature (T_i), etc. Typically, the electron temperature is much higher than the temperatures of ions or neutrals. This asymmetry happens due to the large difference between electron (m_e) and ions (m_i) masses. For example, the lightest ion (proton) is 1836 times heavier than the electron. Therefore, when a plasma is created, electrons are usually heated much faster than ions. Moreover, the heating of ions due to collisions with electrons is a very slow process, because the maximum amount of kinetic energy an electron can transfer to an ion during a collision is $4m_e/m_i \ll 1$. Hence, a gas may be classified as plasma when the electron temperature approaches the ionization energy. It

---

[1]Here and later in the text, the temperature is measured in energy units such as jouls (J) or electronvolts (eV) rather than in Celsius (C) or Kelvins (K). Therefore, the conversion factor — the Boltzmann constant, is omitted throughout the text and words "temperature" and "energies" are used interchangeably.

is one of the important features of plasmas that it can be strongly non-equilibrium and ion temperature can be significantly smaller than the electron temperature.

This thesis is focused on non-relativistic plasmas where the motion of charged particles is governed by classical electromagnetism[2], and the electron temperature is bounded by the electron rest mass energy $T_e < m_e c^2 \approx 0.5$ MeV. Therefore, we are concerned with the state of matter with electron temperatures roughly from ~ 1 eV up to ~ 0.1 MeV, which is the most common state of visible matter in our universe. For example, our sun has a temperature varying from ~ 0.5 eV in the photosphere and up to ~ 1.4 keV in the core.

Above, only an intuitive definition of a plasma state was given. A more precise definition is: plasma is a quasi-neutral gas of charged particles where interactions are predominantly collective. This definition, however, requires further clarifications. Namely, what are **quasi-neutrality** and **collective interactions**?

Quasi-neutrality

A quasi-neutrality (QN) means that the electron charge density (ρ_e) is approximately (on average in time and space) equal to the ion charge density (ρ_i). Separation of the electrons and ions results in the electric field which brings the charges back together. The scale of the separation is limited by the available kinetic (thermal) energy of particles (mostly electrons as the lighter component), which allows a simple estimate for the typical length scale of the charge separation. Assume that the charge separation had occurred and there is a region of size x with only one particle species present, e.g., electrons with charge $-e$ and density n. Then the electric field E can be estimated from Gauss law[3] $\partial_x E = -4\pi n e$, i.e., $E \sim 4\pi n e x$. The separation occurs due to a thermal energy $Ex \sim T_e$, therefore we have

$$x \sim \lambda_D \equiv \sqrt{\frac{T_e}{4\pi n e^2}}, \tag{1.1}$$

where λ_D is a Debye length, which is a charge separation scale length; i.e., if $x \ll \lambda_D$, then $\rho_e \neq \rho_i$, while if $x \gg \lambda_D$, then $\rho_e \approx \rho_i$, with x being a typical scale of interest. The Debye

---

[2] For equations of motion to be classical, quantum effects should be negligible. This happens when plasma density (or average distance between particles) satisfy $n^{-1/3} \gg \lambda_{DB}$, where λ_{DB} is a De Broglie wavelength. This condition is usually satisfied for common plasmas.

[3] Here and later in the text, unless specifically indicated, all formulas are written in Gaussian centimetre–gram–second (CGS) system of units.

length is also the scale length of charge screening. It follows from the accurate solution of the Gauss law (or the Poisson equation) in plasma, that the potential of a test charge q decays with distance r as

$$\phi(r) = \frac{qe^{-r/\lambda_D}}{r}, \tag{1.2}$$

in contrast to the standard Coulomb's law in a vacuum

$$\phi(r) = \frac{q}{r}. \tag{1.3}$$

The additional decay e^{-r/λ_D} occurs due to plasma charges which are getting polarized to compensate for the test charge and screen its electric field.

Using the same estimate for electrostatic potential ($\partial_x\phi \sim 4\pi nex$), we can evaluate the time scale when the fastest (i.e., lightest) species (i.e., electrons) undergoes charge separation. We consider motionless ions with electrons deviated from them by a distance x. Newton's second law ($m_e\ddot{x} = e\partial_x\phi$) yields the equation for periodic oscillation with a characteristic frequency

$$\omega_{pe} = \sqrt{\frac{4\pi ne^2}{m_e}}. \tag{1.4}$$

The quantity ω_{pe} is called the electron plasma frequency or simply plasma frequency. It defines the charge separation time scale and characterizes the most fundamental plasma eigen-mode — the Langmuir wave (or in this approximation Langmuir oscillations).

Let us note that if we combine these two fundamental plasma quantities, we get

$$\lambda_D\omega_{pe} = \sqrt{\frac{T_e}{m_e}} \equiv v_{T_e}, \tag{1.5}$$

the thermal electron velocity v_{T_e}. This is natural because the charge separation occurs due to the thermal motion.

Collective interactions

In neutral gases, particles interact with each other mostly through occasional collisions, where only very close particles are involved (binary collisions). In plasmas, many charged particles can interact simultaneously via the long-range Coulomb forces. The number of interacting particles is limited by the Debye screening (exponential decay in (1.2)). Thus, each particle

5

interacts effectively only with particles inside the Debye sphere with the center at the chosen particle. Therefore, many particles (inside the Debye sphere) can interact simultaneously with each other and it is called a collective interaction. Due to this interactions plasmas respond to large-scale perturbations (i.e., larger than the Debye length) collectively. Such responses are usually manifested as plasma waves and they are called collective phenomena. This makes plasma dynamics significantly different from neutral gas dynamics and results in many complex nonlinear phenomena. We note that collective interactions and collective phenomena are different processes where the former are many-body interactions on the scales smaller than the Debye length, while the latter are collective plasma responses on perturbations which are usually larger than the Debye length, e.g., plasma waves.

The binary interactions in plasma become negligible in comparison with collective interactions, when the potential of a test particle at the mean distance between particles ($r \sim n^{-1/3}$) is much smaller than the plasma thermal energy. Using (1.2), we get

$$\left.\frac{e\phi}{T_e}\right|_{r=n^{-1/3}} \sim \frac{\exp\left((n\lambda_D^3)^{-1/3}\right)}{(n\lambda_D^3)^{2/3}} \sim \frac{1}{(n\lambda_D^3)^{2/3}} \ll 1, \tag{1.6}$$

or in other words

$$n\lambda_D^3 \gg 1. \tag{1.7}$$

Condition (1.7) is a necessary condition for a plasma state and the quantity $n\lambda_D^3$ is known as the plasma parameter. It defines the number of plasma particles in a Debye cube (or sphere).

1.3 Plasma in nature and in the laboratory

Modern plasma physics includes many complex phenomena and has numerous applications. Historically, plasma physics[4] started with Irving Langmuir and Lewi Tonks who studied the physics of tungsten filaments in light bulbs in order to increase their lifetime. Subsequently, they developed a theory of plasma-material interactions and discovered the fundamental plasma waves now called Langmuir waves [121]. Discharge physics covers a variety of phenomena related to electric currents and electromagnetic fields in gas discharges. It deals with

---

[4] It was Langmuir who coined the term "plasma", because it reminded him of blood plasma [102, 120].

relatively cold, partially ionized plasmas with electron temperature of a few electronvolts $T_e \sim (2-3)$ eV and particle densities $n \sim (10^{14} - 10^{18})$ m^{-3}. Typical examples of such plasmas in nature and laboratory are fluorescent lamps, neon lights, electric arcs, hot flames, lightings, etc.

Another early manifestation of plasma physics phenomena came from radiophysics community. It was noticed that radio waves were reflected from upper layers of the atmosphere which makes it possible to transmit radio signals around the globe. It was understood later that the radio waves were reflected from the ionosphere which is a plasma layer located at an altitude of approximately 60 km to 1000 km. Further research revealed complicated physics which closely connects processes in the ionosphere to the whole sun-magnetosphere system. Studies of plasmas in this system led to a new field of space physics which is concerned not only with fundamental questions on how the universe works, but also tries to explain and predict space weather. Thus, it has important implications for everyday life: the operation of satellites, power plants, etc. Space physics deals with a variety of different plasmas. For example, a typical ionosphere electron temperature is $T_e \sim 0.1$ eV and density $n \sim 10^{12}$ m^{-3}, while a typical solar wind (i.e., a plasma emanating from the sun) electron temperature is $T_e \sim 10$ eV, density $n \sim 10^7$ m^{-3} and large mean velocity $v_{drift} \sim 300$ km/s. Plasma systems are also common in deep space and are a major subject of research in modern astrophysics.

1.3.1 Thermonuclear fusion

A large part of plasma physics is focused on the problem of thermonuclear fusion (TF). TF is the energy source of stars such as our sun and the physical phenomenon behind the hydrogen bomb. The main idea is that one needs to combine light nuclei to form heavy ones. This reaction releases energy when combined nuclei are sufficiently lighter than the iron nucleus. For example, dominant fusion reactions inside the Sun are

$$D + D = {}^3He + n + 3.2\text{MeV},$$
$$D + D = T + p + 4.0\text{MeV},$$
$$D + T = {}^4He + n + 17.6\text{MeV},$$
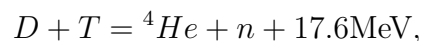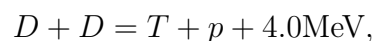
where D is a deuterium nucleus, T is a tritium nucleus, n is a neutron, p is a proton, and $^3He, ^4He$ are helium-3 and helium-4 nuclei respectively.

The important practical question is how one can control nuclear fusion to get almost an inexhaustible energy source. The main difficulty is that in TF reactions one has to combine positively charged particles (ions). Therefore, there is a large energy threshold due to the Coulomb barrier. A rough estimate of the required temperature is $T_e \sim 10$ keV, and it is very difficult to confine very hot plasmas in the laboratory, because it will melt container walls.

One possible and promising solution is to use magnetic confinement. It is well known that the trajectories of charged particles in magnetic fields are helices, tied to magnetic field lines at a distance of the Larmor radius

$$\rho_\alpha = \frac{v_{\perp\alpha}}{\omega_{c\alpha}}, \text{ with } \omega_{c\alpha} = \frac{q_\alpha B}{m_\alpha c}, \tag{1.8}$$

where α denotes particle species (α = electrons, ions, etc.), $v_{\perp\alpha}$ is the particle velocity perpendicular to the magnetic field, $\omega_{c\alpha}$ is the frequency of circular motion around the magnetic field called the gyro frequency, q_α is the particle charge, m_α is the particle mass, c is the speed of light, and B is the magnitude of the magnetic field. Therefore, if the charged particle's Larmor radius is much smaller than the device size, the plasma can be confined in the direction perpendicular to the magnetic field. However, particles can still escape in the direction of the magnetic field. There is a large variety of magnetic configurations which aim to confine plasmas [112], but the most obvious choice is to make magnetic field lines closed. In the simplest case, we get magnetic field lines closed into a torus — a tokamak.[5]

1.3.2   Ion propulsion

Another prominent example of a practically applied plasma system is the Hall thruster (HT), which is one of the most promising ion propulsion systems [99, 97]. It has good efficiency ($50 - 60\%$), a high thrust velocity ($10^4 - 10^5$ m/s), and a relatively simple working principle. HTs have a cylindrical geometry, with an axial electric and a predominantly radial magnetic field as shown in Figure 1.2. Devices are configured to have the ion Larmor radius much

---

[5]The name originates from Russian abbreviation — **то**к**амак**: **то**роидальная **ка**мера с **ма**гнитными **к**атушками, which translates into English as toroidal chamber with magnetic coils

smaller than the system size, making the magnetic field effects on the ion motion negligible. Hence, ions are accelerated by the electric field along the axial direction. At the same time, the electron gyroradius is much smaller than the device size, so they are confined in the device[6]. The reason why a quasi-neutral plasma is important for the HT operation is space charge. If electrons were absent, the ion charge excess would screen the accelerating electric field, limiting the ion current and velocity. This effect is known as the Child-Langmuir Law [32]. Therefore, a plasma overcomes this limit, because an ion charge is neutralized by electrons.
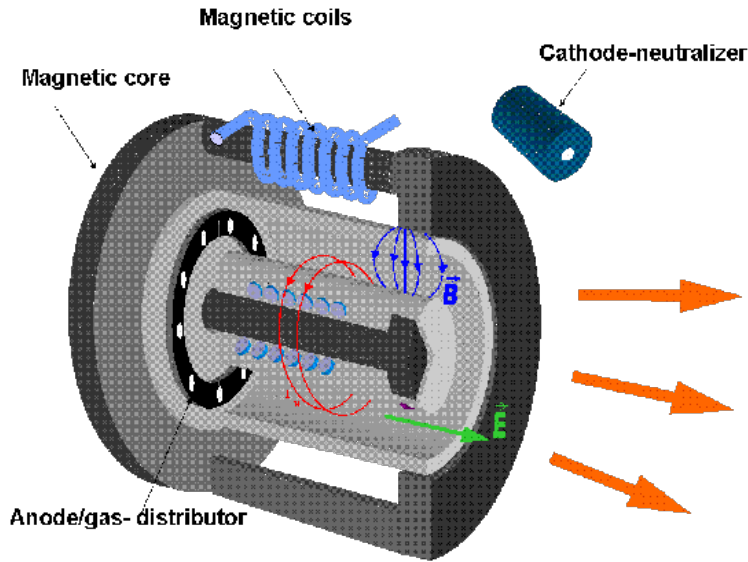
Figure 1.2: Hall thruster scheme (from http://htx.pppl.gov/).

1.3.3   Other plasma applications

Numerous subfields and details of mentioned plasma physics applications in space physics, fusion, etc. were omitted, as well as other diverse fields related to plasma physics. For example, plasma reactors are commonly used for material processing (e.g., magnetrons) or to create lasers. There are new and quickly growing fields such as a plasma medicine, where plasma is created to control chemical reactions in very localized areas in our body.

Despite a variety of applications, plasmas in very different systems share similar properties because universal collective plasma phenomena (e.g., plasma waves) usually define plasma

---

[6] Actually, as will be explained later in the text, electrons move with $\mathbf{E} \times \mathbf{B}$ drift in the azimuthal direction.

dynamics, and, by virtue of a theoretical approach, can be studied with similar tools and techniques. Therefore, the goal of this thesis is to demonstrate how plasma phenomena and applications can be approached by theoretical and numerical techniques.

1.4   Plasma models and scale separation

Plasmas are pervasive in nature and in the laboratory. Therefore, the natural question is how can plasmas be described and studied? A common tool is mathematical modeling which usually results in a system which can be expressed in the form of integro-differential equations.

1.4.1   Kinetic plasma model

Kinetic modeling is a fundamental way to describe plasmas. In these models, the system state is defined by a particle distribution function (PDF) which evolves according to the Vlasov equation. This equation originates from the Boltzmann equation for classical gases. Additionally, it includes effects of long-range electromagnetic fields, and Maxwell's equations are used to compute their evolution. Electromagnetic fields are self-consistent as they depend on the PDF. Therefore, the full kinetic model for plasmas is the Vlasov-Maxwell (VM) system of time-dependent partial differential equations.

As was noted, the Vlasov equation originates from the Boltzmann equation and it is the statement that the PDF changes in time only due to collisions, which follows from Liouville's theorem. Thus, the Boltzmann equation reads

$$\frac{df_\alpha(t, \mathbf{x}, \mathbf{v})}{dt} = \left(\frac{\partial f_\alpha(t, \mathbf{x}, \mathbf{v})}{\partial t} \right)_{coll}, \tag{1.9}$$

and, using the chain rule, the total time derivative in the phase space

$$\frac{d}{dt} = \frac{\partial}{\partial t} + \mathbf{v} \cdot \nabla + \frac{\mathbf{F}(t, \mathbf{x})}{m_\alpha} \cdot \frac{\partial}{\partial \mathbf{v}}, \tag{1.10}$$

where α subscript denotes a plasma species (e.g., electrons, ions, etc.); $f(t, \mathbf{x}, \mathbf{v})$ is a particle distribution function; t, $\mathbf{x}$, $\mathbf{v}$ are time, space and velocity variables, respectively; m_α is a particle mass; $\mathbf{F}(t, \mathbf{x})$ is force acting on particles; the right hand side of equation (1.9) is the rate of PDF change due to collisions between particles.

Vlasov recognized the problem of applying classical gas theory, which uses pair collisions, to the plasma dynamics. He suggested that pair collisions can be neglected, but one needs to include the effect of self-consistent electromagnetic fields, because long-range Coulomb interactions define a plasma dynamics. Therefore, the Vlasov equation yields

$$\frac{df_\alpha}{dt} = \left(\frac{\partial}{\partial t} + \mathbf{v} \cdot \nabla + \frac{q_\alpha}{m_\alpha} \left(\mathbf{E} + \frac{\mathbf{v} \times \mathbf{B}}{c} \right) \cdot \frac{\partial}{\partial \mathbf{v}} \right) f_\alpha = 0, \tag{1.11}$$

where $\mathbf{E} = \mathbf{E}(t, \mathbf{x})$, $\mathbf{B} = \mathbf{B}(t, \mathbf{x})$ are self-consistent electromagnetic fields; q_α is a particle charge; c is the speed of light.

We stress here that not all plasmas are collisionless, i.e., the right hand side of (1.9) is negligible. For example, it is not the case in high density plasmas where the effective collision frequency ν can be comparable to the frequency of collective plasma processes (waves). We are mostly concerned with collisionless plasmas, and we omit the complicated processes of collisions between charged particles, which usually lead to diffusion in the velocity space. We will however consider charge-neutral particle collisions, and will use the most simple approximation for the collision integral

$$\left(\frac{\partial f}{\partial t} \right)_{coll} \approx -\nu(f - f_0), \tag{1.12}$$

where f_0 is a PDF of neutral particle species and ν is an effective collision frequency. The charged-neutral particle collisions are important for cold plasmas, where the fraction of ionized particles is small and there is significant momentum exchange between charged and neutral particles.

We note that the evolution equations for the Vlasov equation characteristics $\mathbf{x}_c(t)$ and $\mathbf{v}_c(t)$,

$$\frac{d\mathbf{x}_c}{dt} = \mathbf{v}_c, \tag{1.13}$$

$$\frac{d\mathbf{v}_c}{dt} = \frac{q_\alpha}{m_\alpha} \left(\mathbf{E} + \frac{\mathbf{v}_c \times \mathbf{B}}{c} \right), \tag{1.14}$$

$$\tag{1.15}$$

are Newton equations for particles in self-consistent electromagnetic fields.

The self-consistent electromagnetic fields can be found from Maxwell's equations

$$\partial_t \mathbf{E} = c \nabla \times \mathbf{B} - 4\pi \mathbf{j}, \tag{1.16}$$

$$\partial_t \mathbf{B} = -c \nabla \times \mathbf{E}, \tag{1.17}$$

$$\nabla \cdot \mathbf{E} = 4\pi \rho, \tag{1.18}$$

$$\nabla \cdot \mathbf{B} = 0, \tag{1.19}$$

with charge and current densities defined via velocity moments of the distribution function

$$\rho = \sum_\alpha q_\alpha \int f_\alpha d^3 v, \tag{1.20}$$

$$\mathbf{j} = \sum_\alpha q_\alpha \int f_\alpha \mathbf{v} d^3 v. \tag{1.21}$$

The full electromagnetic system (1.11), (1.16)-(1.21) is not always needed to describe the considered problem. For example, in the case of longitudinal waves $\mathbf{k} \parallel \mathbf{E}$, where $\mathbf{k}$ is the wave vector, the magnetic field is stationary ($\partial_t \mathbf{B} = 0$). In this case, the system reduces to two equations (1.11), (1.18). This is called the electrostatic approximation and it is used in the rest of this work.

1.4.2 Fluid reduction

The full kinetic system is very difficult to solve analytically or numerically. The intrinsic complexity originates from various factors. First, the VM system's high dimensionality (time and six-dimensional phase space) implies enormous information required to describe the system state. Secondly, a plasma has a wide range of time and spatial scales. For example, the characteristic time scale of electron dynamics is significantly different from that of ions due to their huge mass and temperature differences. Another important scale separation is the large difference between plasma characteristic length scales (e.g., Debye length, Larmor radius, etc.) and the system size. For instance, we may need to resolve waves with wavelengths of about ~ 1 km in space systems of astronomical sizes (e.g., 1 AU$\approx 1.5 \times 10^8$ km). Plasma can also be strongly anisotropic. It is common in highly magnetized plasmas (e.g., tokamaks) that the pressure along and perpendicular to the magnetic field can vary by orders of magnitude.

All of the above, in combination with plasma dynamics being highly turbulent and chaotic, imply that the VM system is very complicated to treat.

The standard way to simplify equations in physics is via scale reduction, where equations are reduced to contain only certain scales. In plasmas, the Vlasov equation (1.11) can be reduced by using a fluid description, which is usually valid for large-scale plasma dynamics. Fluid equations describe the evolution of macroscopic quantities, such as plasma density n_α, plasma flow velocity $\mathbf{V}_\alpha$, pressure p_α, etc. Formally, one can obtain fluid equations, by taking subsequent velocity moments of the Vlasov equation. For example, integration of the Vlasov equation (1.11) over the whole velocity space, gives a mass conservation equation

$$\frac{\partial n_\alpha}{\partial t} + \nabla \cdot (n_\alpha \mathbf{V}_\alpha) = 0, \tag{1.22}$$

where the plasma density and the velocity for the species α were defined as

$$n_\alpha = \int f_\alpha d^3 v, \quad \mathbf{V}_\alpha = \frac{1}{n_\alpha} \int \mathbf{v} f_\alpha d^3 v. \tag{1.23}$$

Every fluid equation defines the time evolution of a macroscopic quantity (e.g., the plasma density) and depends on the divergence of the next order macroscopic quantity. Thus, the density evolution equation (a zero order moment) depends on the divergence of the plasma velocity (a first order moment). Similarly, the evolution equation for the plasma velocity obtained by taking the first order velocity moment of the Vlasov equation — a momentum conservation equation

$$\frac{\partial (n_\alpha \mathbf{V}_\alpha)}{\partial t} + \nabla \cdot \left(n_\alpha \mathbf{V}_\alpha \mathbf{V}_\alpha + \frac{\mathbf{P}_\alpha}{m_\alpha} \right) = \frac{q_\alpha n_\alpha}{m_\alpha} \left(\mathbf{E} + \frac{\mathbf{V}_\alpha \times \mathbf{B}}{c} \right), \tag{1.24}$$

depends on the divergence of the next order pressure tensor

$$\mathbf{P}_\alpha = m_\alpha \int (\mathbf{v}_\alpha - \mathbf{V}_\alpha)(\mathbf{v}_\alpha - \mathbf{V}_\alpha) f_\alpha d^3 v. \tag{1.25}$$

The momentum conservation equation (1.24) is also called the Euler equation and is usually expressed in the following form

$$m_\alpha n_\alpha \left(\frac{\partial}{\partial t} + \mathbf{V}_\alpha \cdot \nabla \right) \mathbf{V}_\alpha + \nabla p_\alpha + \nabla \cdot \mathbf{\Pi}_\alpha = q_\alpha n_\alpha \left(\mathbf{E} + \frac{\mathbf{V}_\alpha \times \mathbf{B}}{c} \right), \tag{1.26}$$

where the mass conservation equation (1.23) was subtracted and the pressure tensor was split $\mathbf{P}_\alpha = p_\alpha \mathbf{I} + \mathbf{\Pi}_\alpha$ ($\mathbf{I}$ is a unit tensor) into the scalar pressure $p_\alpha = (m_\alpha/3) \int (\mathbf{v}_\alpha - \mathbf{V}_\alpha)^2 f_\alpha d^3 v$ and the viscosity tensor $\mathbf{\Pi}_\alpha = \mathbf{P}_\alpha - p_\alpha \mathbf{I}$.

Therefore, the Vlasov equation (and the Boltzmann equation) is equivalent to an infinite number of fluid moments. One way to truncate this system is to use a closure for some moment via lower order moments. For example, a simple approximation is the adiabatic approximation where a non-diagonal anisotropic part of the pressure tensor is neglected ($\mathbf{\Pi} = 0$) and the scalar pressure follows the adiabatic law

$$\mathbf{P}_\alpha \approx p_\alpha \mathbf{I}, \qquad p_\alpha = n_\alpha^{\gamma_a}, \tag{1.27}$$

where γ_a is the adiabatic index.

The mass conservation equations (1.23), the momentum conservation equations (1.24), and other higher order moments (e.g., energy conservation equations) are still complicated PDEs. However, velocity moments usually have a clear physical meaning and can be measured in experiments, unlike the PDF which is more difficult to measure and interpret. Nevertheless, it is usually important to simplify fluid equations further. For example, if the charge separation is neglected ($n_e \approx n_i$), the magnetohydrodynamics (MHD) equations can be recovered, which describe plasmas on scales larger than charge separation scales ($x \gg \lambda_D, t \gg \omega_{pe}^{-1}$); e.g., MHD is a standard model to reproduce large-scale dynamics of the Earth magnetosphere. Typical plasmas are controlled by non linear processes and have a large number of parameters. Therefore, scale reduction and further simplifications are important techniques in plasma physics and it is the underlying theme of this thesis.

1.5 Plasma waves

Due to their origin in conservative laws, most plasma equations (e.g., Vlasov and its moments, etc.) are hyperbolic[7]. Therefore, the plasma dynamics are predominantly wave-like and this thesis focuses on the study of wave-related phenomena in plasmas.

Waves are oscillations that transfer energy through space. A familiar class of waves is those in fluids or gases such as sound waves. They propagate due to compression of the

---

[7] The strict definition of a hyperbolic PDE is not given in this text, but a descriptive definition follows. The representative hyperbolic equation is a wave equation $(\partial_t^2 - c^2\partial_x^2)u = 0$. It can be factorized into two advection equations $\partial_t u \pm c\partial_x u = 0$. So, the hyperbolicity means real characteristics or waves velocity speeds c, thus solutions constitute propagating waves. For a system of PDE $\partial_t \mathbf{U} + \nabla \cdot \mathbf{F}(\mathbf{U}) = 0$, it means real eigenvalues for the Jacobian $\partial \mathbf{F}/\partial \mathbf{U}$.

medium and a returning pressure force. Plasmas also have similar modes (e.g., ion sound wave) where fluid-like mechanisms (e.g., pressure) play an important role. Additionally, charged particles and electromagnetic forces play a crucial role in plasma dynamics, resulting in coupled electromagnetic and fluid wave-like behavior which makes plasma support a large number of eigenmodes of different nature.

1.5.1   Linear waves and phenomena

The first step to study waves is to consider the linear approximation. As an example of the general procedure of linear analysis, we will analyze the most fundamental plasma wave — the Langmuir wave, which is an oscillation of the electron charge density around virtually motionless ions. For simplicity we will use the fluid equations (1.23), (1.26) with the adiabatic closure (1.27).

First, the plasma equilibrium must be found by solving stationary equations of motion. In our case, these are fluid equations with omitted time derivatives. The trivial case of a boundless and uniform plasma in equilibrium with $n_e = n_i = n_0$, given T_e, and zero flow velocity is considered. In this equilibrium, electric and magnetic fields are absent. The next step is to expand our quantities around the equilibrium

$$x = x_0 + \widetilde{x}, \tag{1.28}$$

where x is a plasma quantity (e.g., density, velocity, etc.), x_0 is an equilibrium value, and $\tilde{x}$ is a perturbed value. Then we substitute the expansion (1.28) into fluid equations and use linear approximation $x_0 \gg \tilde{x}$; i.e., we neglect nonlinear terms. After linearization, the electron fluid equations and the adiabatic closure read

$$\frac{\partial \tilde{n}_e}{\partial t} + n_0 \nabla \cdot \widetilde{\mathbf{V}}_e = 0, \tag{1.29}$$

$$m_e n_0 \frac{\partial \widetilde{\mathbf{V}}_e}{\partial t} + \nabla \widetilde{p}_e = -e n_0 \widetilde{\mathbf{E}}, \tag{1.30}$$

$$\nabla \widetilde{p}_e = \gamma_a T_e \nabla \tilde{n}_e. \tag{1.31}$$

We can close this system by assuming motionless ions ($\tilde{n}_i = \widetilde{\mathbf{V}}_i = 0$) and using the linearized Gauss's law (1.18)

$$\nabla \cdot \widetilde{\mathbf{E}} = -4\pi e \tilde{n}_e. \tag{1.32}$$

Let us notice that equations (1.29)-(1.32) are a linear system of homogeneous differential equations with constant coefficients. The homogeneity appears because zero order terms are canceled out due to equilibrium; the linearity follows from linear approximation (i.e., higher order terms were neglected); coefficients are constant because equilibrium profiles are homogeneous in space. Such equations can be readily solved with the Fourier method. Equivalently, we can consider only one monochromatic mode with frequency ω and wave vector $\mathbf{k}$

$$\widetilde{x} = \left(\widetilde{n_e}, \widetilde{\mathbf{V}}_e, ...\right) \sim e^{-i\omega t + i\mathbf{k}\cdot\mathbf{x}}. \tag{1.33}$$

After some trivial algebra and using (1.33), the system (1.29)-(1.32) reduces to

$$\left(\omega^2 - \omega_{pe}^2 - \gamma_a v_{T_e}^2 k^2\right) \widetilde{\mathbf{E}} = 0. \tag{1.34}$$

Therefore, the system has nontrivial solution ($\widetilde{\mathbf{E}} \neq 0$) only when frequencies and wave vectors satisfy the equation

$$\omega^2 = \omega_{pe}^2 + \gamma_a v_{T_e}^2 k^2, \tag{1.35}$$

which is called the Bohm-Gross dispersion relation and describes Langmuir waves. This wave was first discovered by Irving Langmuir and Lewi Tonks in the 1920 [121].

The absence of nonlinearity makes linear wave modes independent from each other, so each mode can be independently described with an algebraic dispersion equation, like (1.35). Let us assume that we have some initial density profile $\widetilde{n}_e(t = 0, \mathbf{x})$, and we are looking for further evolution in time of electron density $\widetilde{n}_e(t, \mathbf{x})$ according to the the dispersion equation $\omega = \omega(\mathbf{k})$. First, we expand the initial profile in the Fourier series

$$\widetilde{n}_e(t = 0, \mathbf{x}) = \int \widehat{n}_e(\mathbf{k}) e^{i\mathbf{k}\cdot\mathbf{x}} d^3 k, \tag{1.36}$$

and the time evolution follows

$$\widetilde{n}_e(t, \mathbf{x}) = \int \widehat{n}_e(\mathbf{k}) e^{-i\omega(\mathbf{k})t + i\mathbf{k}\cdot\mathbf{x}} d^3 k. \tag{1.37}$$

Therefore, the algebraic dispersion equation is sufficient to describe the linear plasma dynamics.

Now we comment on how the equation (1.35) can be modified in the comprehensive kinetic model. First of all, the dispersion relation which follows from the Vlasov equation is

not algebraic and it involves a complicated transcendental plasma dispersion function [119]. In the long-wavelength limit ($k\lambda_D \ll 1$), the Bohm-Gross dispersion is recovered with the adiabatic index $\gamma_a = 3$, as was first shown by Vlasov [128] and then by Bohm and Gross [14]. The rigorous analysis performed by Landau [82] showed that the frequency of a Langmuir wave has a negative imaginary component $\gamma < 0$, in $\omega = \omega_r + i\gamma$. In this case, the mode $e^{-i\omega t} \sim e^{\gamma t}$ damps in time exponentially. This effect is called Landau damping. In the long wavelength limit, the Landau damping rate takes the form

$$\gamma = \frac{2\pi^2 e^2}{m_e k^2} \omega \left.\frac{\partial f_e}{\partial v}\right|_{v=\omega/k}. \tag{1.38}$$

For wavelengths comparable to the Debye length $k\lambda_D \sim 1$ and smaller, when the dispersion equation (1.35), (1.38) becomes inaccurate, the Landau damping becomes very strong, so that $\omega \sim \gamma$ and Langmuir waves do not exist.

Imaginary solutions to dispersion equations play an important role in plasma dynamics. In gases, collisions serve as the main mechanism to establish equilibrium. Indeed, if there is a prominent non-equilibrium, like a density gradient, collisions may act to remove it. In collisionless plasmas, collisions are too rare to provide such mechanism; however long-range electromagnetic interactions can redistribute the energy. Usually, those interactions are exhibited in the form of plasma waves. Therefore, in the presence of some free energy sources (e.g., fast beams, density gradients, etc.), plasma waves are excited to drive a system into an equilibrium state. Such wave excitations are called plasma instabilities and are an important part of plasma dynamics which are studied in conjunction with plasma waves. In the linear approximation, instabilities take the form of complex solutions to dispersion equations with positive imaginary parts $\gamma > 0$. Similarly to the Landau damping example, in the case of the positive imaginary part, the mode will exponentially grow in time $e^{-i\omega t} \sim e^{\gamma t}$. For example, the Landau damping rate (1.38) can turn positive when the distribution function has a positive slope ($\partial_v f > 0$). It is a common situation in non-equilibrium plasmas; e.g., in the presence of a particle beam. This wave excitation is called Cherenkov radiation or inverse Landau damping. The instabilities discussed above occur at every space point simultaneously, so they are called absolute instabilities. There is another instability type — a convective instability. It happens when the dispersion equation with fixed frequency and a direction of

propagation $\mathbf{k}/k$ has imaginary wave number roots [119]. Therefore, a wave can grow while propagation in space $e^{ikx} \sim e^{\kappa x}$ ($\kappa = -\text{Im}(k)$). Convective instabilities are not considered in this thesis.

1.5.2 Nonlinear effects

The study of linear stability and plasma waves is crucial for understanding plasma dynamics, But plasma instabilities make the wave energy grow exponentially in time and, at some point, the linear approximation breaks. For this reason, in may cases plasma waves in nature and in the laboratory are in a nonlinear state. This highlights the importance of understanding nonlinear plasma dynamics. In general, we cannot solve nonlinear PDEs analytically, and numerical solutions are also hard to obtain. The main difficulty is due to the fact that solutions to nonlinear PDEs are usually turbulent and chaotic which means a strong sensitivity to initial conditions (ICs) (solutions to chaotic PDEs corresponding to very similar ICs may diverge exponentially in time[8] as illustrated in Figure 1.3). Nevertheless, nonlinear coherent structures coexist with turbulent fields and chaos. In other words, there is an order in chaos, as was illustrated, for example, by famous Lorenz attractors [88].
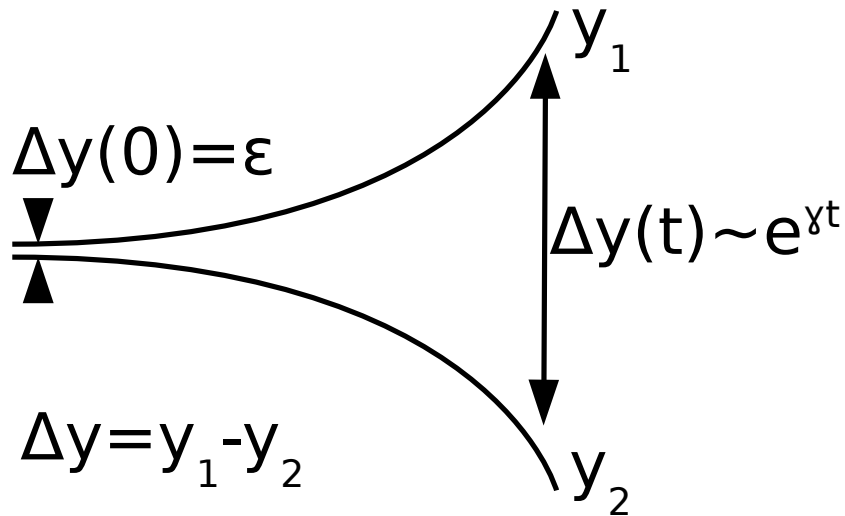
Figure 1.3: Illustration of chaotic PDE solution trajectories ($y_1 = y_1(t), y_2 = y_2(t)$) diverging in time from initial proximity ($|y_1(0) - y_2(0)| \sim 0$).

---

[8] This property of nonlinear PDEs inspired a famous quote by Edward Lorenz known as the "Butterfly effect": The flap of a butterfly's wings in Brazil set off a tornado in Texas.

In plasmas, nonlinear effects and turbulence[9] produce numerous important phenomena such as zonal flows [43] and anomalous resistivity [54], as well as trigger fundamental plasma process such as wave-wave and wave-particle interactions. Therefore, understanding of nonlinear effects is vital in plasma physics. Here, we will outline some theoretical techniques available to study nonlinear waves.

Three wave interactions and modulational instability

When wave amplitudes become sufficiently large, wave-wave interactions could become important. Moreover, nonlinear coupling between different modes leads to energy exchange between them and may produce instabilities due to a nonlinear driving. Here we will consider the simplest interaction between Langmuir and ion sound waves. We note, however, that similar interactions can happen between many other plasma modes and it is one of the most fundamental nonlinear plasma processes. Physically, it is very similar to parametric resonance in mechanics, where a pendulum excites oscillations in a connected pendulum. Mathematically, it is described with the Mathieu equation, where the frequency of a simple pendulum equation, $y'' + \omega^2 y = 0$ is modulated by oscillations of the external pendulum $\omega^2 \to \omega^2(1 - \epsilon \cos(\omega_0 t))$. Wave interactions are more complicated, because instead of simply oscillation frequencies, waves have both frequencies and wave vectors which are interconnected through the dispersion relation $\omega = \omega(\mathbf{k})$.

Because of a strict restriction on frequencies and wavenumbers, the resonance condition from mechanics $\omega_0 = 2\omega$ cannot be satisfied. Instead, the condition can usually be satisfied for three waves

$$\omega_0 = \omega_1 + \omega_2, \tag{1.39}$$

as well as similar condition for wave numbers

$$\mathbf{k}_0 = \mathbf{k}_1 + \mathbf{k}_2. \tag{1.40}$$

Therefore, in an elementary wave-wave interaction, at least three waves are involved.

---

[9] By turbulence we mean a plasma state where numerous wave modes are excited and are interacting with each other.

Before we proceed, we first introduce an ion sound wave. The ion sound wave is a fundamental electrostatic wave in plasmas without a magnetic field (or propagating along magnetic field $\mathbf{k} \parallel \mathbf{B}$). It is similar to a normal sound wave in gases because the wave propagates due to the compression of the ion density, but the restoring force involves the electron pressure which is transferred to ions by the electric field. The wave exists only when the ion temperature is much smaller than the electron temperature, because otherwise, strong Landau damping will damp the wave. So in the limit $T_e \gg T_i$ and $k\lambda_D \ll 1$, when the wave exists, one can obtain (analogous to the analysis done in Section 1.5.1)

$$(\omega^2 - k^2 c_s^2)\widetilde{n}_e = 0, \tag{1.41}$$

where $c_s^2 = T_e/m_i$ is the ion sound speed.

Low frequency ion sound waves act on Langmuir waves by modulation of the plasma density. Therefore, by analogy with the Mathieu equation, the plasma density in equation (1.34) is modulated (the plasma density is included in the plasma frequency $\omega_{pe}^2 \sim n_e = n_0(1 + \widetilde{n}_e/n_0)$). We translate the equation (1.34) back into real space, including modulation and considering only a one dimensional plasma slab $\widetilde{\mathbf{E}} \to \widetilde{E}$

$$\left(\partial_t^2 - \omega_{pe}^2 - 3v_{T_e}^2 \partial_x^2\right)\widetilde{E} = \omega_{pe}^2 \widetilde{E}\frac{\widetilde{n}_e}{n_0}, \tag{1.42}$$

where $\widetilde{n}_e$ is a density perturbation caused by the ion sound wave and ω_{pe} is the plasma frequency without modulation.

As mentioned, in the ion sound wave, the restoring force that acts on ions is the electric field from electrons. At the same time, electrons are in a quasi-static state $p_e + e\phi = const$ for the considered time scale. Therefore, the main effect of electron oscillations (i.e., Langmuir wave) on the ion sound is a ponderomotive force, i.e., $p_e \to p_e + \widetilde{E}^2/16\pi$ (the electron pressure is implicitly present in equation (1.41) via the ion sound speed $c_s^2 \widetilde{n}_e = \widetilde{p}_e/m_i$). Thus, equation (1.41) gets modified to

$$(\partial_t^2 - c_s^2 \partial_x^2)\widetilde{n}_e = \partial_x^2 \widetilde{E}^2/(16\pi m_i), \tag{1.43}$$

where $\widetilde{E}$ is an electric field of the Langmuir wave. Equations (1.42), (1.43) describe the nonlinear interactions between ion sound and Langmuir waves in the main order. The strongest interaction happens when resonance conditions (1.39), (1.40) are satisfied, which

can be seen from the Fourier transform of the quadratic nonlinearity, i.e., the convolution $\partial_t^2 \widetilde{n}_e \sim \int E_{k'} E_{k''} \delta(k - k' - k'') dk' dk''$.

In plasmas, Langmuir waves excite ion sound waves, so to quantify this energy transfer, we consider a large pump Langmuir wave with amplitude E_0, a wave number k_0, and a frequency ω_0, which will excite an ion sound wave with an amplitude $\widetilde{n}_e$, a wave number k, and a frequency ω, as well as a Langmuir sideband with an amplitude E_1, a wave number $k_0 - k$, and a frequency $\omega_0 - \omega$. Thus, substituting the three wave structure

$$\widetilde{n}_e \sim e^{-i\omega t + ikx}, \quad E \sim E_0 e^{-i\omega_0 t + ik_0 x} + E_1 e^{-i(\omega_0 - \omega)t + i(k_0 - k)x}, \tag{1.44}$$

into our equations (1.42), (1.43), and considering the amplitude of the pump wave E_0 fixed, we find the imaginary shift of the ion sound wave frequency

$$\gamma^2 = \frac{E_0^2/16\pi}{n_0 T_e} \omega_l \omega_s / 4, \tag{1.45}$$

where $\omega_l^2 = \omega_{pe}^2 + 3v_{T_e}^2 k^2$ and $\omega_s = kc_s$. The expression of nonlinear growth rate confirms the energy transfer from the Langmuir pump wave into the ion sound mode as well as into Langmuir sideband.

Here the nonlinear fundamental process of wave-wave interaction was considered, where only three waves were accounted for. This procedure is essentially the next step beyond the linear approximation, where nonlinear interactions are taken into account perturbatively. The next step beyond three-wave interactions is quasilinear theory, where instead of a fixed pump wave, a large spectrum of weakly interacting waves is considered

$$E_0^2 \to \sum_k E_k^2. \tag{1.46}$$

The evolution of the wave ensemble (1.46) within the quasilinear theory is described by equations

$$\frac{dE_k^2}{dt} = 2\gamma(k) E_k^2, \tag{1.47}$$

where $\gamma(k)$ is the linear growth rate. The resulting system is called weak turbulence approximation for wave-wave interactions[10].

---

[10] Quasilinear theory can also be applied to wave-particle interaction, which is described with equations similar to (1.38).

Careful investigation of quasilinear theory based on wave-wave interactions shows [54] that energy in a plasma system may be transferred into long wavelengths, constituting a so-called inverse energy cascade. This is opposite to the well known Kolmogorov energy cascade in fluids. For example, as was described above in this section, Langmuir waves with wave number k_0 were unstable and the energy was transferred into the ion sound waves with smaller wave numbers $k < k_0$. This is an inverse energy cascade mechanism. As we will see later, the inverse cascade is an important plasma phenomenon which universally happens in many plasma systems.

Numerical methods

Great insight into the behavior of nonlinear systems can be obtained from analytical techniques. Unfortunately, pure theory is not enough to study nonlinear plasma dynamics and numerical methods (NMs) should be employed in conjunction with theory. NMs are used to get insights and advance the analytical theory of plasma dynamics. At the same time, analytical tools are used to aid advancing NMs, sometimes just to use them and sometimes to construct new methods.

The main idea behind NMs is to approximate continuous functions and operators with their discrete counterparts. Once done, the PDE system can be translated into matrix equations[11] and solved numerically. In general, NMs in plasma physics can be roughly[12] separated into two main categories: NMs for fluid models and NMs for kinetic models.

Fluid methods allow simulations of large systems for long times with high resolution since they are computationally cheaper due to low dimensionality. They include only selected physical effects, which can be an advantage or a disadvantage. The main difficulty comes with the large variety of fluid models, each requiring a NM to suit the problem. Therefore, it is difficult to develop and use NMs for fluids models, because one has to understand how solutions of selected equations would behave. In this thesis, all fluid simulations were performed with BOUT++ [45], which is a efficient highly parallelized framework for plasma

---

[11] Not all NMs are represented as matrix equations, but in principle, they can be.

[12] Those two categories can intersect forming hybrid methods, where kinetic method solves one part of the problem and a fluid method another.

fluid simulations in 3D curvilinear coordinates.

Kinetic methods are usually focused on solving the kinetic equation; e.g., Vlasov-Maxwell equations. Therefore, they are usually computationally more expensive and many important physical effects are included. There are various ways to solve the VM system numerically; one example is the Eulerian-Vlasov methods [30, 118, 50], where phase space is discretized using a Eulerian computational grid. Another approach is the class of spectral methods [6, 110, 64, 108]. In spectral methods, the distribution function is expanded in a series of basis functions similar to the fluid expansion based on velocity moments. The oldest, most popular, and well-established technique to study the kinetics of plasmas is the particle-in-cell (PIC) method. It was first used in Los Alamos National Laboratory in 1955 [60] to study hydrodynamics of fluids. Approximately five years later, particle methods [19, 37] were started to be applied in plasma physics. One of the first prominent PIC successes, which led to the wide adoption, was the discovery of previously predicted Landau damping [82] in PIC simulations before it was discovered experimentally [38].

Today PIC is a standard numerical method in plasma physics and it is widely adopted in other branches of physics such as fluid dynamics, astrophysics, etc. A thorough description of PIC can be found in texts [12, 62, 127]. In recent years, the advances of high-performance computing have boosted the progress in many scientific areas including kinetic plasma simulations with PIC. The optimal parallel implementations of PIC have been investigated and developed for CPU based supercomputer environments [86, 42, 27] as well as for modern computer architectures such as graphics processing units (GPU) [39, 27, 40].

1.6 Drift waves in fully magnetized plasma

The density gradient is an intrinsic property of laboratory plasmas. A fundamental wave supported in fully magnetized plasmas with a gradient in density is a drift wave. A comprehensive review of drift waves in plasmas can be found in the Ref. [65]. Here we illustrate the basic drift wave propagation mechanism.

Let us imagine an ion density perturbation δn localized in a magnetized plasma. Then, a local electric field $\mathbf{E}$ produced by this charge will cause plasma around the perturbation

to drift with velocity $\mathbf{V}_E \sim \mathbf{E} \times \mathbf{B}$ perpendicular to the magnetic field. In homogeneous plasmas, the whole system will rotate with zero density flux. In the presence of a density gradient, however, the total density flux $\mathbf{\Gamma}_n$ will be in the direction of the diamagnetic drift $\mathbf{\Gamma}_n \sim \nabla n \times \mathbf{B}$ and the perturbation δn will propagate in this direction. This is a basic drift wave mechanism.
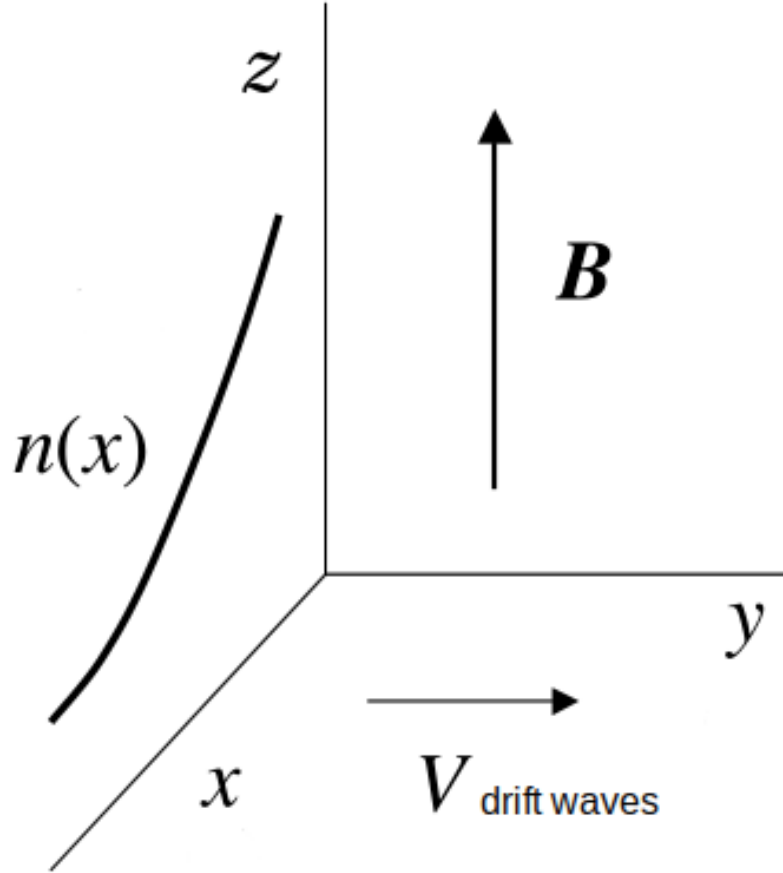
Figure 1.4: Geometry of a drift wave propagation in magnetized plasmas.

Now we quantify this process. We will use the geometry shown in Figure 1.4 with the magnetic field along the z axis and the density decaying in the x direction. First, we consider cold ions $0 \sim T_i \ll T_e$, and a strong magnetic field $\omega_{ci} t \gg 1$, where t is the considered time scale and $\omega_{ci} = eB/m_i c$ is the ion cyclotron frequency. In this limit, it follows from Euler's equation (1.26), that ions would respond to an electric field perturbation $\widetilde{\mathbf{E}}$, with the electric

24

drift

$$\widetilde{\mathbf{V}}_i = \mathbf{V}_E = c\frac{\widetilde{\mathbf{E}} \times \mathbf{B}}{B^2} = -c\frac{\nabla\widetilde{\phi} \times \mathbf{B}}{B^2}, \tag{1.48}$$

where $\mathbf{B}$ is a stationary magnetic field, and it has been taken into account that, in a strong magnetic field, the electrostatic approximation is valid, so the electric field can be expressed via the electrostatic potential $\widetilde{\mathbf{E}} = -\nabla\widetilde{\phi}$. Let us notice that in a uniform magnetic field, this drift is incompressible; i.e., $\nabla \cdot \mathbf{V}_E = 0$. Therefore, the mass conservation equation for ions will take the form

$$\frac{\partial n_i}{\partial t} + \mathbf{V}_E \cdot \nabla n_i = 0. \tag{1.49}$$

Expanding density around its equilibrium value $n_i = n_0(x) + \widetilde{n}_i$, neglecting nonlinear terms, using the geometry defined in Figure 1.4, and considering a monochromatic mode $\sim e^{-i\omega t + i\mathbf{k}\cdot\mathbf{x}}$, we get

$$\omega\widetilde{n}_i + \frac{cn_0}{BL_n}k_y\widetilde{\phi} = 0, \tag{1.50}$$

where ω is a perturbation frequency, k_y is a perturbation wave number in the y direction, and $L_n^{-1} = \partial_x n_0/n_0$ is the density gradient scale length.

For electrons, we use the Boltzmann approximation

$$\widetilde{n}_e = n_0\frac{e\widetilde{\phi}}{T_e}, \tag{1.51}$$

which comes from the projection of the Euler equation (1.26) for electrons onto the magnetic field direction, when the electron inertia ($m_e \sim 0$) is neglected (i.e., $\omega \ll k_z v_{T_e}$ and the electrons are in the quasi-stationary state $\partial_z p_e = en_e\partial_z\widetilde{\phi}$).

Closing the system of equations with the quasi-neutrality condition $n_e \approx n_i$, we finally get the dispersion equation for drift waves

$$\omega = v_d k_y, \tag{1.52}$$

with the drift wave velocity

$$v_d = -\frac{cT_e}{eBL_n}. \tag{1.53}$$

Now we can see that drift waves propagate in the y direction according to the geometry of Figure 1.4 ($L_n < 0$).

1.6.1 Hasegawa-Mima equation

We will introduce a reduced fluid model for the nonlinear interaction of drift waves, called the Hasegawa-Mima equation which is a natural next step after the linear model. It was first derived by Akira Hasegawa and Kunioki Mima to describe turbulence in tokamaks [61]. The geometry shown in Figure 1.4 and ordering from previous section are

$$\frac{\widetilde{n}_i}{n_0} \approx \frac{\widetilde{n}_e}{n_0} \approx \frac{e\widetilde{\phi}}{T_e} \sim \frac{\omega}{\omega_{ci}} \sim \frac{1}{k_y L_n} \ll 1. \tag{1.54}$$

Using this ordering we can further expand the Euler equation (1.26) for ions beyond simple $\mathbf{E} \times \mathbf{B}$ drift (1.48). Hence,

$$\widetilde{\mathbf{V}}_i = \mathbf{V}_E + \mathbf{V}_p, \tag{1.55}$$

where the notation for $\mathbf{E} \times \mathbf{B}$ drift $\mathbf{V}_E$ and polarization drift $\mathbf{V}_p$ were introduced

$$\mathbf{V}_E = -c\frac{\nabla\widetilde{\phi} \times \mathbf{B}}{B^2}, \qquad \mathbf{V}_p = -\frac{1}{\omega_{ci}B}\left(\frac{\partial}{\partial t} + \mathbf{V}_E \cdot \nabla\right)\nabla\widetilde{\phi}. \tag{1.56}$$

Notice that the polarization drift has two parts: an inertial part due to the time derivative and an advectional part due to the Lagrangian advection. The latter serves as the main nonlinear mechanism of wave-wave interactions in drift waves.

Plugging the ion velocity expression (1.55) into the ion mass conservation equation, in one order above the linear approximation, we get

$$\left(1 - \rho_s^2\nabla_\perp^2\right)\frac{\partial}{\partial t}\frac{e\widetilde{\phi}}{T_e} + v_d\frac{\partial}{\partial y}\frac{e\widetilde{\phi}}{T_e} - \rho_s c_s\left\{\frac{e\widetilde{\phi}}{T_e}, \rho_s^2\nabla_\perp^2\frac{e\widetilde{\phi}}{T_e}\right\} = 0, \tag{1.57}$$

where $\rho_s = c_s/\omega_{ci}$ is called the ion sound Larmor radius which is the ion Larmor radius computed with the electron temperature, $\nabla_\perp$ is a gradient perpendicular to the magnetic field, $\{f, g\} = \partial_x f \partial_y g - \partial_y f \partial_x g$ is the Poisson bracket. Here, we note that the inertial part of the polarization drift produces a linear term proportional to $\nabla_\perp^2 \partial_t \widetilde{\phi}$ and the Lagrangian advection adds a Poisson bracket term.

Let us note that the dynamics described by the Hasegawa-Mima equation is pseudo two-dimensional. Indeed, all spatial derivatives are perpendicular to the magnetic field, because the strong magnetic field separates time and spatial scales along and perpendicular to it. Therefore, we can consider only two dimensional dynamics $\widetilde{\phi} = \widetilde{\phi}(x, y)$. However, we should

also note that fast electron dynamics along magnetic field ($\omega \ll k_z v_{T_e}$) is important, as it provides a Boltzmann equilibrium for the electron density perturbation (1.51).

1.6.2   Zonal flow

The Hasegawa-Mima equation (1.57) is a minimal reduced fluid model for drift wave nonlinear interactions which lead to stochastic solutions and turbulence [65]. It is not known how to solve the Hasegawa-Mima equation, but one can apply perturbative techniques to investigate regimes of weak nonlinearity, similar to what was shown in Section 1.5.2. This analysis will be conducted in Chapter 2. Here we will outline a qualitative picture of the nonlinear dynamics.

Similar to the parametric instability (also called modulational instability) discussed in Section 1.5.2, where energy is transferred to large-scale ion sound waves from small-scale Langmuir waves, Hasegawa-Mima describes a modulational instability where energy is transferred from small-scale drift waves to a large scale zonal flow.
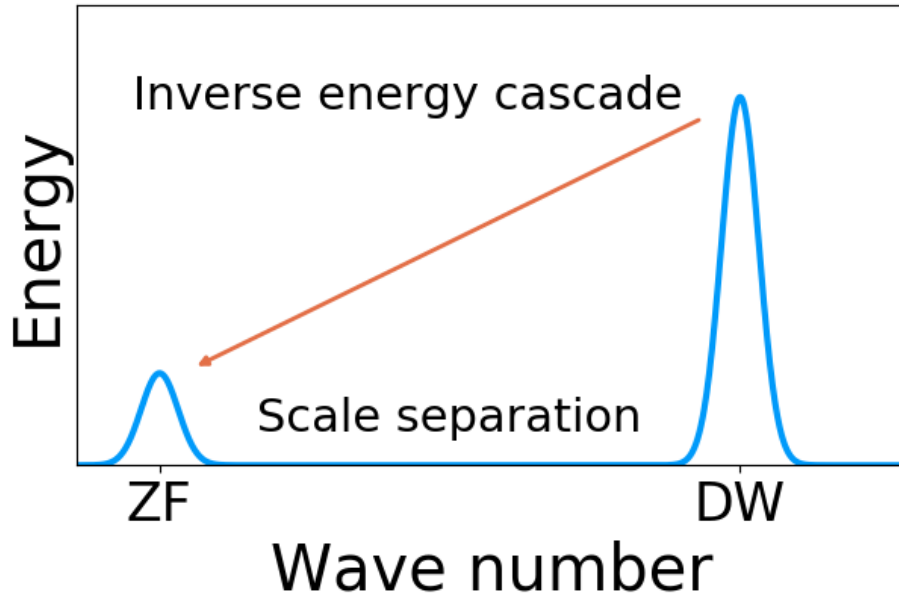
Figure 1.5: Schematic representation of the inverse energy cascade in drift waves/zonal flow system.

Unlike the ion sound wave, which is a linear plasma eigen-mode, zonal flows are a nonlinear self-organized structure which emerges from turbulence and does not exist in the linear regime. The schematic representation of energy transfer into the larger scales (inverse energy

cascade) is shown in Figure 1.5. This happens because the parametric instability excites the mode via nonlinear forcing (with frequency Ω and wave number q) which do not exist in the linear limit

$$\partial_t \phi_q \sim \phi_{\pm k} \phi_{\mp k+q}, \tag{1.58}$$

where ϕ_q is the amplitude of the zonal flow, and $\phi_{\pm k}, \phi_{\mp k+q}$ are drift wave and sideband amplitudes, respectively. Analysis similar to that in Section 1.5.2 shows that the nonlinear effects in the Hasegawa-Mima equation shift the zonal flow frequency by

$$\frac{\Omega^2}{\omega_{ci}^2} = -2k^4 q^4 \rho_s^8 \left| \frac{e\phi_k}{T_e} \right|^2, \tag{1.59}$$

making it unstable $(Im(\Omega) > 0)$ in the presence of drift waves.

Zonal flows cannot grow indefinitely, and must saturate at some amplitude. For example, the zonal flow growth can be limited by the drift wave energy, so it will saturate when the pump wave (drift wave) is exhausted. However, as we will show in Chapter 2, the saturation may happen before the drift wave energy is exhausted due to nonlinear zonal flow self-interaction.

Finally, we note that the study of zonal flows have numerous practical applications [43]. First, zonal flows occur in tokamaks [65], where they significantly reduce radial transport and improve plasma confinement. Furthermore, the term zonal flow originates from meteorology, where it refers to an atmospheric circulation in a predominantly latitudinal direction. This phenomenon occurs in all rotating fluids (e.g., Earth atmosphere) and the zonal flow can be described with the same Hasegawa-Mima equation, which was discovered independently in the geophysics community, and is called Charney–Obukhov equations [26]. In the atmosphere, zonal flows appear from Rossby wave turbulence which governs our weather, and the role of the magnetic field is played by the Coriolis force.

1.7 Drift waves, instabilities and transport in partially magnetized plasma

Partially magnetized plasmas (or Hall plasmas) have a number of important applications such as Hall thrusters for electric propulsion, magnetrons and some regions of the ionosphere.

The crucial feature of these applications is that the ion Larmor radius ρ_i is much larger than the length scale of the interest L, which could be device size and/or the wavelength of the perturbations. As a result, ions do not feel the magnetic field and can be freely accelerated by the electric field, e.g., as in the electric propulsion systems. The electron Larmor radius is much smaller, so the electrons gyrate around the magnetic field lines and are well confined. This confinement is not ideal and electrons do move in the direction of the external electric field when some additional processes (collisions and turbulence) are included.

Electron collisions with neutrals represent a classical mechanism for the electron current across the magnetic field (along the direction of the external electric field). Numerous experiments [99, 69, 93] and numerical simulations [113, 2, 7, 3, 10, 73] of practical devices with partially magnetized plasmas, however, indicate that the electron current is orders of magnitude larger than the collisional transport predictions; this current is called the anomalous current.

In application to Hall thrusters, there are two main mechanisms proposed to explain the anomalously high electron cross-field current: (i) electron-wall collisions [17, 101], or so-called near-wall conductivity, and (ii) turbulence driven by micro-instabilities [69]. The near-wall conductivity mechanism is based on the observation that the mean free path of particles is much smaller than the effective thruster size. Thus, effective collision frequency due to interaction with the wall is larger than the classical collision frequency; this increases transport coefficients and axial current. It has been pointed out, however, that the near-wall conductivity alone is not able to explain fully the anomalous current [72]. Moreover, the near-wall conductivity is not operating outside of the thruster (i.e., no walls) where the level of the current is still high (anomalous).

In this thesis, we consider the wave processes that may result in the turbulent transport in partially magnetized plasmas and we start by describing a linear theory of density gradient driven modes (similar to drift waves).

Magnetically confined electrons are subject to the $\mathbf{E} \times \mathbf{B}$ drift ($\mathbf{V}_E$) and thus their dynamics is described by the equation

$$\frac{\partial \widetilde{n}_e}{\partial t} + \mathbf{V}_E \cdot \nabla n_0 = 0, \tag{1.60}$$

which gives (similar to equation for ions (1.50) in drift wave dynamics)

$$\omega \widetilde{n}_e - \frac{cn_0}{BL_n} k_y \widetilde{\phi} = 0. \tag{1.61}$$

Ions are not magnetized and follow the inertial (ballistic response) determined by the equations

$$\frac{\partial \widetilde{n}_i}{\partial t} + n_0 \nabla \cdot \widetilde{\mathbf{V}}_i = 0, \tag{1.62}$$

$$\frac{\partial \widetilde{\mathbf{V}}_i}{\partial t} = -\frac{e}{m_i} \nabla \widetilde{\phi}, \tag{1.63}$$

which gives

$$\frac{\widetilde{n}_i}{n_0} = \frac{k^2 c_s^2}{\omega^2} \frac{e\widetilde{\phi}}{T_e}. \tag{1.64}$$

Using the quasi-neutrality, one obtains the dispersion relation for "anti-drift waves" [52]

$$\omega = \frac{k^2 c_s^2}{k_y v_d}, \tag{1.65}$$

with $k = |\mathbf{k}|$. Here, we call these waves the Hall drift waves. These waves may become unstable in plasmas with external electric field $\mathbf{E}_0$ where

$$(\mathbf{k} \cdot \mathbf{B} \times \nabla n_0)(\mathbf{k} \cdot \mathbf{B} \times \mathbf{E}_0) > 0, \tag{1.66}$$

and it is called the Simon-Hoh instability [115]. Simon-Hoh type instability is a building block of turbulence in $\mathbf{E} \times \mathbf{B}$ Hall plasma devices.

1.7.1 Reduced nonlinear model for dynamics of partially magnetized plasmas

In this section, we describe the advanced nonlinear fluid model that we will be using to describe wave turbulence and transport in partially magnetized plasmas. In addition to the anti-drift mode described by the equation (1.65), our model also includes the lower hybrid and ion sound modes as well as the effects of the electron Larmor radius and collisions. The model was first proposed in Ref [115].

First of all, we use standard fluid equations with the assumption that ions are not magnetized. Hence,

$$\partial_t n_i + \nabla \cdot (n_i \mathbf{V}_i) = 0, \tag{1.67}$$

$$\partial_t \mathbf{V}_i + \nabla \left(\frac{\mathbf{V}_i^2}{2} \right) - \mathbf{V}_i \times (\nabla \times \mathbf{V}_i) = -\frac{e}{m_i} \nabla \phi, \tag{1.68}$$

where n_i is the ion density, $\mathbf{V}_i$ is the ion velocity, ϕ is the electrostatic potential, and the Reynolds stress was expanded with the well-known vector identity $\mathbf{V}_i \cdot \nabla \mathbf{V}_i = \nabla(\mathbf{V}_i^2/2) - \mathbf{V}_i \times (\nabla \times \mathbf{V}_i)$. Here, the ion temperature, and thus pressure effects, were neglected because the dominant part of ion energy is in their axial velocity. Then, we expand our equations around the equilibrium — ions have equilibrium velocity $\mathbf{V}_{i0}$, and there is a constant electric field $\mathbf{E}_0$,

$$n_i(t, \mathbf{r}) = n_0(\mathbf{r}) + \widetilde{n}_i(t, \mathbf{r}), \tag{1.69}$$

$$\mathbf{V}_i(t, \mathbf{r}) = \mathbf{V}_{i0} + \widetilde{\mathbf{V}}_i(t, \mathbf{r}), \tag{1.70}$$

$$\widetilde{\mathbf{V}}_i(t, \mathbf{r}) = -\nabla \widetilde{\chi}(t, \mathbf{r}), \tag{1.71}$$

$$\nabla \phi = -\mathbf{E}_0 + \nabla \widetilde{\phi}, \tag{1.72}$$

here we neglected the divergence-free component of the ion velocity, as ions are assumed to have a ballistic response to the predominantly axial electric field. Thus taking the divergence of the Euler equation finally gives

$$(\partial_t + \mathbf{V}_{i0} \cdot \nabla)\, \widetilde{n}_i - n_0 \nabla^2 \widetilde{\chi} - \nabla n_0 \cdot \nabla \widetilde{\chi} - \nabla \widetilde{n}_i \cdot \nabla \widetilde{\chi} - \widetilde{n}_i \nabla^2 \widetilde{\chi} = 0, \tag{1.73}$$

$$(\partial_t + \mathbf{V}_{i0} \cdot \nabla)\, \nabla^2 \widetilde{\chi} = \nabla^2 \left(\frac{1}{2}(\nabla \widetilde{\chi})^2 + \frac{e}{m_i} \widetilde{\phi} \right), \tag{1.74}$$

where the $\mathbf{V}_{i0} \cdot \nabla n_0$ term was neglected, because of the assumption that the equilibrium is supported by external forces (external forces were not included in (1.67), (1.68)).

In order to derive the evolution equations for electrons, we employ the assumption that they are strongly magnetized and consider time scales much slower than electrons gyro motion $t\omega_{ce} \gg 1$. We start with the Euler equation for electrons (1.26)

$$\partial_t \mathbf{V}_e + (\mathbf{V}_e \cdot \nabla)\mathbf{V}_e = \frac{e}{m_e} \nabla \phi - \omega_{ce} \mathbf{V}_e \times \mathbf{b} - \frac{1}{n_e m_e} \nabla p_e - \frac{1}{n_e m_e} \nabla \cdot \mathbf{\Pi}_e - \nu \mathbf{V}_e, \tag{1.75}$$

where $\mathbf{b} = \mathbf{B}/B$ is a unit vector in the direction of the magnetic field, and the friction force $-\nu\mathbf{V}_e$ due to collisions with neutrals was added with an effective collision frequency ν. We can now proceed in a similar fashion as in the derivation of the Hasegawa-Mima equation (1.57); in other words, we expand the Euler equation for electrons (instead of the Euler equation for ions in Hasegawa-Mima) in a series of $1/\omega_{ce}$

$$\mathbf{V}_e = \mathbf{V}_E + \mathbf{V}_d + \mathbf{V}_I + \mathbf{V}_\nu + \mathbf{V}_\Pi, \tag{1.76}$$

where

$$\mathbf{V}_E = v_{T_e}\rho_e\mathbf{b} \times \nabla\frac{e\phi}{T_e}, \tag{1.77}$$

$$\mathbf{V}_d = -\frac{1}{n_e m_e \omega_{ce}}\mathbf{b} \times \nabla p_e, \tag{1.78}$$

$$\mathbf{V}_I = -\frac{1}{\omega_{ce}}\mathbf{b} \times \left(\partial_t(\mathbf{V}_E + \mathbf{V}_d) + ((\mathbf{V}_E + \mathbf{V}_d) \cdot \nabla)(\mathbf{V}_E + \mathbf{V}_d)\right), \tag{1.79}$$

$$\mathbf{V}_\nu = -\frac{\nu}{\omega_{ce}}\mathbf{b} \times (\mathbf{V}_E + \mathbf{V}_d), \tag{1.80}$$

$$\mathbf{V}_\Pi = -\frac{1}{n_e m_e \omega_{ce}}\mathbf{b} \times \nabla \cdot \mathbf{\Pi}_e. \tag{1.81}$$

Here we note that this expansion is valid only for electron dynamics perpendicular to the magnetic field (notice the $\mathbf{b}\times$ term in all expressions for the velocities). The parallel dynamics is neglected in this model and will be considered in future work.

To close the system, we use the gyro viscous cancellation as our closure [16]

$$n_e m_e(\mathbf{V}_d \cdot \nabla)(\mathbf{V}_E + \mathbf{V}_d) + \nabla \cdot \mathbf{\Pi}_e = 0. \tag{1.82}$$

Finally, we substitute the electron velocity expansion into the continuity equation

$$\partial_t n_e + \nabla \cdot (n_e\mathbf{V}_e) = 0. \tag{1.83}$$

After some algebraic manipulations and expanding around the equilibrium,

$$n_e(t, \mathbf{r}) = n_0(x) + \widetilde{n}_e(t, \mathbf{r}), \tag{1.84}$$

$$\nabla\phi = -\mathbf{E}_0 + \nabla\widetilde{\phi}, \tag{1.85}$$

we finally get, to main order (see details in [115]),

$$\partial_t\widetilde{\eta} + \mathbf{V}_{e0} \cdot \nabla\widetilde{\eta} + \nu(\widetilde{\eta} - \widetilde{n}_e) + v_{T_e}\rho_e\left(\mathbf{b} \times \nabla\frac{e\widetilde{\phi}}{T_e}\right) \cdot \nabla n_0 + v_{T_e}\rho_e\left\{\frac{e\widetilde{\phi}}{T_e}, \widetilde{\eta}\right\} = 0, \tag{1.86}$$

with generalized vorticity defined as

$$\widetilde{\eta} = \widetilde{n}_e + \rho_e^2 \left(n_0 \nabla^2 \frac{e\widetilde{\phi}}{T_e} - \nabla^2 \widetilde{n}_e \right), \tag{1.87}$$

where the equilibrium electron velocity is $\mathbf{V}_{e0} = c\mathbf{E}_0 \times \mathbf{b}/B$, and the coordinate system invariant definition of the Poisson bracket is $\{f, g\} = (\mathbf{b} \times \nabla f) \cdot \nabla g$.

Equations (1.73), (1.74), (1.86) together with quasi-neutrality condition $n_e \approx n_i$ form a reduced fluid model, which we will use to investigate waves in Hall thruster plasmas. The structure of equation (1.86) is very similar to the Hasegawa-Mima equation (1.57). Indeed, the fourth term in the left-hand side of the equation (1.86) is analogous to the drift wave term in Hasegawa-Mima equation, and it also produces waves analogous to drift waves in fully magnetized plasmas; we call them Hall drift waves. The first and last terms in (1.86) are also present in the Hasegawa-Mima equation, and they come from the polarization drift. A new second term in (1.86) is just the equilibrium electron $\mathbf{E} \times \mathbf{B}$ drift and the third term comes from the friction force due to electron collisions with neutrals.

1.8 Langmuir wave turbulence

We move to waves and turbulence in the comprehensive kinetic model; i.e., the Vlasov equation (1.11). The analytical theory for the Vlasov equation is complicated and is out of the scope of this text. The standard numerical approach, the PIC method, is unfortunately ill-suited for wave/turbulence problems, since it requires a high resolution and the PIC method is very noisy. Indeed, it can be shown with the aid of the fluctuation-dissipation theorem [79, 84] that the particle noise decreases as the inverse square root of macro-particle number ($\sim 1/\sqrt{N_p}$). A macro-particle is a computational particle that represents many real particles and if you need to increase a resolution by one order, you need one hundred times more particles, which usually means one hundred times more computational time and space. This is unacceptable for many problems; e.g., plasma turbulence. The good solution is to use spectral methods [6, 110, 64, 108], as they are famous for their exponential convergence. In collisionless plasmas, however, the PDF can be highly deformed, thus causing slow convergence of spectral methods. This problem is absent in PIC codes because all particle methods

can easily represent a very complicated PDF. In Chapter 7, we will investigate the possibility of combining spectral and PIC methods to improve convergence of the spectral method and the accuracy of PIC. For this matter, we will use the simplest plasma turbulence problem, Langmuir turbulence, which happens when an electron beam interacts with plasmas. Here we will briefly outline this classical problem. For a more thorough description, refer to the references [125, 70].
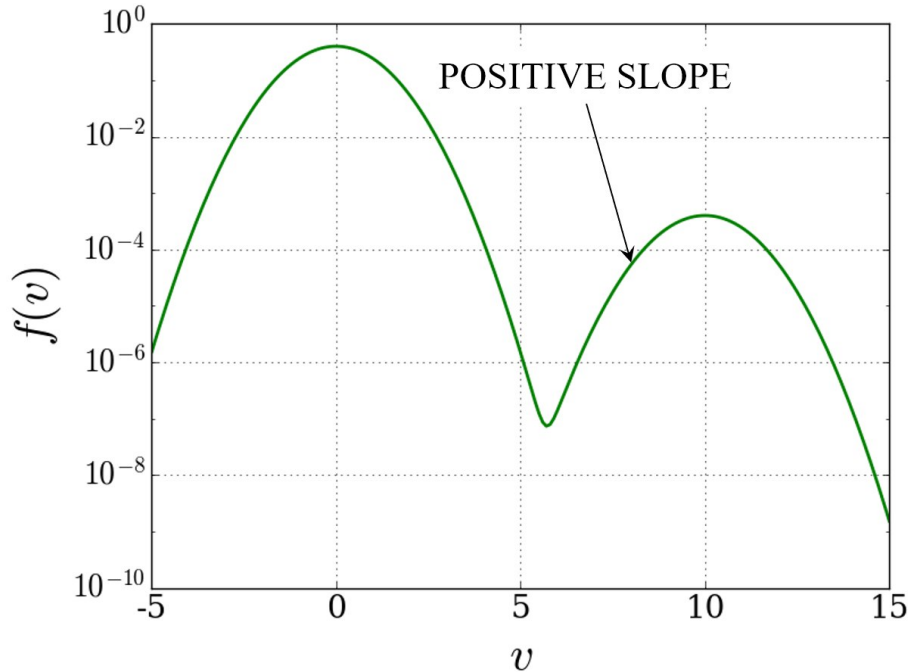
Figure 1.6: Particle distribution function of a system where a beam penetrates plasma.

When a low-density beam penetrates a plasma, the distribution function will take on a form similar to that shown in Figure 1.6. This PDF has a positive slope ($\partial_v f > 0$) which will cause instability, due to inverse Landau damping (i.e., the Landau damping rate (1.38) will become positive), which excites Langmuir waves. This is also called Cherenkov radiation. The physical mechanism of this instability can be explained as follows. In the reference frame moving with the wave, the particle sees the wave as a potential well ($\phi \sim \sin x$). If the particle moves with a speed close to the wave speed $v_{particle} \approx v_{wave}$, it will be trapped in this well. If it is slightly faster than the wave, it will reflect from the wave potential and slow down. The residual energy will go into the wave itself. If on the contrary, the particle is slightly slower than the wave, it will reflect and accelerate, removing energy from the wave.

34

Therefore, if there are more particles slower than the wave (negative slope, $\partial_v f(v_{wave}) < 0$), the wave will damp — Landau damping. If there are more fast particles, the wave will be excited — Cherenkov radiation.

Thus, when there is a particle beam, plasmas are unstable and Langmuir waves will be excited. Waves will grow taking energy from the beam, and thus disrupting it. Quasilinear theory shows that particles will diffuse in velocity space removing the instability source (i.e., flattening the positive slope). Finally, the saturation stage will be reached when the beam is fully deformed into a plateau in velocity space. This is a typical situation in plasmas with beams and is a challenging problem for both pure PIC and spectral methods. For PIC, the challenge comes with low beam densities, as instability growth rate decreases with beam density $\gamma \sim n_{Beam}/n_{Plasma}$, therefore requiring higher resolution. For the spectral method, it may be difficult to converge to the plateau type distribution function. In Chapter 7, we propose a new hybrid method, which overcomes those difficulties.

Chapter 2

Nonlinear damping of zonal flows

2.1 Preface

In this chapter, we study nonlinear dynamics of drift waves and zonal flows with the minimal reduced fluid model, the Hasegawa-Mima equation (1.57), as introduced in Section 1.6.1. The modulational instability theory is extended to higher-order which allows us to quantify the formation and saturation mechanisms of zonal flows. The material in this chapter is based on a paper published in Plasma Physics Reports [77].

2.2 Abstract

The modulational instability theory for the generation of large scale (zonal) modes by drift modes has been extended to the second order including the effects of finite amplitude zonal flows, ϕ_q. The nonlinear (second order) sidebands are included in the perturbative expansion to derive the nonlinear equation for the evolution of ϕ_q. It is shown that effects of finite ϕ_q reduce the growth rate of zonal flow with a possibility of oscillatory regimes at a later stage.

2.3 Introduction

Drift waves (DW) and instabilities are common for many confined plasmas. Nonlinear interactions of drift waves have been studied in various settings in attempts to understand anomalous transport in controlled fusion systems such as tokamaks. The nonlinear Hasegawa-Mima equation is often used as a simplest model for drift waves and generation of large scale structures such as zonal flows (ZF). Similar phenomena occurs in geostrophic fluids (shallow

water on a rotating sphere) such as the atmosphere and ocean, where the analogous Charney-Obukhov equation is employed to describe Rossby waves. Zonal flow structures have been a topic of intense interest due to their role in controlling the drift turbulence by taking energy away from small scale fluctuations as well by a direct mechanism via the reduction of the radial correlation length [22].

The basic dynamics in drift wave - zonal flow systems can be characterized by a predator-prey model [43, 68], where drift waves are the pray while zonal flow is the predator who "feeds" on drift waves. In this model, the evolution of zonal flow energy is described by the equation,

$$\frac{\partial W_{ZF}}{\partial t} = \kappa W_{DW} W_{ZF} - \gamma_{damp} W_{ZF} - \gamma_{NL}(W_{ZF}) W_{ZF}, \qquad (2.1)$$

where W_{ZF}, W_{DW} - are zonal flow and drift wave energy, respectively.

The first term on the right side of Eq. (2.1) describes nonlinear coupling between drift wave and zonal flow. This coupling is manifested as a zonal flow instability which has a growth rate proportional to the drift wave intensity, $\gamma = \kappa W_{DW}$. The modulational instability theory of drift waves is the simplest model that describes zonal flow growth [117, 116, 90, 55, 29, 58, 5, 4]. Such analytical calculations are generally consistent with the results of direct numerical simulations [96, 90, 34]. The second term in Eq. (2.1) describes the linear ZF damping rate, e.g. collisional or neoclassical nature [43]. The last term in Eq. (2.1) describes nonlinear damping of ZF. In the simplest case, it can be represented in the form $\gamma_{NL} = \alpha W_{ZF}$ where α is the so-called Landau constant [83]. Nonlinear damping may suppress the zonal flow instability. Eq. (2.1) gives a simple estimate for the zonal flow energy (amplitude) at saturation

$$W_{ZF}^{max} \sim \frac{\gamma}{\alpha}. \qquad (2.2)$$

Several different mechanisms resulting in nonlinear damping of zonal flow are possible (e.g. effect of broad drift wave spectra, secondary instabilities of zonal flows, interaction with mean flow [122] (MF), etc. [43]). In this work we focus on generalizing modulation instability theory for the case of finite ZF amplitude by nonlinear modification of Reynolds stress tensor drive. Generally speaking this effect is a nonlinear expansion of the coupling with drift waves (first term in Eq. (2.1))

$$\kappa = \kappa_0 + \kappa_1 W_{ZF} + O(W_{ZF}^2). \qquad (2.3)$$

Similar studies were conducted by Mendonca [94] using the wave kinetic equation. Here we employ the direct perturbation theory for several coupled modes.

The physical nature of considered nonlinear damping is ZF interaction with itself. In some sense (mathematically) our ZF-ZF interaction is similar to stabilization via ZF-MF interaction considered by K. Uzawa et al [122]. K. Uzawa concluded that taking into account leading stabilization term is sufficient, and one does not need to include higher side-bands. In our system the leading stabilizing effect is due to self ZF interaction. Moreover, in real systems, the importance of ZF-MF interaction against ZF-ZF interaction would be determent by ZF/MF energy balance.

The paper is organized as follows. In Sec. 2.4 we introduce simple modulation instability theory of ZF/DW to derive the linear growth rate ($\gamma = \kappa W_{DW}$) in Eq. (2.1). In Sec. 2.5 we extend the results of Sec. 2.4 for the case of finite ZF amplitude by taking into account the second order sidebands. This allows us to estimate saturation amplitude Eq. (2.2) and nonlinear damping coefficient ($\alpha = \gamma_{NL}/W_{ZF}$). We provide a summary of the manuscript results in Sec. 2.6.

2.4 Drift waves-zonal flows interactions in Hasegawa-Mima model

To derive the coupling coefficient (κ_0 in Eq. (2.3)) from modulational instability theory we use Fourier decomposition of the standard Hasegawa-Mima equation [61]:

$$D_k(\omega)\phi_k(\omega) + \sum_{k=k'+k''} B_{k',k''}\phi_{k'}(\omega')\phi_{k''}(\omega'') = 0, \tag{2.4a}$$

$$D_k(\omega) = -i\omega(1 + \rho_s^2 k^2) + i\mathbf{V}_* \cdot \mathbf{k}, \tag{2.4b}$$

$$B_{k',k''} = \frac{c\rho_s^2}{B_0}(\hat{\mathbf{z}} \cdot \mathbf{k}' \times \mathbf{k}'')(k'^2 - k''^2), \tag{2.4c}$$

where ϕ_k - Fourier transform of electrostatic potential corresponding to $e^{i(\mathbf{k}\cdot\mathbf{x}-\omega t)}$ mode (here and later ω - dependence is omitted for convenience), $\mathbf{V}_* = V_*\hat{\mathbf{y}}$ - electron diamagnetic drift velocity, ρ_s - gyroradius, c - speed of light, B_0 - stationary magnetic field.

The nonlinear part of Eq. (2.4) is a sum of 3-wave interactions. The linear stage of zonal

flow instability is obtained by truncating nonlinear part of Eq. (2.4) and including only the primary drift wave $(\omega, \mathbf{k})$ mode, the zonal flow $(\Omega, \mathbf{q})$ mode and two sidebands $(\Omega \pm \omega, \mathbf{q} \pm \mathbf{k})$ modes. The fact that electrostatic potential is observable physical quantity implies this constrain which we will use later

$$\phi_j^* = \phi_{-j}, \quad \mathbf{k}_{-j} = -\mathbf{k}_j.$$

Then, the electrostatic potential is represented in the form

$$\phi(t, \mathbf{r}) = (\Phi_k^\omega + \text{C. C.}) + \Phi_q^\Omega + \Phi_{q+k}^{\Omega+\omega} + \Phi_{q-k}^{\Omega-\omega}, \tag{2.5}$$

where

$$\Phi_k^\omega = \phi_k e^{-i\omega t + i\mathbf{k}\cdot\mathbf{r}}.$$

Basically the truncation (2.5) is a first-order perturbation expansion with ZF amplitude as a small parameter $(\phi_q \ll \phi_k)$. This is true because side-bands amplitude is proportional to the ZF amplitude or more generally $|\phi_{nq+k}| \sim |\phi_q|^n$. To obtain the dispersion equation for the ZF in this limit, we substitute the truncated form of the electrostatic potential (2.5) in the equation (2.4). Thus, evolution equations for ϕ_q and $\phi_{q\pm k}$

$$D_q \phi_q + B_{k,q-k}\phi_k\phi_{q-k} + B_{-k,q+k}\phi_{-k}\phi_{q+k} = 0, \tag{2.6}$$

$$D_{q\pm k}\phi_{q\pm k} + B_{\pm k,q}\phi_{\pm k}\phi_q = 0, \tag{2.7}$$

where

$$D_q = -i\Omega(1 + \rho_s^2 q^2),$$

$$D_{q\pm k} = -i\left[(\Omega \pm \omega) - \mathbf{V}_* \cdot (\mathbf{q} \pm \mathbf{k}) + \rho_s^2(\Omega \pm \omega)(\mathbf{q} \pm \mathbf{k})^2\right],$$

$$B_{\pm k,q} = \pm\frac{c\rho_s^2}{B_0}\hat{\mathbf{z}} \cdot \mathbf{k} \times \mathbf{q}(k^2 - q^2).$$

In the leading order, the primary wave amplitude does not change, giving the linear dispersion equation for drift wave $(D_k = 0)$

$$\omega = \frac{V_* k_y}{1 + \rho_s^2 k^2}. \tag{2.8}$$

Eliminating sidebands amplitudes $(\phi_{q\pm k})$ from Eqs. (2.6,2.7), we have

$$D_q = |\phi_k|^2 \left[\frac{B_{k,q-k}B_{-k,q}}{D_{q-k}} + \frac{B_{-k,q+k}B_{k,q}}{D_{q+k}}\right], \tag{2.9}$$

where

$$B_{\pm k, q \mp k} = \frac{c\rho_s^2}{B_0} \hat{\mathbf{z}} \cdot \mathbf{k} \times \mathbf{q}(2\mathbf{q} \cdot \mathbf{k} \mp q^2).$$

The explicit form of the dispersion equation can be written as

$$[\Omega (1 + Q) - qV_{gx}]^2 = \left[\omega Q - \frac{\Omega}{\omega} qV_{gx}\right]^2 - 2\omega_{ci}^2 \left|\frac{e\phi_k}{T_e}\right|^2 k_y^2 q^4 (k^2 - q^2)\rho_s^8 K, \qquad (2.10)$$

where

$$V_{gx} = -\frac{2\omega\rho_s^2 k_x}{1 + \rho_s^2 k^2}, \quad Q = \frac{q^2\rho_s^2}{1 + k^2\rho_s^2}, \quad K = \frac{1 + \rho_s^2 k^2 + \rho_s^2 q^2 - 4\rho_s^2 k_x^2}{(1 + \rho_s^2 q^2)(1 + \rho_s^2 k^2)^2},$$

and $\omega_{ci} = eB_0/m_i c$ - ion gyrofrequency, m_i - ion mass, e - electron charge, T_e - electron temperature.

In the long wavelength limit ($k\rho_s \ll 1$ and $q\rho_s \ll 1$) and when $\mathbf{q} \cdot \mathbf{k} = 0$ the solution to Eq. (2.10) have a simple form

$$\Omega^2 = q^4\rho_s^4 \left(\omega^2 - 2\left|\frac{e\phi_k}{T_e}\right|^2 k^4 c_s^2 \rho_s^2\right). \qquad (2.11)$$

This equation shows that the zonal flow instability occurs for a sufficiently large amplitude of the primary drift wave (see Malkov and others [89, 5, 90])

$$\left|\frac{e\phi_k}{T_e}\right| > \frac{1}{kL_n}, \qquad (2.12)$$

where L_n is a scale of density change ($L_n = n_0/|\nabla n_0| \sim c_s\rho_s/V_*$), and $c_s = T_e/m_i$ - ion sound velocity. Note that the amplitude threshold in Eq. (2.11) is somewhat equivalent to the linear damping term γ_{damp} in Eq. (2.1). It is interesting that the threshold amplitude of the unstable primary wave is of the order of the mixing length amplitude.

2.5   Effects of finite amplitude of zonal flow

The leading order of perturbation expansion of ZF frequency (growth rate) Eq. (2.11) does not depend on the ZF amplitude. In this section we derive this dependence with second-order perturbation expansion. The second-order term is a nonlinear self damping of ZF (the third term in Eq. (2.1)). To do so, we are extending the model from Sec. 2.4 by including second

order sidebands $(\pm 2\mathbf{q} \pm \mathbf{k})$

$$
\begin{aligned}
\phi(t, \mathbf{r}) =& (\Phi_k^\omega + \text{C. C.}) + (\Phi_q^\Omega + \text{C. C.}) \\
&+ (\Phi_{q+k}^{\Omega+\omega} + \text{C. C.}) + (\Phi_{q-k}^{\Omega-\omega} + \text{C. C.}) + \Phi_{2q+k}^{2\Omega+\omega} + \Phi_{2q-k}^{2\Omega-\omega}.
\end{aligned}
\tag{2.13}
$$

It is worth noting that the main assumption $(\phi_q \ll \phi_k)$ still holds as we omitted higher order sidebands (e.g. $\pm 3\mathbf{q} \pm \mathbf{k}$). Repeating the procedure from Sec. 2.4, the dispersion equation is obtained as

$$
\begin{aligned}
D_q =& |\phi_k|^2 \left[\frac{B_{k,q-k} B_{-k,q}}{D_{q-k}} + \frac{B_{-k,q+k} B_{k,q}}{D_{q+k}} \right] + \\
&+ |\phi_q|^2 |\phi_k|^2 \left[\frac{B_{-q+k,2q-k} B_{k,-q} B_{q-k,q} B_{q,-k}}{D_{-q+k} D_{2q-k} D_{q-k}} + \frac{B_{-q-k,2q+k} B_{-k,-q} B_{q+k,q} B_{q,k}}{D_{-q-k} D_{2q+k} D_{q+k}} \right],
\end{aligned}
\tag{2.14}
$$

where

$$
\begin{aligned}
D_{2q+k} &= D_{q+k}(\Omega \to 2\Omega, \mathbf{q} \to 2\mathbf{q}), \\
B_{\pm k, -q} &= -B_{\pm k, q} = \mp \frac{c\rho_s^2}{B_0} \hat{\mathbf{z}} \cdot \mathbf{k} \times \mathbf{q}(k^2 - q^2), \\
B_{q, q\pm k} &= \frac{c\rho_s^2}{B_0} \hat{\mathbf{z}} \cdot \mathbf{k} \times \mathbf{q}(2\mathbf{q} \cdot \mathbf{k} \pm k^2), \\
B_{-q\pm k, 2q\mp k} &= \frac{c\rho_s^2}{B_0} \hat{\mathbf{z}} \cdot \mathbf{k} \times \mathbf{q}(2\mathbf{q} \cdot \mathbf{k} \mp 3q^2).
\end{aligned}
$$

The Eq. (2.14) differs from simplified version Eq. (2.9) by the additional part which is quadratic in respect to ZF amplitude $(|\phi_q|)$. The last bracket of Eq. (2.14) resembles "α" Landau constant which implies that the sign of the term in the last bracket governs saturation while the ratio of the terms in the first and second brackets defines the saturation amplitude. The explicit dispersion equation is cumbersome in this limit, so we leave only main terms in $\Omega, \mathbf{q}$ - Taylor series. This is justified because zonal flow does not exist in linear limit $(\Omega_{lin} = 0)$ and is induced only via nonlinear interactions with drift waves, so $\Omega \ll \omega$ and $q \ll k$.

$$
\Omega = \frac{2\omega_{ci}^2 \Omega \left| \frac{e\phi_k}{T_e} \right|^2 q^4 k_y^2 (k^2 - q^2) \rho_s^8 K}{\left(\omega Q - \frac{\Omega}{\omega} q V_{gx} \right)^2 - (\Omega(1 + Q) - q V_{gx})^2} + \frac{\omega_{ci}^4 \left| \frac{e\phi_k}{T_e} \right|^2 \left| \frac{e\phi_q}{T_e} \right|^2 q^6 k_y^4 k^4 \rho_s^{14} [\Omega M - q V_{gx} L]}{(\Omega - q V_{gx})^4},
\tag{2.15}
$$

where

$$
M = \frac{(16 k_x^2 k^2 \rho_s^4 - \rho_s^2 (1 + \rho_s^2 k^2)(3k^2 + 4k_x^2))}{(1 + \rho_s^2 q^2)(1 + \rho_s^2 k^2)^4}, \quad L = \frac{\rho_s^2 (k^2 - 4k_x^2)}{(1 + \rho_s^2 q^2)(1 + \rho_s^2 k^2)^3}.
$$

As before, we consider the long wavelength limit and the case when ZF propagate perpendicular to the primary wave ($\mathbf{q} \cdot \mathbf{k} = 0$). In this situation, the solution of (2.15) simplifies significantly. Considering the primary wave above the threshold (Eq. 2.11), one writes:

$$(\Omega_{\pm}/\omega_{ci})^2 = -\left|\frac{e\phi_k}{T_e}\right|^2 k^4 q^4 \rho_s^8 \pm \sqrt{\left|\frac{e\phi_k}{T_e}\right|^4 k^8 q^8 \rho_s^{16} - 3\left|\frac{e\phi_q}{T_e}\right|^2 \left|\frac{e\phi_k}{T_e}\right|^2 k^{10} q^6 \rho_s^{16}}. \qquad (2.16)$$

The solution with negative sign (corresponding to the ZF instability) can be expanded giving

$$(\Omega_{-}/\omega_{ci})^2 \simeq -2\left|\frac{e\phi_k}{T_e}\right|^2 k^4 q^4 \rho_s^8 + \frac{3}{2}\left|\frac{e\phi_q}{T_e}\right|^2 k^6 q^2 \rho_s^8. \qquad (2.17)$$

This equation shows that finite amplitude ϕ_q results in stabilization of ZF instability. The amplitude of stabilized ZF is of the order

$$\left|\frac{e\phi_q}{T_e}\right|_{max} \sim \frac{q}{k}\left|\frac{e\phi_k}{T_e}\right|. \qquad (2.18)$$

Strictly speaking, this value is at the limit of applicability of the perturbation expansion ($\phi_q \ll \phi_k$). However taking into account that $q \ll k$, the Eq. (2.18) yields the main assumption $\phi_q \ll \phi_k$. Thus, one can expect that the above estimate is still valid as an order of magnitude estimate. In Eq. (2.18) regime, ZF dynamics becomes oscillatory (with $\Re(\Omega) \neq 0$) which is common in numerical ZF simulations.

It was pointed out by Manfredi [90] that at some point the amplitude of DW is starting to decrease resulting in saturation of ZF growth. It is possible to estimate ZF amplitude using these considerations (see J. Anderson et al [5]). However this effect will be important when the amplitude of ZF is comparable to DW amplitude ($|\phi_q| \sim |\phi_k|$) and is not considered in our paper. Simulation results that J. Anderson et al [5] used to support their estimate, that $\phi_q \gamma_q$ grows as ϕ_k^2 – agrees with our results because γ_q growth as ϕ_k, so ϕ_q grows as ϕ_k as in Eq. (2.18).

2.6 Summary

In this article, we discussed the evolution of zonal flow in the framework of the drift wave turbulence model described by Hasegawa-Mima equation. Within the qualitative picture of the predator-prey model, Eq. (2.1), zonal flow dynamics is governed by the competition of

the zonal instability and nonlinear saturation. The focus of our work was on the derivation of nonlinear damping term via direct perturbation theory.

The dispersion of drift waves results in the amplitude threshold in Eq. (2.11) effectively equivalent to the linear damping term in zonal flow model equation (2.1). The nonlinear damping of zonal flow (the last term in Eq. (2.1)) was obtained by expanding the coupling to higher order, Eq. (2.3), by including effects of finite amplitude of ZF. Nonlinear dispersion equation for zonal flow instability (2.15) was derived. It is shown that in the long wavelength limit, the nonlinear effects stabilize zonal flow growth. The estimate for the maximum ZF amplitude was obtained (2.18).

It is understood that ZF is important in the Dimits shift [44] formation process. Thus, one can envisage that the stabilization mechanism due to a finite amplitude of ZF flow may be operative and shift the instability boundary. However, it is really speculative, since we do not consider the really unstable modes (such as ITG) mode. Our model is based on the Hasegawa-Mima equation, for the conditions of the tokamak, the zonal flow with $m = 0$, will not follow the Boltzmann distribution for ions, so the Hasegawa-Mima equation should be modified [116]. That analysis has to be modified [116] and the $k^2\rho^2$ will be different (smaller) see [116, 90].

Acknowledgments

Chapter 3

Anomalous electron mobility and inverse energy cascade in partially magnetized plasmas with crossed ExB fields

3.1   Introduction

As discussed in Chapter 1, partially magnetized plasmas support a type of drift waves which is different from the standard drift waves in fully magnetized plasmas (e.g., described by the Hasegawa-Mima equation). Such waves, the so-called anti-drift waves [52], or Hall drift waves, as they are called in this thesis, together with ion sound and lower hybrid waves are the basic waves that define the turbulent behavior of partially magnetized plasmas such as Hall thrusters.

Experimental studies show that Hall thrusters are in turbulent state exhibiting a wide range of oscillations [21, 33]. Anomalous electron current was also studied in a number of experiments and numerical simulations; however, the exact nature of fluctuations and anomalous current remain poorly understood. Most of the existing first principle simulations are based on the full kinetic PIC method [1] and thus are unable to model the full discharge due to excessive computational requirements even for modern computers.

A fluid approach, such as developed in this thesis, allows faster simulations and better insight into the underlying physical phenomena. In this thesis, we present nonlinear simulations from first principle of the anomalous current due to wave turbulence in partially magnetized plasmas. Our work is among first few (along with Ref [51]) in the field which predict, from fluid theory, the level of anomalous current generally consistent with experi-

mental values [115].

Hall truster plasmas demonstrate fluctuations in a wide range of frequencies $1\,\text{kHz} - 1\,\text{GHz}$ of waves [33], including the slow azimuthal oscillations (10-25) kHz [69, 47, 31, 103, 69, 47], also known as spokes. The spoke is an azimuthally rotating structure of high density, so it emits in the visible range. It is accompanied by fluctuations in electron density and electrostatic potential [69]. As a result, the presence of the spoke strongly affects the anomalous current in Hall thrusters and much of the anomalous current passes through the spoke region [46]. The velocity of the spoke is much smaller than the $\mathbf{E} \times \mathbf{B}$ drift velocity of electrons, thus it is not directly the electron rotation and ion inertia plays an important role. Linear instabilities typically have growth rates higher for short wavelength (i.e., high $m \gg 1$ modes have larger growth rates [115], where m is azimuthal mode number). At the same time, the spoke has low mode number $m = 1, 2, 3$. Thus, it cannot be explained as a simple linear instability and its nature remains unknown.

It was suggested that spokes originate from small-scale turbulence driven by the density gradient via an inverse energy cascade [115]. The example of the inverse energy cascade in fully magnetized plasmas was considered in Chapter 2 where the formation of large-scale zonal flows from small-scale drift waves was discussed. In this chapter, we present evidence for inverse energy cascade and formation of large scale nonlinear structures (c.f., zonal flow) in partially magnetized plasma turbulence driven by a density gradient [115] which supports a possible spoke formation mechanism from small-scale turbulence.

3.2 Reduced fluid model and the spectra of linear instabilities

We use the reduced fluid model derived in Section 1.7.1 which was first proposed in Ref [115] to describe the nonlinear interaction of Hall drift waves. Two-dimensional slab geometry perpendicular to the magnetic field is used. The equilibrium electric field $\mathbf{E}_0$ and equilibrium ions velocity $\mathbf{V}_{i0}$ are along the $\hat{\mathbf{x}}$ axis. The equilibrium electron velocity ($\mathbf{E} \times \mathbf{B}$ drift $\mathbf{V}_{e0}$) is

along the $\hat{\mathbf{y}}$ axis. Thus, the reduced model can be written as

$$(\partial_t + v_0\partial_x)n = (n_0 + n)\nabla^2\chi + \nabla n \cdot \nabla\chi, \tag{3.1}$$

$$(\partial_t + v_0\partial_x)\chi = c_s^2\frac{e\phi}{T_e} + \frac{1}{2}(\nabla\chi)^2, \tag{3.2}$$

$$(\partial_t + u_0\partial_y)\eta = -n_0 v_d\partial_y\frac{e\phi}{T_e} - \nu(\eta - n) + v_{T_e}\rho_e\left\{\frac{e\phi}{T_e}, \eta\right\}, \tag{3.3}$$

$$\eta = n + \rho_e^2\left(n_0\nabla^2\frac{e\phi}{T_e} - \nabla^2 n\right), \tag{3.4}$$

where $v_0 = |\mathbf{V}_{i0}|$ is the ion equilibrium speed, $u_0 = |\mathbf{V}_{e0}|$ is the electron equilibrium speed, $v_d = v_{T_e}\rho_e/L_n$ is the diamagnetic drift speed, $n = \tilde{n}_e = \tilde{n}_i$ is the density perturbation, and tildes in the perturbation terms (i.e., n, χ, ϕ, η) were omitted for convenience. The density gradient effect on ions was neglected because its effect is negligible in comparison with the ion equilibrium flow. Finally, the Laplacian was integrated out from the ion Euler equation.

The first step to study the reduced model is a local linear approximation. Therefore, we neglect nonlinear terms and assume monochromatic response ($\sim e^{-i\omega t + i\mathbf{k}\cdot\mathbf{x}}$). The dispersion equation follows

$$\frac{c_s^2 k^2}{(\omega - v_0 k_x)^2} = \frac{v_d k_y + \rho_e^2 k^2(\omega - u_0 k_y + i\nu)}{\omega - u_0 k_y + \rho_e^2 k^2(\omega - u_0 k_y + i\nu)}. \tag{3.5}$$

The dispersion equation (3.5) was first discovered in Ref [115] and analyzed in detail. Here we note that equation (3.5) is a combination of the Simon-Hoh instability [111, 63] (the excitation of a low frequency anti-drift mode $\omega = k^2 c_s^2/v_d k_y$ by the equilibrium electron flow u_0) with a low hybrid mode $\omega = \omega_{LH} = \sqrt{\omega_{ce}\omega_{ci}}$ and an ion sound mode $\omega = kc_s$. In this text, we call those waves Hall drift waves.

In this chapter we will use typical Hall thruster parameters which in dimensionless form are $\nu = 0.28\omega_{LH}$, $v_0 = 3.72c_s$, $L_n = 48.8\rho_e$, $\sqrt{m_i/m_e} = 427$, $u_0 = 241.8c_s$. Using these parameters, a solution to the dispersion equation (3.5) is shown in Figure 3.1a. The figure clearly shows strong instabilities with growth rate $\gamma = Im(\omega) \sim 4\omega_{LH}$ driven by the density gradient.

Figure 3.1a hides another instability which appears due to electron collisions with neutrals and an ion equilibrium flow. This is a weak axial instability for $k_y = 0$, with growth rate shown in Figure 3.2. An in-depth analysis of this instability is left for Chapter 4. Here, we

(a) $v_0 = 3.72c_s$, $\nu = 0.28\omega_{LH}$ **(b)** $v_0 = 0$, $\nu = 0$
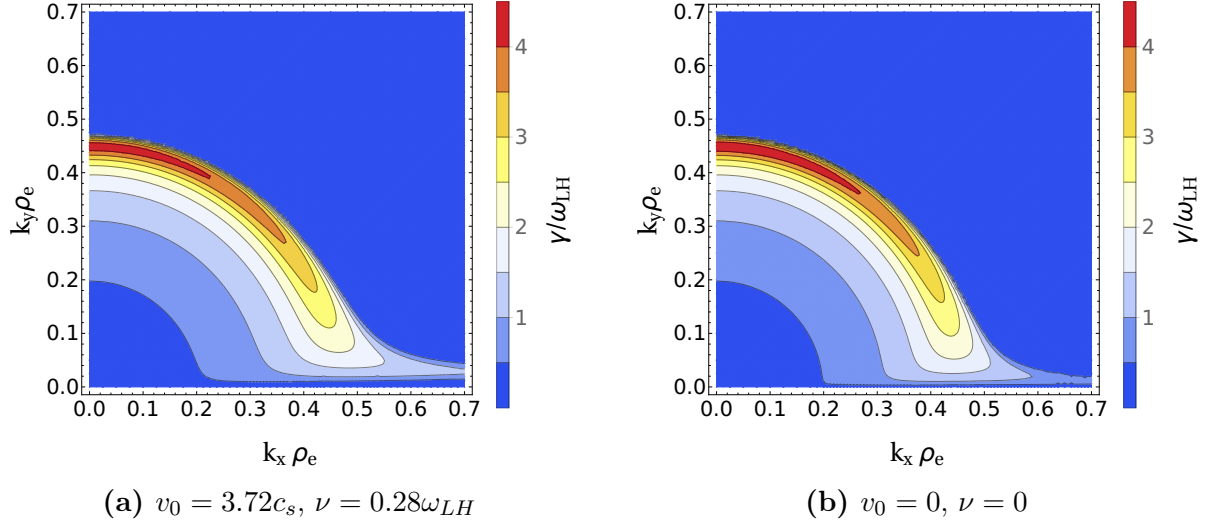
Figure 3.1: Solution to the dispersion equation (3.5) with parameters $L_n = 48.8\rho_e$, $\sqrt{m_i/m_e} = 427$, $u_0 = 241.8c_s$.

proceed by neglecting ions axial flow ($v_0 = 0$, which is the case for Penning trap devices) and electron-neutral collisions ($\nu = 0$). The structure of the Hall drift waves instability is not significantly affected by this approximation as shown in Figure 3.1b. As will be discussed later in Chapter 6, the nonlinear dynamics of gradient driven/axial instabilities interactions is relevant only for time scales larger than considered in this chapter. Therefore, we study nonlinear structures and inverse energy cascade separately from the axial instability and the full system will be considered in Chapter 6.
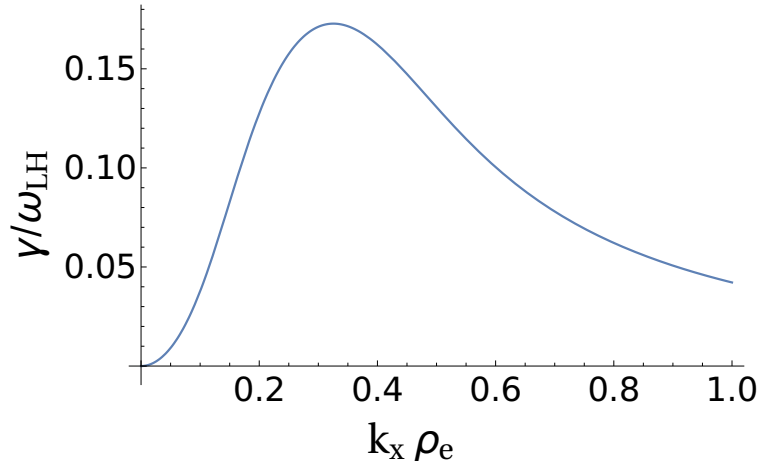
Figure 3.2: Solution to the dispersion equation (3.5) along the axial direction $k_y = 0$ with parameters $\nu = 0.28\omega_{LH}$, $v_0 = 3.72c_s$, $L_n = 48.8\rho_e$, $\sqrt{m_i/m_e} = 427$, $u_0 = 241.8c_s$.

3.3 Results of nonlinear simulations

We perform nonlinear simulations with the aid of the fluid simulation framework BOUT++ [45] to investigate the nonlinear dynamics of Hall drift waves. The system (3.1)-(3.4) is supplied with periodic boundary conditions (PBC). The PBC in the azimuthal direction is natural, but for the axial direction, it is an approximation which simplifies the study of nonlinear dynamics. Next, the system is modified with the addition of artificial hyperviscosity, which is chosen not to disrupt the linear spectrum of Hall drift wave instabilities. The artificial hyperviscosity is a standard technique to avoid spectral blocking; i.e., energy accumulation in short wavelength modes ($k\Delta x \sim 1$ were Δx is a spatial discretization step size) [15]. Benchmark tests of the linear spectrum were performed and confirm the growth rates shown in Figure 3.1b with an error under 10%.

We monitor the evolution of a turbulence state with the quantities

$$E_n = \sqrt{\frac{1}{L_x L_y} \int \left(\frac{n}{n_0}\right)^2 dxdy}, \qquad E_\eta = \sqrt{\frac{1}{L_x L_y} \int \left(\frac{\eta}{n_0}\right)^2 dxdy}, \tag{3.6}$$

where L_x, L_y are system sizes in x and y dimensions respectively and the integration is performed over the whole spatial domain. Their evolution is shown in Figure 3.3 where we can clearly see the linear phase $n \ll n_0$ where amplitudes grow exponentially consistent with the maximum growth rate $\gamma = 4.43\omega_{LH}$ predicted from linear theory in Figure 3.1b. When the wave amplitudes are comparable to the equilibrium profiles, $n \sim n_0$, linear growth slows down due to nonlinear effects; then, a saturation level is reached.

Azimuthal turbulent fluctuations result in the axial electron current

$$I_e \sim \left\langle \widetilde{n}_e \widetilde{E}_{azimuthal} \right\rangle, \tag{3.7}$$

where angular brackets $<,>$ indicate spatial average, $\widetilde{n}_e$ is a turbulent density fluctuation and $\widetilde{E}_{azimuthal}$ is a turbulent electric field fluctuation in the azimuthal direction. We use the simulations to measure the anomalous axial electron current density, which occurs due to the $E \times B$ drift from a turbulent electric field in the azimuthal direction $-\partial_y \phi$

$$j_e = -en\frac{c\partial_y \phi}{B_0}, \tag{3.8}$$
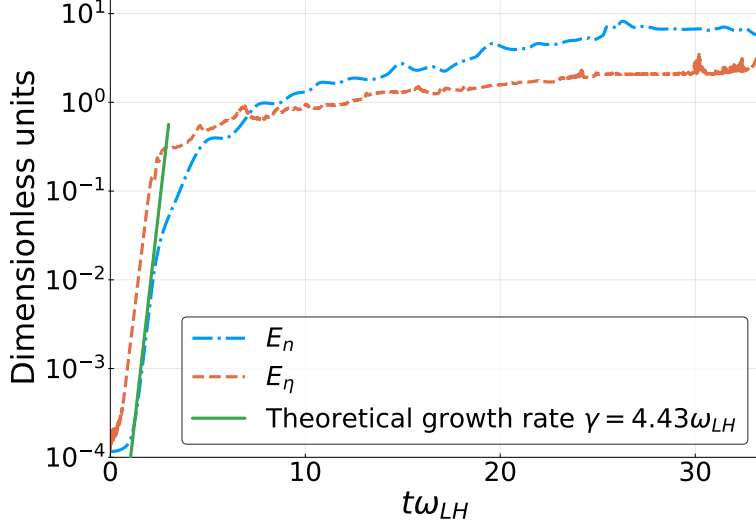
Figure 3.3: Time evolution of (3.6) with parameters $\nu = 0$, $v_0 = 0$, $L_n = 48.8\rho_e$, $\sqrt{m_i/m_e} = 427$, $u_0 = 241.8c_s$.

where B_0 is the equilibrium magnetic field. The computed axial anomalous currents are shown in Figure 3.4, where current is averaged in space

$$J_e = \frac{1}{L_x L_y} \int j_e dxdy, \tag{3.9}$$

and measured in units of classical current J_ν with collisional conductivity

$$\sigma_\nu = \frac{e^2 n_0 \nu}{m_e \omega_{ce}}, \tag{3.10}$$

where we used typical value of collision frequency $\nu = 0.28\omega_{LH}$; however, in the simulation, collisions are absent, $\nu = 0$. Notice that at the time when nonlinear dynamics become important ($n \sim n_0$, $t\omega_{LH} \sim 2.6$), current is enhanced by two orders of magnitude above the classical current.

Next, we analyze the time evolution of the generalized vorticity spatial profiles and its spectrum. The simulation was initialized with the sum of test waves and, after a short time, only unstable modes remain relevant. In Figure 3.5 the spatial profile and its spectrum for normalized generalized vorticity η/n_0 are shown at time when the most unstable modes are exponentially growing in the linear phase. The spectrum is in full agreement with analytical theory shown in Figure 3.1b.

After some time, when nonlinear terms become relevant, linear modes interact with each other and produce other modes. The beginning of the nonlinear stage is shown in Figure 3.6

49
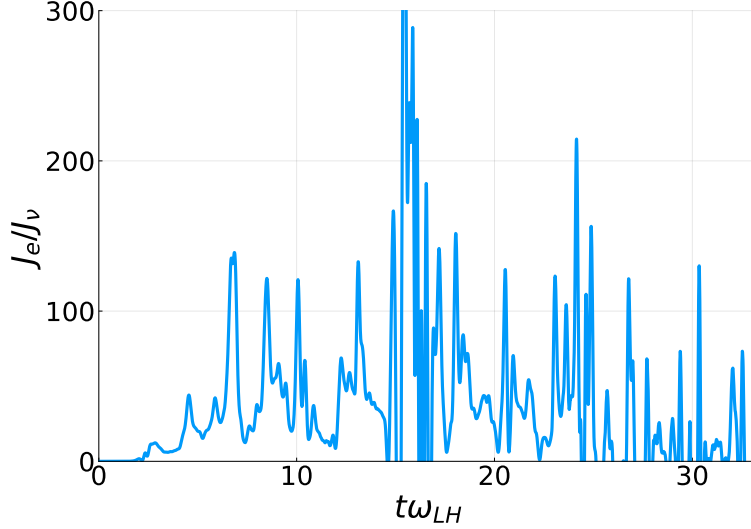
Figure 3.4: Anomalous axial electron current in units of classical collisional current with parameters $\nu = 0, \quad v_0 = 0, \quad L_n = 48.8\rho_e, \quad \sqrt{m_i/m_e} = 427, \quad u_0 = 241.8c_s$. The current was smoothed with window function of order 30.

at the time $t\omega_{LH} = 2.6$ when linear modes are still dominant, but nonlinear interactions significantly modify the plasma dynamics.

The nonlinear evolution continues and, at some point, a strong shear azimuthal flow appears as shown in Figure 3.7. At that stage, energy cascades into large structures (small k) as shown in the spectrum.

The strong azimuthal shear flow reverses direction and eventually forms vortices as shown in Figure 3.8. Vortices are large-scale structures (as well as flows) and are the evidence of the inverse energy cascade. The large shear flows are analogous to zonal flow in fully magnetized plasmas discussed in Chapter 2. Vortices can stay for some extended time $t\omega_{LH} \sim 1$, and then again collapse back into the shear flow which then again forms vortices. As shown in sequential snapshots, Figures 3.9, 3.10. At a later time, the biggest possible vortex (i.e., the size of the simulation box) is formed (see Figure 3.11) and energy can no longer flow into smaller k and saturation is reached. The biggest vortex still can collapse into the shear flow and form again.

50

(a) Spatial profile

(b) Spectrum
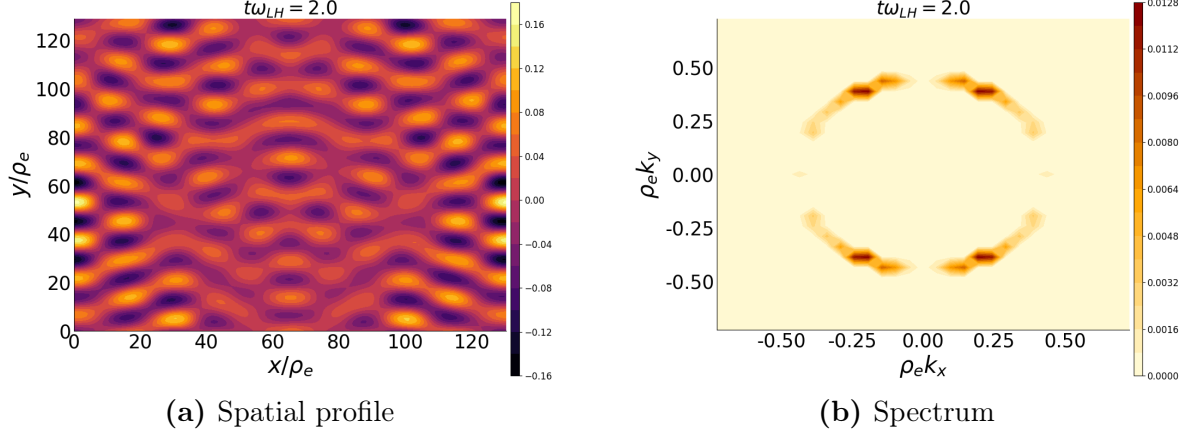
Figure 3.5: Normalized generalized vorticity η/n_0 spatial and spectral profiles at time $t\omega_{LH} = 2.0$ — linear stage. Parameters are $\nu = 0$, $v_0 = 0$, $L_n = 48.8\rho_e$, $\sqrt{m_i/m_e} = 427$, $u_0 = 241.8c_s$.

(a) Spatial profile

(b) Spectrum
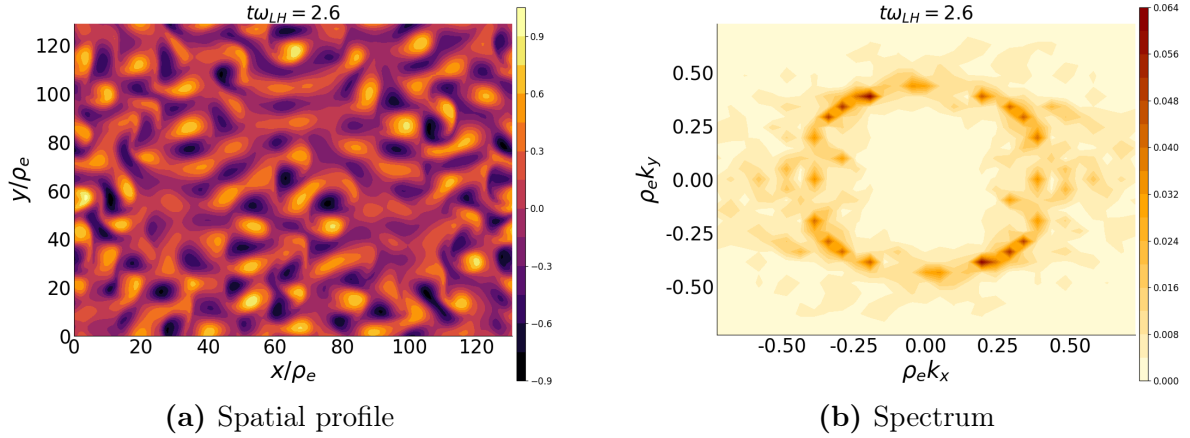
Figure 3.6: Normalized generalized vorticity η/n_0 spatial and spectral profiles at time $t\omega_{LH} = 2.6$ — beginning of nonlinear stage. Parameters are $\nu = 0$, $v_0 = 0$, $L_n = 48.8\rho_e$, $\sqrt{m_i/m_e} = 427$, $u_0 = 241.8c_s$.

3.4 Summary

The nonlinear reduced fluid model, proposed in [115], describes the nonlinear evolution of partially magnetized plasma systems such as Hall thrusters. The model predicts strong linear instabilities of Hall drift waves (a combination of anti drift and low hybrid modes), with a growth rate $\gamma \sim 4.43\omega_{LH}$ and a weak axial instability with growth rate $\gamma \sim 0.17\omega_{LH}$ for typical Hall thruster parameters ($\nu = 0.28\omega_{LH}, v_0 = 3.72c_s, L_n = 48.8\rho_e, \sqrt{m_i/m_e} = 427, u_0 = 241.8c_s$). The former modes are destabilized due to strong equilibrium electron $E \times B$ flow u_0 and density anisotropy L_n, while the later modes are unstable due to strong equilibrium

(a) Spatial profile

(b) Spectrum
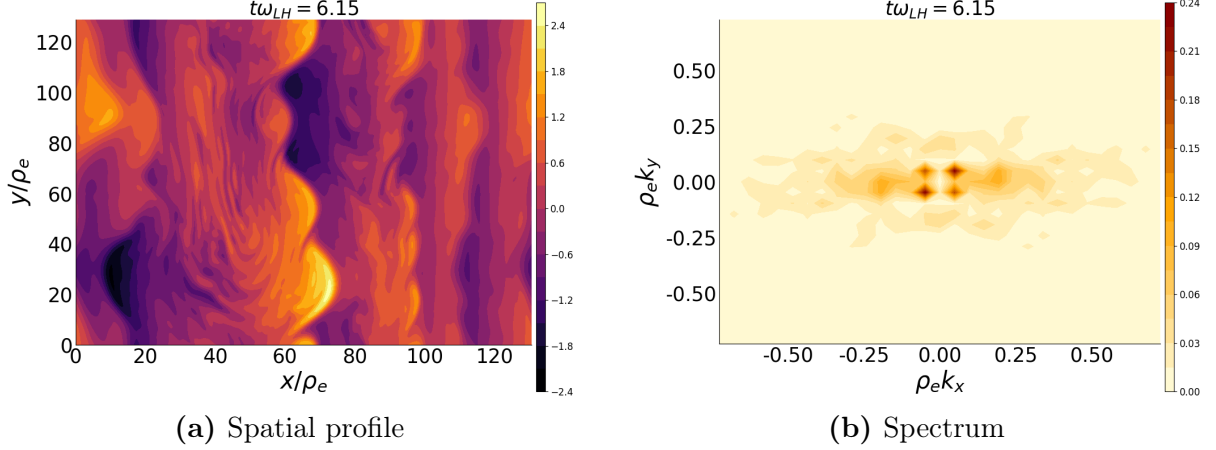
Figure 3.7: Normalized generalized vorticity η/n_0 spatial and spectral profiles at time $t\omega_{LH} = 6.15$ — nonlinear phase and formation of shear. Parameters are $\nu = 0$, $v_0 = 0$, $L_n = 48.8\rho_e$, $\sqrt{m_i/m_e} = 427$, $u_0 = 241.8c_s$.

ion flow v_0 and electron-neutral collisions ν. For the purpose of this chapter, axial modes were artificially neglected ($v_0 = 0, \nu = 0$) and the nonlinear dynamics of Hall drift waves were studied numerically. Simulations were performed with the aid of the fluid simulation framework BOUT++. The linear phase of simulations was shown to be in perfect agreement with linear theory (growth rate and spectrum structure). The simulations showed that in the nonlinear phase, the Hall drift wave turbulence produces anomalous axial electron current which exceeds typical values for current due to electron-neutral collisions by at least two orders of magnitude. This occurs in conjunction with the formation of shear azimuthal flows which are similar phenomena to zonal flows in fully magnetized plasmas. Counterstreaming flows tend to form large vortices (similar to the Kelvin-Helmholtz instability) which can stay for long periods of time ($t\omega_{LH} \sim 1$). The spectrum of flows and vortex formations have dominant energy residing in small wave numbers which supports the existence of the inverse energy cascade. Finally, nonlinear saturation is reached when the biggest possible vortex is formed (size of the simulation box).

(a) Spatial profile

(b) Spectrum
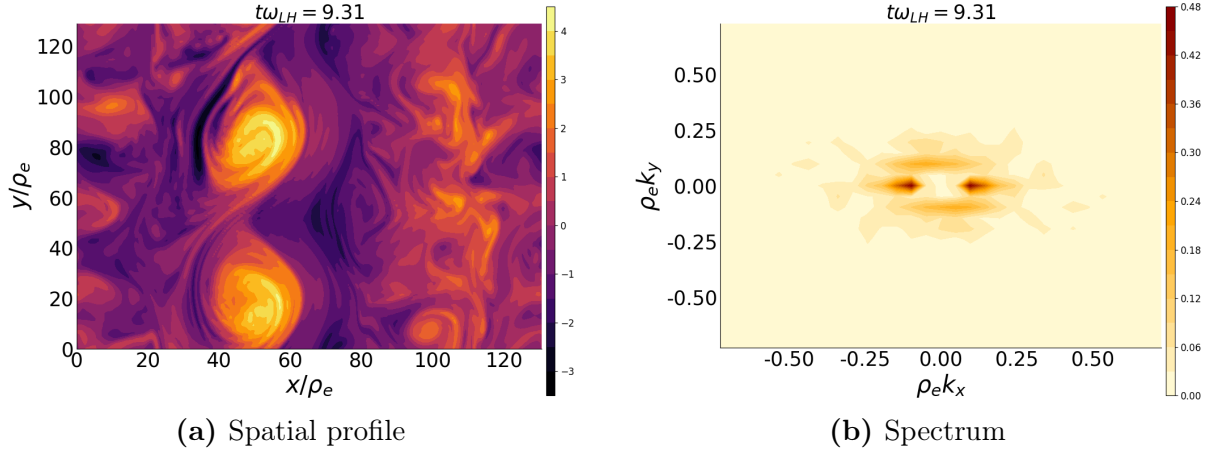
Figure 3.8: Normalized generalized vorticity η/n_0 spatial and spectral profiles at time $t\omega_{LH} = 9.31$ — nonlinear phase and formation of vortices. Parameters are $\nu = 0$, $v_0 = 0$, $L_n = 48.8\rho_e$, $\sqrt{m_i/m_e} = 427$, $u_0 = 241.8c_s$.

(a) Spatial profile

(b) Spectrum
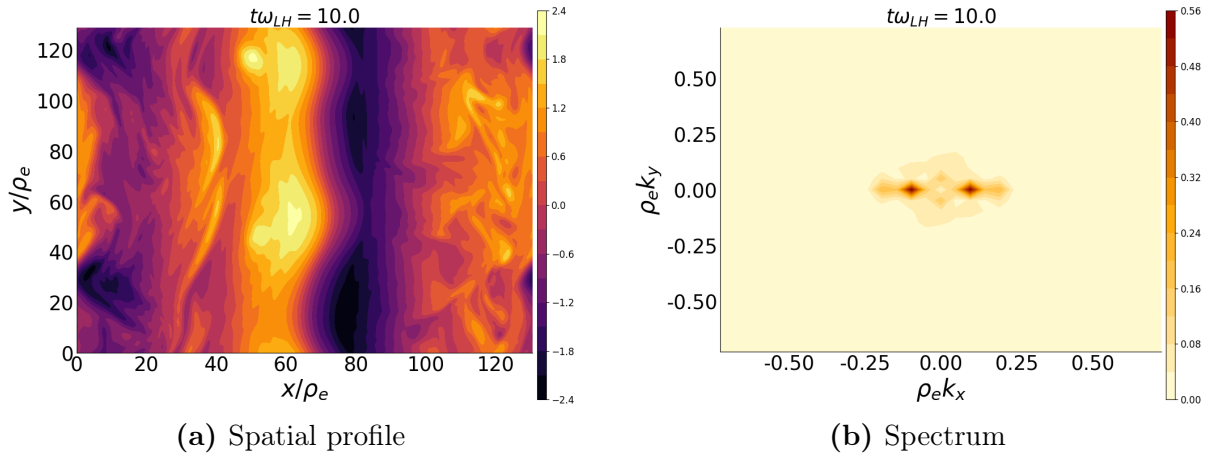
Figure 3.9: Normalized generalized vorticity η/n_0 spatial and spectral profiles at time $t\omega_{LH} = 10$ — nonlinear phase and formation of shear flow. Parameters are $\nu = 0$, $v_0 = 0$, $L_n = 48.8\rho_e$, $\sqrt{m_i/m_e} = 427$, $u_0 = 241.8c_s$.

(a) Spatial profile

(b) Spectrum
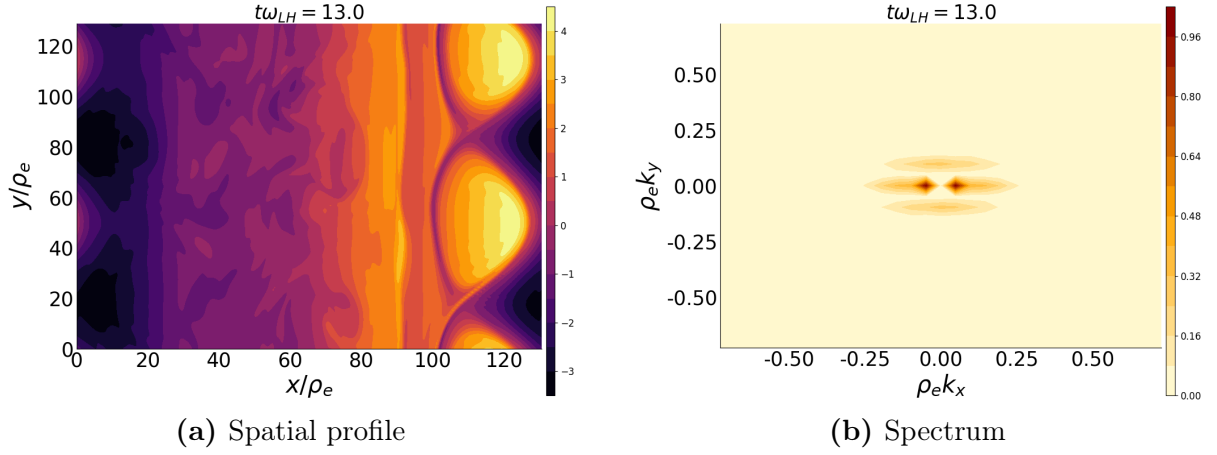
Figure 3.10: Normalized generalized vorticity η/n_0 spatial and spectral profiles at time $t\omega_{LH} = 13$ — nonlinear phase and formation of vortices. Parameters are $\nu = 0$, $v_0 = 0$, $L_n = 48.8\rho_e$, $\sqrt{m_i/m_e} = 427$, $u_0 = 241.8c_s$.

(a) Spatial profile

(b) Spectrum
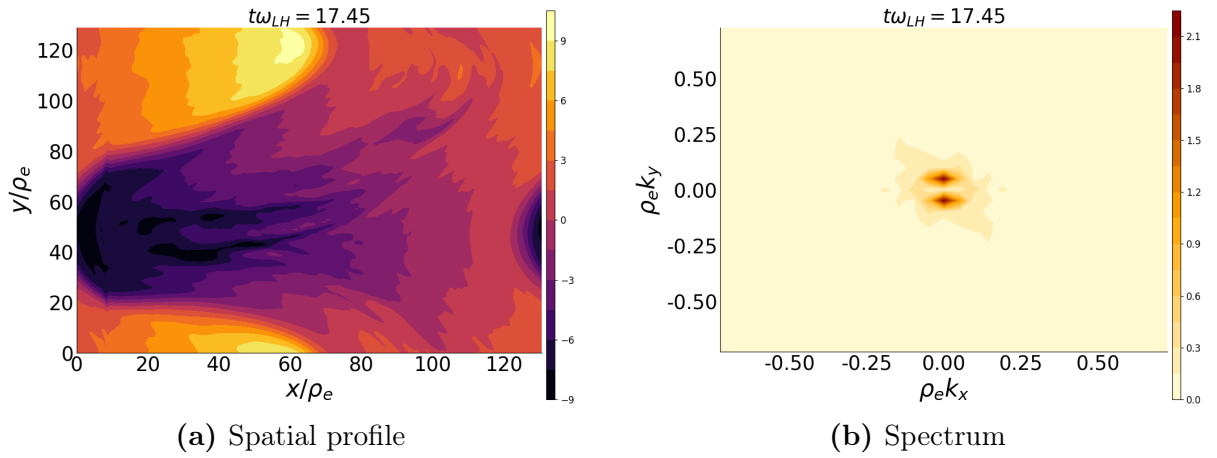
Figure 3.11: Normalized generalized vorticity η/n_0 spatial and spectral profiles at time $t\omega_{LH} = 17.45$ — nonlinear phase and formation of vortices. Parameters are $\nu = 0$, $v_0 = 0$, $L_n = 48.8\rho_e$, $\sqrt{m_i/m_e} = 427$, $u_0 = 241.8c_s$.

Chapter 4

Current flow instability and nonlinear structures in dissipative two-fluid plasmas

4.1 Preface

In the previous Chapter, we have considered the waves and instabilities driven by the electron $\mathbf{E} \times \mathbf{B}$ flow in presence of density gradient and electron-neutral collisions. In many $\mathbf{E} \times \mathbf{B}$ systems, an external electric field results in ion acceleration and thus to the stationary ion beam flow. For the geometry of the Hall thrusters, this flow is in the axial direction. This flow, which was neglected in Chapter 3, provides an additional source of free energy and thus results in axial mode instabilities. The linear and nonlinear regimes of these instabilities due to the equilibrium axial ion flow and axial electron transport (e.g. due to electron-neutral collisions) are studied in this chapter. The material in this chapter is based on the paper published in Physics of Plasmas [78].

4.2 Abstract

The current flow in two-fluid plasma is inherently unstable if plasma components (e.g. electrons and ions) are in different collisionality regimes. A typical example is a partially magnetized $\mathbf{E} \times \mathbf{B}$ plasma discharge supported by the energy released from the dissipation of the current in the direction of the applied electric field (perpendicular to the magnetic field). Ions are not magnetized so they respond to the fluctuations of the electric field ballistically on the inertial time scale. On the contrary, the electron current in the direction of the applied electric field is dissipative supported either by classical collisions or anomalous processes. The

instability occurs due to a positive feedback between electron and ion current coupled by the quasi-neutrality condition. The theory of this instability is further developed taking into account the electron inertia, finite Larmor radius, and nonlinear effects. It is shown that this instability results in highly nonlinear quasi-coherent structures resembling breathing mode oscillations in Hall thrusters.

4.3   Introduction

Systems away from the equilibrium naturally evolve back toward the equilibrium state by compensating the deviation from the equilibrium. In plasmas which support many different wave eigenmodes, the deviations from the equilibrium often result in the development of various instabilities. The nature of such instabilities depends on the type of plasma state and its deviation from the equilibrium. One class of instabilities results from the non-equilibrium which can be characterized by gradients in the velocity space, e.g. plasma-beam instabilities or instabilities due to plasma pressure anisotropy [95]. The non-equilibrium states with relative streaming of electrons and ions are often unstable too. Buneman type instabilities [18] occurs due to the relative motion of electron and ions in the collisionless plasma. In strongly collisional plasmas, the electron drift gives the Farley-Buneman instability [20, 48]. Simon-Hoh type instabilities (both collisional [111, 63] and collisionless version [107, 51, 115]) result from the relative motion of electrons and ions in crossed electric and magnetic fields $\mathbf{E} \times \mathbf{B}$. The Simon-Hoh instability is typically studied for modes propagating in the direction of the $\mathbf{E} \times \mathbf{B}$ drift and typically require a density gradient (and/or magnetic field gradient [51, 115]) for the excitation.

Here we discuss the axial instability of the modes along the direction of the current flow. Essentially, instabilities of this type were considered in Refs. [24, 49]. The basic instabilities in Refs. [24, 49] exist in neglect of the electron inertia. The resistive instability of the lower-hybrid mode which requires the electron inertia (but no density gradient) considered in Ref. [87] can also be referred as the current flow instability of this type. Such instabilities occur due to the phase shift in the response of electrons and ions to the quasi-neutral perturbation of the electric field. In this paper, we consider the axial flow instability in conditions

typical of $\mathbf{E} \times \mathbf{B}$ discharge such as in Hall thrusters and magnetrons. In this case, the axial current is due to the dissipative flow of the electrons and the flow of accelerated ions; both in the direction of the externally applied electric field. We consider the linear and nonlinear regimes of this instability and show that it results in nonlinear quasi-coherent structures. It was earlier suggested [24] that this instability mechanism plays an important role in breathing mode oscillations [99].

4.4   Instability mechanism

Most simply the mechanism can be described on the example of the current flow in the $\mathbf{E} \times \mathbf{B}$ device such as Hall thruster. Consider the configuration supported by the electric current in axial direction (along z) due to the electric field $\mathbf{E} = E\hat{\mathbf{z}}$ applied across the magnetic field. We generally characterize the electron current in z direction in the form $J_e = \sigma E$, where σ can be simply collisional electron conductivity across the magnetic field, $\sigma_c = e^2 n_0 \nu_{en} / (m_e \omega_{ce}^2)$, or some anomalous conductivity which may include as well the effects of near wall conductivity [99]. In the rest of the paper, we do not specify the mechanism of the electron transport, generally parameterizing it with σ (or ν introduced later). The ion current $J_i = en v_i$ is supported by free streaming of unmagnetized ions. We consider quasi-neutral oscillations so that

$$\frac{\partial}{\partial z} \left(J_e + en v_i \right) = 0. \tag{4.1}$$

The dynamics of unmagnetized ions is described by standard equations

$$\frac{\partial}{\partial t} n + \frac{\partial}{\partial z} \left(n v_i \right) = 0, \tag{4.2}$$

$$\frac{\partial}{\partial t} v_i + v_i \frac{\partial}{\partial z} v_i = \frac{e}{m_i} E. \tag{4.3}$$

Linearizing equations (4.1)-(4.3) for perturbations (denoted by tilde) in the form $\left(\tilde{n}, \tilde{E}, \tilde{v}_i, \tilde{J}_e \right) \sim \exp\left(-i\omega t + kz \right)$, and taking into account that ions have the equilibrium velocity v_{i0}, one easily finds the dispersion relation

$$\frac{1}{(\omega - kv_{0i})^2} = \frac{i}{\omega} \frac{\sigma m_i}{e^2 n_0}. \tag{4.4}$$

57

The right hand side of the dispersion equation can also be written as

$$\frac{\sigma m_i}{e^2 n_0} = \frac{\nu}{\omega_{LH}^2},\tag{4.5}$$

where $\omega_{LH}^2 = \omega_{ce}\omega_{ci}$, and ν is either the frequency of the electron-neutral collisions, or parametrization of combined effects of anomalous collisions and near-wall conductivity. This dispersion relation was obtained in Ref. [24] by using kinetic theory for ions and later in Ref [49] from the fluid model.

The axial modes described by the dispersion relation (4.4) are unstable due to the phase shift between the perturbed electron and ion currents, which can be seen from these expressions

$$\widetilde{J}_e = \sigma \widetilde{E},\tag{4.6}$$

$$\widetilde{J}_i = \frac{e^2 n_0}{m_i} \frac{i\omega}{(\omega - kv_{i0})^2} \widetilde{E}.\tag{4.7}$$

The delay introduced by the finite ion flow results in the positive feedback loop leading to the amplification of the initial perturbation. In absence of the flow $v_{i0} = 0$, the dispersion relation (4.4) describes a damped mode with

$$\omega = -i\frac{\omega_{LH}^2}{\nu}.\tag{4.8}$$

However, in the presence of large equilibrium flow velocity, $kv_{i0} > \omega$, one has the negative-diffusion-type instability. From the equation (4.4), the growth rate scales with wave vector as $\gamma \approx \nu k^2 v_{i0}^2/\omega_{LH}^2$ for small $kv_{0i} \ll \omega_{LH}^2/\nu$ and as $\gamma \approx \omega_{LH}\sqrt{kv_{i0}/(2\nu)}$ for large $kv_{0i} \gg \omega_{LH}^2/\nu$. These asymptotics are valid for small $k\rho_e \ll 1$ but for larger values $k\rho_e \sim 1$ other effects become important as discussed in the following sections. The solution to (4.4) is shown in Figure 4.1a.

4.5 Mode stabilization at short wave-lengths due to the effects of diffusion, inertia and finite Larmor radius

The instability with $\gamma \sim k^2$ (or $\sim \sqrt{k}$) in combination with nonlinear effects may produce the explosive growth of the perturbations. However the unlimited growth rate (with k) is
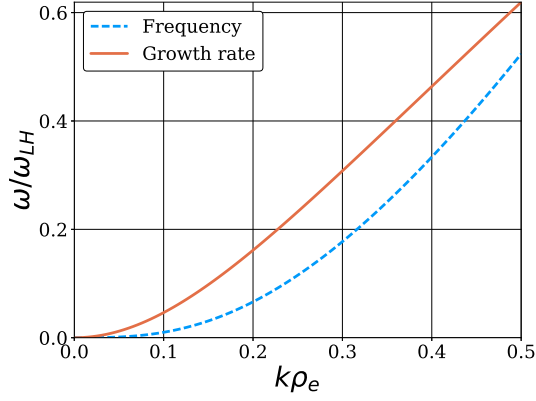
(a) Simplest electron transport model $J_e = \sigma E$, $\gamma \sim k^2$, Eq. (4.4)
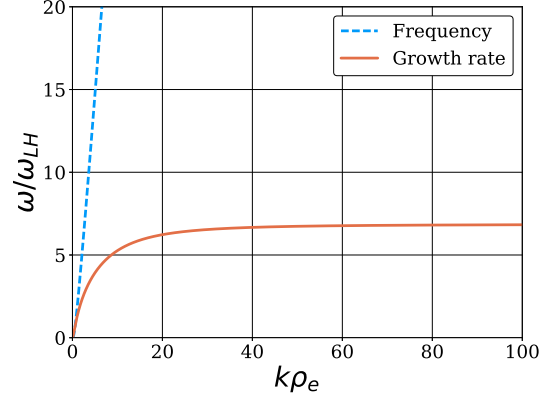
(b) Eq. (4.11) with electron diffusion
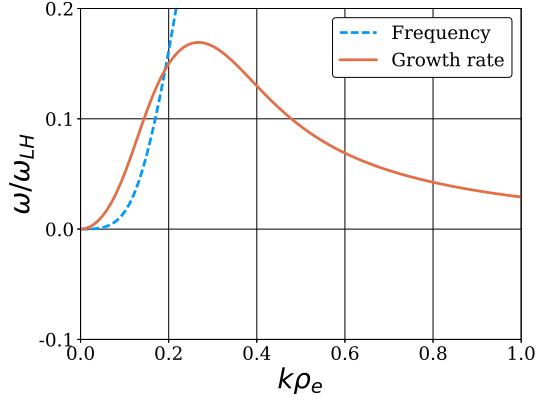
(c) Eq. (4.13) with diffusion, inertia and FLR
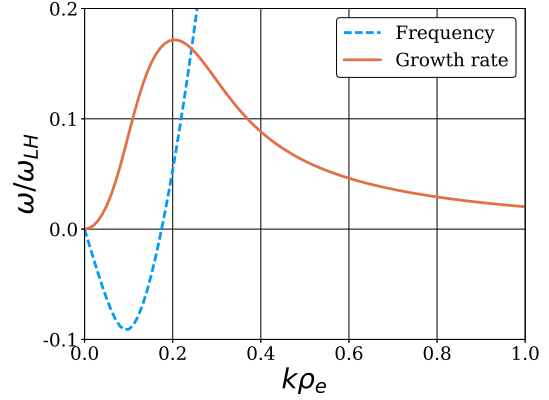
(d) Eq. (4.14) with diffusion, inertia, FLR and finite electron velocity

Figure 4.1: Solution to dispersion equations (4.4), (4.11), (4.13), (4.14) for different electron transport models are shown for typical Hall truster parameters: $v_{i0} = 4.45\omega_{LH}\rho_e$, $v_{e0} = -1.33\omega_{LH}\rho_e$, $\nu = 0.25\omega_{LH}$.

unphysical and it also presents a problem in numerical simulations because the instability will occur at the largest possible wave-vectors ($k_{max} \sim 1/\Delta x$, where Δx is the smallest resolution length scale, e.g., mesh size). This will result in piling up of the energy at the smallest resolution length scale. Therefore the simulation results will never converge to a single solution. It is therefore important to incorporate physics which is relevant on smaller scales thus limiting the growth at large wave-vectors. One of such effects is the diffusion flux which was first added in Ref [49]. Effects of the diffusion can be included via the pressure driven electron current in the generalized Ohm's law

$$J_e = \sigma E + eD\frac{\partial n}{\partial z},$$
(4.9)

where

$$D = \nu \rho_e^2.$$
(4.10)

Once again, the ν should be understood either as the classical electron-neutral, near-wall or anomalous collisional frequency. Repeating the derivations in (4.1)-(4.3) one can get the following dispersion equation which takes into account both electron mobility and diffusion

$$\frac{1}{(\omega - kv_{0i})^2} = \frac{i\nu}{\omega_{LH}^2 \left(\omega + i\nu k^2 \rho_e^2\right)}.$$
(4.11)

The solution of this equation is shown in Figure 4.1b. One can see from (4.11), that the diffusion does not stabilize high $k\rho_e$ completely, but limits the mode growth at the constant level

$$\gamma \approx \frac{\omega_{LH}(v_{0i} - \omega_{LH}\rho_e)}{2\nu\rho_e}.$$
(4.12)

Therefore it is important to incorporate higher order effects such as electron inertia and related effects of the electron finite Larmor radius (FLR) effect which bring in the lower-hybrid modes [36, 87]. These effects may be included following the derivations in Ref. [115]. The respective equation that includes the electron inertia, mobility, diffusion and FLR reads

$$\frac{1}{(\omega - kv_{0i})^2} = \frac{(\omega + i\nu)}{\omega_{LH}^2 \left[\omega + k^2\rho_e^2 \left(\omega + i\nu\right)\right]}.$$
(4.13)

The solution to the above equation is shown in Figure 4.1c, which shows that electron inertia and FLR effects stabilize the modes for high $k\rho_e$. It is important to note that the electron

inertia and FLR effects alone (without electron transport $\nu = 0$) do not make the system unstable.

Our derivations so far have fully neglected the effect of the equilibrium electron velocity. It can be easily included in the consideration, resulting in the dispersion equation

$$\frac{1}{(\omega - kv_{0i})^2} = \frac{(\omega - kv_{0e} + i\nu)}{\omega_{LH}^2 \left[\omega - kv_{0e} + k^2\rho_e^2 (\omega - kv_{0e} + i\nu)\right]}. \tag{4.14}$$

The results for the final dispersion equation (4.14) is shown in Figure 4.1d. Note that in absence of dissipation this equation describes stable lower-hybrid modes modified by the Doppler shift and the effects of the finite electron Larmor radius [115]. The addition of the electron equilibrium velocity results in the Doppler shift kv_{0e} in the electron response which has a significant impact on the real part of the frequency of unstable modes: for v_{0e} has the opposite sign to the v_{0i}, the account of the equilibrium electron flow reduces the phase velocity of unstable modes and may even result in the change of the sign of the phase velocity.

The final dispersion equation (4.14) depends on three important parameters: ion equilibrium velocity v_{0i}, electron equilibrium velocity v_{0e}, and electron collision frequency ν (classical or anomalous). Therefore, to complete the physical picture of effects discussed in this section, we demonstrate how external parameters change the frequency and growth rate of the unstable mode. The effect of collisional frequency is shown in Figure 4.2a,4.2b where we varied the parameter from typical Hall thruster classical value $\nu \approx 0.1\omega_{LH}$ up to the anomalous $\nu = 2.5\omega_{LH}$. One can see that the increase of the collision frequency enhances the linear instability and moves the most unstable wavenumber to the shorter wavelengths. At larger values, the collisions suppress the instability, as shown in Figures 4.2c,4.2d. It is worth noting that results for high (anomalous) collisionality $\nu \gg \omega_{LH}$, should be viewed as the illustration of a general trend rather than a quantitative description of the nonlinear effects (anomalous mobility). Though the often used Bohm diffusion would correspond to anomalously high values of the electron collision frequency (as large as ω_{ce}), the form of the nonlinear (anomalous) mobility and its proper parametrization is still unknown at this time.

Next, we investigate the effects of the ion equilibrium velocity, which is shown in Figure 4.3. To see the effect more clearly, the electron equilibrium velocity was set to zero. The ion flow velocity enhances the instability moving the maximum growth rate to the longer

61

(a) Frequency

(b) Growth rate

(c) Frequency

(d) Growth rate

Figure 4.2: Solution to the dispersion equations (4.14) for different values of electron collision frequency ν and typical Hall truster parameters: $v_{i0} = 4.45\omega_{LH}\rho_e$, $v_{e0} = -1.33\omega_{LH}\rho_e$.

wavelengths where the effects of a finite length of the system may become important [71, 76]. We will employ the correct boundary conditions in the next section.

The experimental data indicate [98] that typically the electron flow is a fraction of the ion flow ($v_{0e} \approx -(0.3 \div 0.5)v_{0i}$). The larger values of the equilibrium electron flow shifts the maximum of the growth rate toward the longer wavelengths and also reversing the phase velocity to the negative direction for the most unstable modes, as is shown in Figure 4.4.

4.6 Nonlinear evolution and structures

The linear theory described in the previous section predicts axial flow instability with a maximal growth rate which is determined by the competition of the instability and stabilizing

(a) Frequency

(b) Growth rate
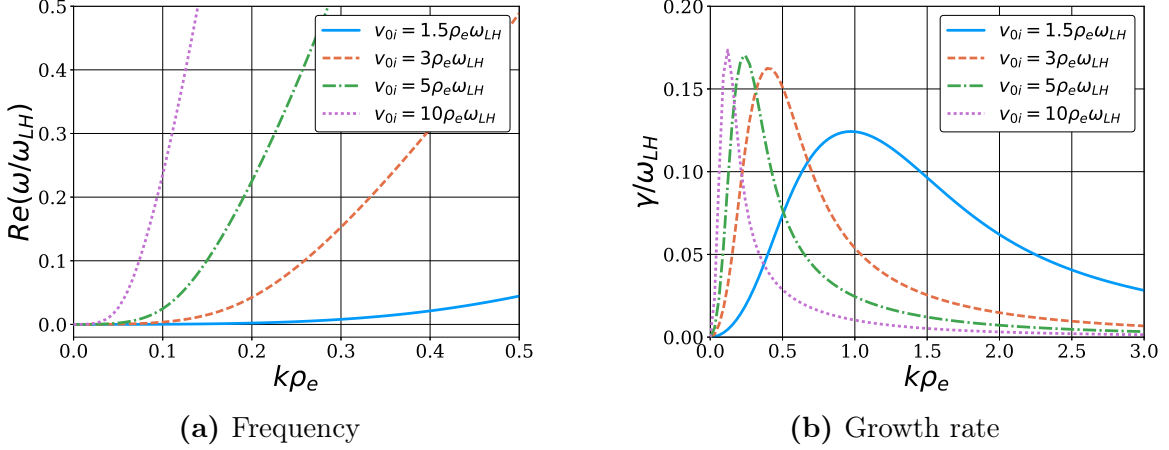
Figure 4.3: Solution to the dispersion equations (4.14) for different values of equilibrium ion velocity, zero equilibrium electron velocity and collision frequency $\nu = 0.25\omega_{LH}$.

effects of the diffusion, inertia and FLR effects. To investigate the nonlinear evolution of these modes we perform nonlinear simulations using the model which was developed in Ref [115] and includes the nonlinear equations for ion density (continuity) and velocity in addition with the electron dynamics equation. In one dimensional case the nonlinear ion continuity and momentum balance equations (4.2)-(4.3) have the form

$$\left(\frac{\partial}{\partial t} + v_{0i}\frac{\partial}{\partial z}\right)\widetilde{n} = n_0\frac{\partial^2\widetilde{\chi}}{\partial z^2} + \widetilde{n}\frac{\partial^2\widetilde{\chi}}{\partial z^2} + \frac{\partial\widetilde{n}}{\partial z}\frac{\partial\widetilde{\chi}}{\partial z}, \tag{4.15}$$

$$\left(\frac{\partial}{\partial t} + v_{0i}\frac{\partial}{\partial z}\right)\widetilde{\chi} = \frac{e}{m_i}\widetilde{\phi} + \frac{1}{2}\left(\frac{\partial\widetilde{\chi}}{\partial z}\right)^2, \tag{4.16}$$

where the potential was introduced for the ion velocity $\widetilde{v}_i = -\partial\widetilde{\chi}/\partial z$. The electron transport model includes the electron diffusion, inertia and FLR. In the Boussinesq approximation the electron dynamics is linear and described by the equation

$$\left(\frac{\partial}{\partial t} + v_{0e}\frac{\partial}{\partial z}\right)\widetilde{\eta} = -\nu(\widetilde{\eta} - \widetilde{n}), \tag{4.17}$$

with the electron generalized vorticity defined as

$$\widetilde{\eta} = \widetilde{n} + n_0\rho_e^2\frac{\partial^2}{\partial z^2}\left(\frac{e\widetilde{\phi}}{T_e} - \frac{\widetilde{n}}{n_0}\right). \tag{4.18}$$

Typical Hall thruster axial length is around $L \sim (25 \div 100)\rho_e$, therefore for modes with the wave number $k\rho_e \approx 0.1$ the realistic boundary conditions are important. We use boundary

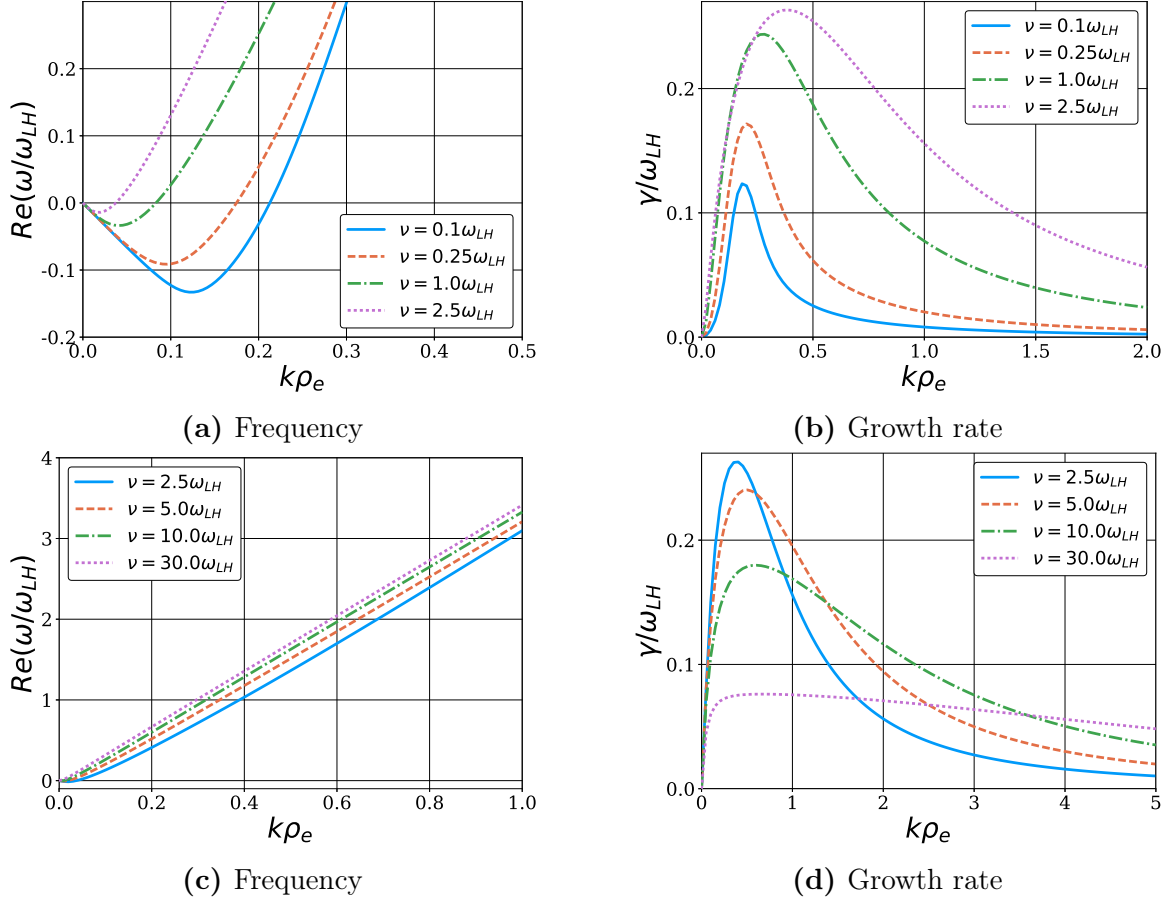**(a)** Frequency   **(b)** Growth rate
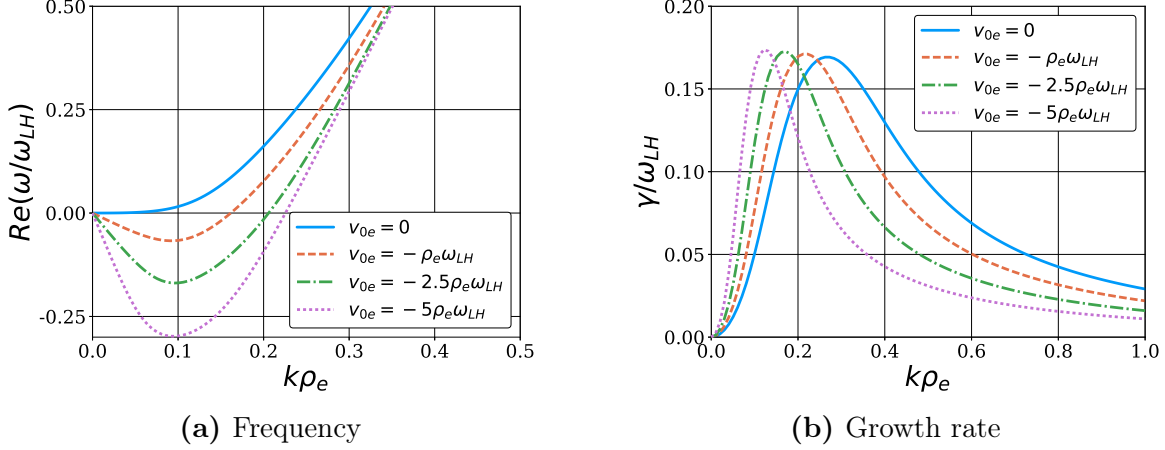
Figure 4.4: Solution to the dispersion equations (4.14) for different values of equilibrium electron velocity and typical Hall thruster parameters $v_{i0} = 4.45\omega_{LH}\rho_e$, $\nu = 0.25\omega_{LH}$.

conditions corresponding to the absence of perturbation at the left ($z = 0$) and open boundary at the right ($z = L$):

$$\widetilde{n}(0) = \widetilde{n}'(L) = \widetilde{\chi}(0) = \widetilde{\chi}'(L) = \widetilde{\eta}(0) = \widetilde{\eta}'(L) = \widetilde{\phi}(0) = \widetilde{\phi}(L) = 0, \tag{4.19}$$

where prime denotes spatial derivatives.

We performed the nonlinear simulations of the system (4.15)-(4.19) using the BOUT++ plasma fluid simulation framework [45], which was modified for the case of partially magnetized plasma [115] and extensively benchmarked. The nonlinear simulations are monitored with energy-like functionals

$$E_n = E\left[\frac{\widetilde{n}}{n_0}\right], \quad E_\eta = E\left[\frac{\widetilde{\eta}}{n_0}\right], \quad E_\phi = E\left[\frac{e\widetilde{\phi}}{T_e}\right], \tag{4.20}$$

with

$$E[f] = \sqrt{\frac{1}{L}\int_0^L dz|f(z)|^2}. \tag{4.21}$$

The time evolution of (4.20) is shown in Figure 4.5 for typical Hall truster parameters: $\nu = 0.25\omega_{LH}$, $v_{0i} = 4.45\omega_{LH}\rho_e$, $v_{0e} = -0.3v_{0i}$, $L = 106\rho_e$. One can see a distinct linear growth phase in the initial stage $t\omega_{LH} \sim 0 \div 70$. The maximum theoretical growth rate obtained from the equation (4.14) is shown in the Figure 4.5 by a purple solid line which shows a good agreement between theory and simulations. At later times $t\omega_{LH} \geq 70$, when

$E_n \sim E_\eta \sim 1$, nonlinear dynamics start to dominate and fluctuations saturate at constant values.
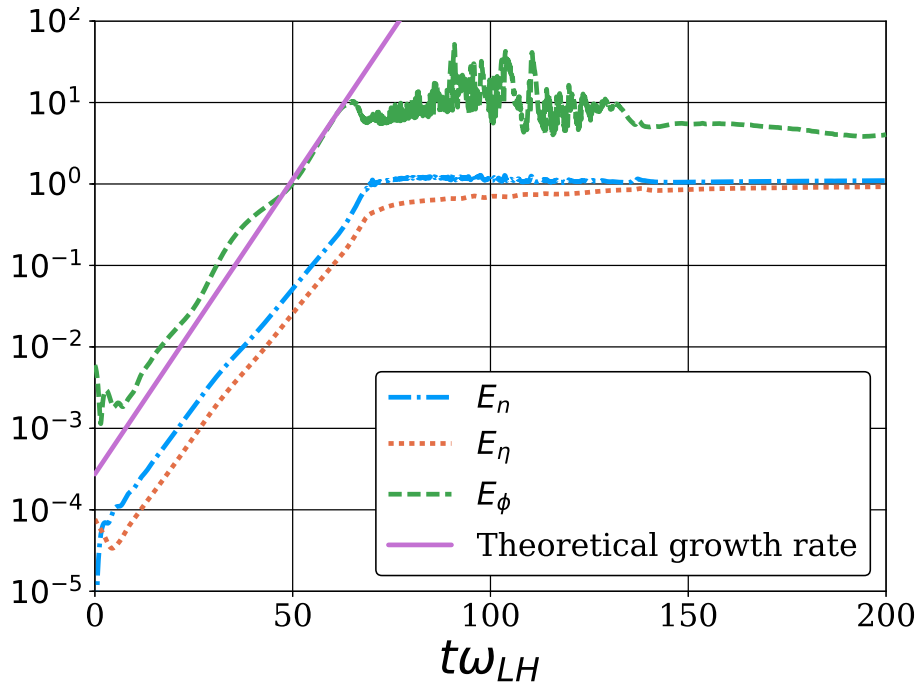
Figure 4.5: Dashed lines represent time evolution of energy like functionals (4.20) for parameters: $\nu = 0.25\omega_{LH}$, $v_{0i} = 4.45\omega_{LH}\rho_e$, $v_{0e} = -0.3v_{0i}$, $L = 106\rho_e$; purple solid line is a maximum theoretical growth rate obtained from the equation (4.14).

The evolution of density $\widetilde{n}$ and generalized electron vorticity $\widetilde{\eta}$ in time and space is shown in Figures 4.6,4.7. As shown in Figures 4.6, in the linear stage ($\widetilde{n}/n_0 \sim \widetilde{\eta}/n_0 \ll 1$) density and vorticity perturbations are growing and slowly moving to the right. This corresponds to the linear picture shown in Figure 4.1d where the most unstable modes have small positive phase velocity.

As amplitude fluctuations is increasing ($\widetilde{n}/n_0 \sim \widetilde{\eta}/n_0 \sim 1$) nonlinear effects become important resulting in formation of strongly nonlinear quasi-periodic waves, see Figs. 4.7. It is interesting to note that as the mode amplitude grows and nonlinear effects become more important, the velocity of nonlinear waves reduces and eventually becomes negative, so they start moving in opposite direction (to the left). This effect is attributed to the electron equilibrium flow, which is in the negative direction (to the left).

The nonlinear evolution in the case of zero electron flow $v_{0e} = 0$ is similar, with the exception that the velocity of nonlinear structures does not change the direction.

4.7   Conclusion

We have analyzed the axial instability of the current flow due to the phase shift in the electron and ion response to the perturbations of the electric field. This is a particular example of a general class of instabilities for the modes propagating along the direction of the current flow, which do not need density gradient as is required for Simon-Hoh instabilities [111, 63]. Dispersion relation similar to (4.4) was obtained in Ref. [24] where it was concluded that this instability is an important ingredient of breathing oscillations [13]. Similar dispersion equation was also obtained in Ref. [49] where the effects of the diffusion were added. As was noted in Ref. [24] the dispersion relation (4.4) is analogous to the one obtained in Ref. [87] for the resistive instability of the azimuthal modes driven by $\mathbf{E} \times \mathbf{B}$ flow.

Our model for the instability additionally includes the effects of electron inertia and finite Larmor radius which are important for the correct description of the modes at high k values.

It is important to note that the discussed instability occurs due to the phase shift between the inertial response of ions and dissipative electron response. The exact mechanism of electron current (classical collisional) or anomalous (turbulent) [59] is not so critical as long as the perturbations of the electron current are in phase with the electric field. Thus one can expect that this mechanism will be operative when the electron flow is anomalous and some scale/time separation exists between fast electron processes that determine anomalous transport and slow evolution of this instability.

The axial flow instability discussed in this paper has relatively low growth rate compared to azimuthal modes of higher frequencies which are driven by collisions and density gradients [51, 115]. Its significance, however, is in the high amplitude of the saturated modes. The mode saturation occurs due to ion dynamics resulting in appearance of high amplitude quasi-coherent structures resembling the cnoidal waves [35]. The theory of such highly nonlinear (non-perturbative) waves is described in Ref. [35]. The nonlinear coherent structures observed in our simulations appear to be an example of such large amplitude waves born out of the instability. The electron nonlinearity is weak as it appears in the higher order polarization drift and only for non-Boussinesq approximation. In this paper, we consider the Boussinesq approximation so the electron dynamics is linear while all explicit nonlinear

effects originate in ion dynamics. The electron inertia and FLR effects are important here as a mechanism of stabilization of the instability at large k (due to coupling to lower-hybrid dynamics).

It has been suggested [24] that the instability of this type is a crucial ingredient of breathing oscillations often observed in Hall thruster discharges supported by the axial electron current. Our basic model given by equations (4.1)-(4.3) is a subset of the full systems of equations typically considered for description of the breathing mode [100, 98, 99]. Our simulations show that the considered instability results in the formation of nonlinear quasi-coherent structures which are indeed similar to those observed in breathing mode [13, 8]. The slow moving coherent structures formed as a result of axial flow instability discussed here could also be the sources of non-monotonous profiles of the electric field observed experimentally in Ref. [123].

The finite velocity of ions plays a critical role in the axial current flow instability discussed in our paper. The characteristic time scale associated with ion velocity, $\omega \simeq v_i/L$, where L is the characteristic length is typically considered to be in the range of the so-called transit instabilities [9, 124], which have higher frequencies compared to the breathing oscillations. In our model, the real part of the unstable modes is considerably lower than $\omega \simeq v_i/L$, in part due to the inclusion of the electron flow velocity. One should note though that in present paper we consider the case of constant ion velocity v_{0i} , while in real configurations the effects of the axial dependence $v_{i0}(x)$ could be important [9, 124]. Consideration of this, a more general case, is left for future publication.

Acknowledgments

(a) Density
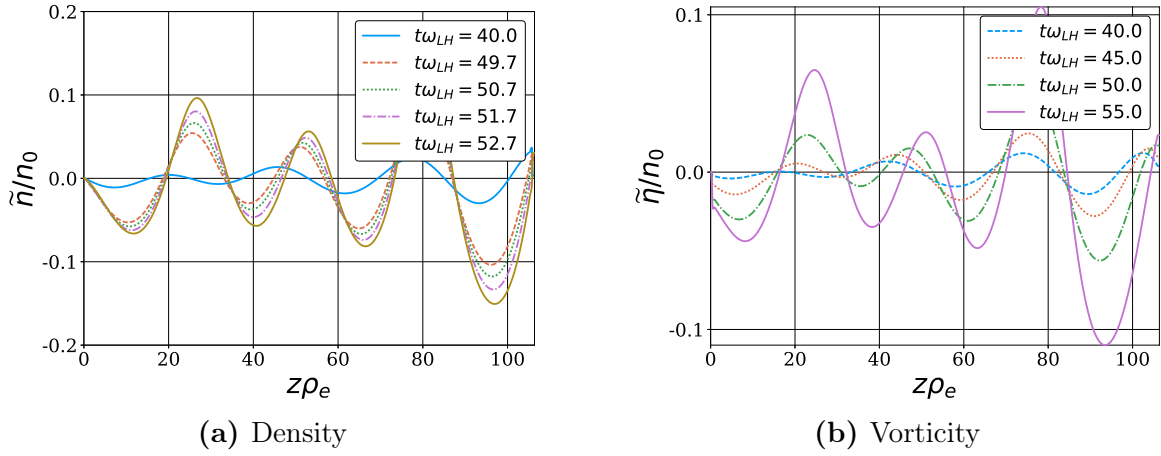
(b) Vorticity

Figure 4.6: Spatial profiles of density $\widetilde{n}$ and generalized vorticity $\widetilde{\eta}$ (linear dynamics).

(a) Density

(b) Vorticity

(c) Density
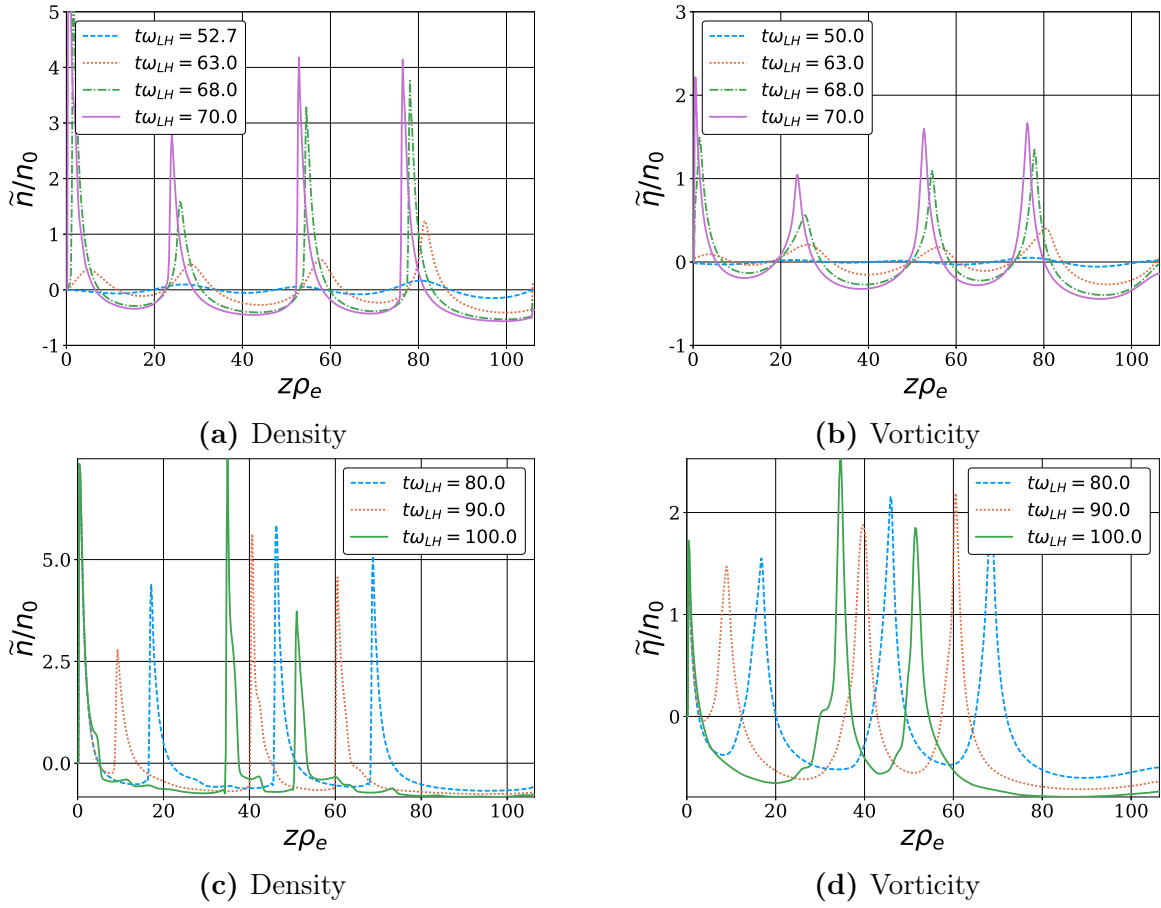
(d) Vorticity

Figure 4.7: Spatial profiles of density $\widetilde{n}$ and generalized vorticity $\widetilde{\eta}$ (nonlinear dynamics).

Chapter 5

Nonlinear structures of lower-hybrid waves driven by the ion beam

5.1 Preface

In Chapter 4 we have studied nonlinear dynamics of axial instabilities in partially magnetized plasmas caused by ion flow and electron cross-field current due to resistivity whilst neglecting the ion flow velocity. In a finite length system with boundaries, the ion beam may be a source of another instability due to coupling of negative and positive energy wave under reflection from the boundaries [76, 71]. In this chapter, we investigate the nonlinear dynamics of the axial instabilities in partially magnetized plasma caused by the ion flow and boundary effects. The material in this chapter is based on a paper submitted to Physics of Plasmas.

5.2 Abstract

The lower-hybrid waves can be driven unstable by the transverse ion beam in partially magnetized plasma of a finite length. This instability mechanism, which relies on the presence of fixed potential boundary conditions, is of particular relevance to axially propagating modes in Hall effect thruster. The linear and nonlinear regimes of this instability are studied here with numerical simulations. In the linear regime, our results agree with analytical theory. It is shown that in nonlinear regimes the mode saturation results in coherent nonlinear structures. For the aperiodic instability (with $Re(\omega) = 0$ — odd Pierce zones), the unstable eigen-function saturates into new stationary nonlinear equilibrium. In the case of oscillatory instability ($Re(\omega) \neq 0$ — even Pierce zones), the instability results in the nonlinear oscillat-

ing standing wave. It is also shown that finite Larmor radius effects stabilize instability for parameters corresponding to large number Pierce zones, therefore only a few first zones are relevant.

5.3 Introduction

Partially magnetized plasmas where electrons undergo fast gyro rotation, while ions dynamics is not significantly affected by the magnetic field, are common in many applications such as Hall-effect thrusters, magnetrons, and some regions of the ionosphere. This is the typical regime of the so-called $\mathbf{E} \times \mathbf{B}$ discharges, e.g., Hall thrusters for electric propulsion [114] and magnetrons [67]. Plasmas in such discharges are typically strongly turbulent, exhibit fluctuations of different temporal and spatial scales, and are characterized by anomalous current. Understanding of the nature and sources of these instabilities is an area of active research.

Local plasma gradients, such as in density, temperature, and magnetic field are usually identified as sources of free energy resulting in plasma instabilities and turbulence. These instabilities referred as drift instabilities have also been studied in partially magnetized plasmas [95, 115].

In the short wavelength limit, linear plasma dynamics is local and is formally described by linear partial differential equations (PDE) with constant coefficients. However, when the mode wavelength is of the order of the system size or/and plasma equilibrium length scale, the wave dynamics becomes nonlocal. In particular, the role of boundary conditions becomes non-trivial, which may result in new nonlocal instabilities mechanisms. An example is the Pierce instability [104], in which plasma flow in a finite length plasma with boundaries, results in the instability, whereas in the periodic (infinite) plasmas such flow would only lead to a trivial Doppler frequency shift. Such instabilities driven by boundary effects for ion sound type waves and electric charge waves in non-compensated diodes were studied in a number of experimental and theoretical works, see e.g. Refs. [76, 74, 105, 81] and references therein.

It was recently shown that the lower-hybrid waves can be driven by the transverse ion-beam in a finite length system via the mechanism similar to the Pierce instability in which

the role of boundaries is crucial for the instability [71]. The present paper is devoted to the investigation of nonlinear regimes of this instability and its consequences.

The lower-hybrid mode is among the most important modes in partially magnetized plasmas relevant to electric propulsion [115]. The nonlinear dynamics of resistive lower hybrid instability induced by ions flow was recently studied in Ref. [78]. This instability is relevant to axial (along the direction of the electric field) modes of $\mathbf{E} \times \mathbf{B}$ plasma discharges such as Hall-effect thrusters and magnetrons[24]. In the previous work[78], it was shown that numerical simulations confirm the predictions of the local theory for the most unstable modes in periodic geometry. It was also shown that in the nonlinear stage the highly localized (cnoidal-like type) wave structures are formed. The mechanism of this instability is local and related to the phase shift between the perturbations of the electron and ion currents. The electron current is supported by plasma conductivity across the magnetic field which may have classical (collisional) or anomalous (turbulent and/or wall conductivity) nature. At the same time, the ion current is due to inertial response to the electric field and thus is shifted in phase due to the Doppler effect. It was shown in Ref. [71] the lower hybrid waves can be driven unstable by the ion beam due to boundary effects. The wavelengths of those modes usually are of the order of the system length, therefore the dynamics is highly nonlocal.

Both of these instabilities mechanisms are relevant to the axially propagating modes in the Hall thruster (e.g., breathing modes) which are known to significantly affect the ion thrust [13, 8]. Modes exited by boundary effects are highly nonlocal in comparison with modes induced by the resistive electron current. Therefore, the nonlinear dynamics is expected to be different. The objective of this work is to investigate linear and nonlinear stage of the instability described in Ref. [71]. For this purpose, the nonlinear simulations were performed with BOUT++ plasma fluid simulation framework [45].

The paper is organized as follow. In Section 5.4 the nonlinear two-fluid model for low-hybrid instability is discussed. Results for linear instability from Ref. [71] are recovered in Section 5.5. In Section 5.6 the numerical solution to full nonlinear model is obtained. The effect of finite Larmor radius on the linear instability is analyzed in Section 5.7. Finally, the conclusions and discussions are in Section 5.8.

5.4 One dimensional model for lower-hybrid waves in partially magnetized plasmas

In this section, we introduce one-dimensional axial fluid model for partially magnetized plasmas used in Ref. [71] to describe the ion beam instability in bound plasma systems. The dynamics of unmagnetized ions is considered along constant equilibrium electric field in the x-direction, while magnetized electrons (i.e., equilibrium electric and magnetic fields are perpendicular) assumed to have zero collisional mobility along this direction and quasi-neutrality is supported by electron polarization drift.

Following the derivation in Ref. [71], two-fluid approximation with unmagnetized cold singly ionized ions and magnetized cold electrons are used. One dimensional mass and momentum conservation equations for ions written for perturbations around equilibrium yield

$$\partial_t n + n_0 \partial_x v + v_0 \partial_x n + v \partial_x n_0 + n \partial_x v_0 + \partial_x (nv) = 0, \tag{5.1}$$

$$\partial_t v + v_0 \partial_x v + v \partial_x v + v \partial_x v_0 + \frac{e}{M} \partial_x \phi = 0, \tag{5.2}$$

with equilibrium profiles

$$n_0 = \frac{n_{00} v_{00}}{v_0}, \quad v_0 = \sqrt{v_{00}^2 + \frac{2eE_0}{M} x}, \tag{5.3}$$

where ∂_t, ∂_x are time and space derivatives respectively; $n_0 = n_0(x), v_0 = v_0(x)$ are equilibrium profiles of ion density and velocity respectively; $n_{00} = n_0(0), v_{00} = v_0(0)$; n, v are perturbed ion density and velocity respectively; ϕ is a electrostatic potential perturbation; E_0 is a constant electric field along the x direction; $x \in [0, L]$ is a spatial domain of length L; e is an absolute value of an electron charge; M is an ion mass. We note that the assumption of constant electric field $E_0 = const$, implies the equilibrium electrostatic potential to grow as $\phi_0 \sim x$.

In the absence of collisions and in the strong magnetic field, the electron inertial response is compensated by the polarization drift in axial direction. The electron dynamics can be recovered from mass conservation equation

$$\partial_t n + n_0 \partial_x u + u \partial_x n_0 = 0, \tag{5.4}$$

where the electron velocity perturbation in axial direction (u) is supported by polarization drift (in the main order of strong magnetic field expansion $\partial_t \ll \omega_{ce}$)

$$u = \frac{e}{m\omega_{ce}^2}\partial_t\partial_x\phi, \tag{5.5}$$

where m is an electron mass, and ω_{ce} is an electron cyclotron frequency. Hence, the final electron equation reads

$$\partial_x^2\phi + \frac{1}{n_0}\partial_x n_0 \partial_x\phi + \frac{m\omega_{ce}^2}{en_0}n = 0. \tag{5.6}$$

Note that the electron equation is linear, as leading order nonlinear term disappears in one dimensional geometry [115].

The system is closed with standard [71] boundary conditions

$$\phi(0) = \phi(L) = n(0) = v(0) = 0. \tag{5.7}$$

5.5   Linear instability

In the linear approximation, the system of equations (5.1)-(5.6) reduces to

$$\partial_t n + n_0\partial_x v + v_0\partial_x n + v\partial_x n_0 + n\partial_x v_0 = 0, \tag{5.8}$$

$$\partial_t v + v_0\partial_x v + v\partial_x v_0 + \frac{e}{M}\partial_x\phi = 0, \tag{5.9}$$

$$\partial_x^2\phi + \frac{1}{n_0}\partial_x n_0 \partial_x\phi + \frac{m\omega_{ce}^2}{en_0}n = 0. \tag{5.10}$$

Note, that in the local approximation, when equilibrium profiles can be considered constant $(\partial_x n_0 \approx \partial_x v_0 \approx 0)$, the system (5.8)-(5.10) is reduces to Pierce equations [104] which can be solved analytically.

As was shown in Ref. [71] the boundary conditions (5.7) make the system of equations (5.8)-(5.10) unstable similar to the Pierce instability. The growth rate of this system was extensively studied in Ref. [71] and we reproduce those results in Figure 5.1. The figure shows the growth rate normalized to low hybrid frequency $\omega_{LH} = \omega_{ce}\sqrt{m/M}$ as a function of a Pierce parameter $\alpha = \omega_{LH}L/v_{0d}$ with $v_{0d} = v_0(L)$ being the equilibrium ion outflow velocity. The initial equilibrium ion velocity value was chosen as in Ref. [71] $v_{00} = 0.2v_{0d}$.

Growth rate values were benchmarked with the Table 1 in Ref. [71] and differ with those results by no more than 3%. Notice, that values in the Table 1 in Ref. [71] are obtained for a different normalization. Therefore, to recover them, one needs to multiply γ/ω_{LH} by α.

As was shown in Ref. [71], the discussed model has only two external parameters: α and $q = 1 - (v_{00}/v_{0d})^2$. Here we use v_{00}/v_{0d} instead of q.

Figure 5.1 shows four Pierce instabilities zones [104]. For $\alpha < 0.7\pi$ the plasma is stable, while for large α there will appear more zones. Each odd zone (counting starts from the small α) has aperiodic instability $Re(\omega) = 0$, while even zones have oscillatory instabilities $Re(\omega) \neq 0$. For example, Figure 5.1 shows two aperiodic zones for $\alpha \sim \pi$, $\alpha \sim 2.2\pi$ and two oscillatory zones $\alpha \sim 1.49\pi$, $\alpha \sim 2.7\pi$. The zone number also defines the number of zeros of unstable eigenfunction, therefore higher zones correspond to higher effective wave-numbers. This means that to consider higher number zones one needs to take into account small-scale effects such as finite Larmor radius effect or charge separation.
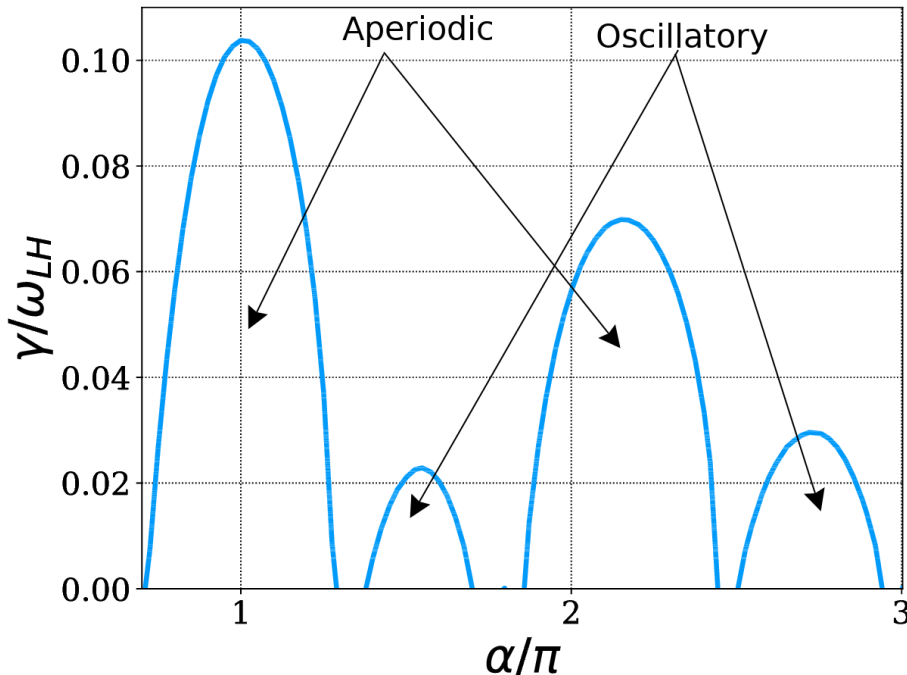
Figure 5.1: Growth rate dependence on the Pierce parameter $\alpha = \omega_{LH} L/v_{0d}$ with initial ion velocity $v_{00} = 0.2 v_{0d}$.

5.6 Nonlinear evolution

The main objective of this paper is to track a nonlinear evolution of the instability discussed in Section 5.5. Therefore, the full system of equations (5.1)-(5.7) was solved numerically. In order to track the stage of nonlinear evolution we define energy-like functionals and follow their time evolution

$$E_n = E\left[\frac{n}{n_{00}}\right], \quad E_v = E\left[\frac{v}{v_{00}}\right], \quad E_\phi = E\left[\frac{e\phi}{Mv_{00}^2/2}\right], \text{ with } E[f] = \sqrt{\frac{1}{L}\int_0^L dz|f(z)|^2}.$$

$$(5.11)$$

The temporal evolution of energy-like functionals for aperiodic ($\alpha = 1.05\pi$) and oscillatory ($\alpha = 1.55\pi$) Pierce zones are shown in Figures 5.2. The evolution for both zones clearly shows a linear growth phase with transition into nonlinear saturation.

(a) Aperiodic zone with $\alpha = 1.05\pi$ (b) Oscillatory zone with $\alpha = 1.55\pi$
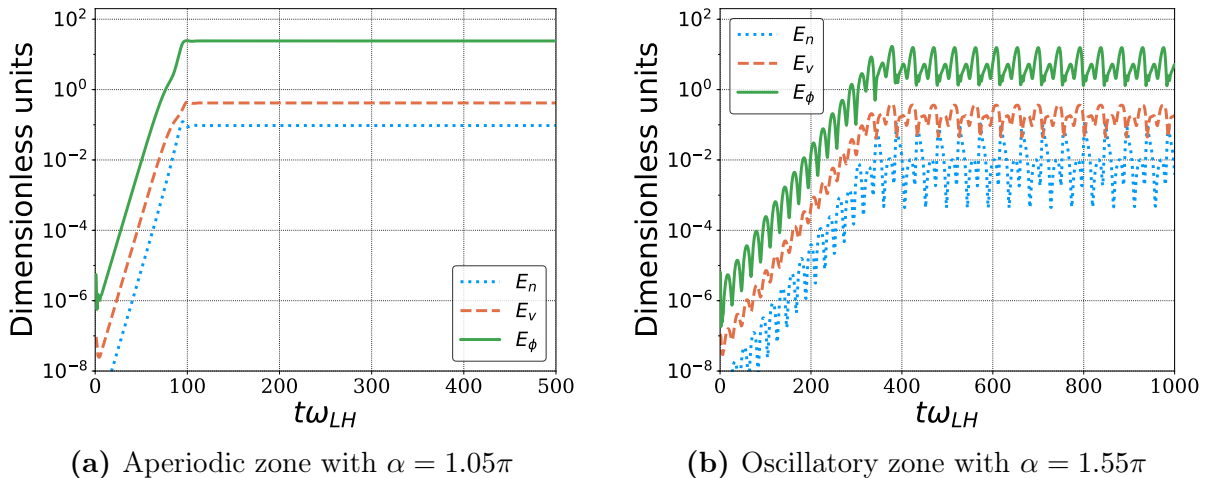
Figure 5.2: Time evolution of functionals (5.11) with initial ion velocity $v_{00} = 0.2v_{0d}$.

5.6.1 The aperiodic instability zone

In the aperiodic zone, for sufficiently small initial condition, the unstable eigenfunction starts growing exponentially with time. The linear growth phase corresponds to the time $t\omega_{LH} < 100$ in Figure 5.2a. The shape of the unstable eigenfunction in the first Pierce zone is shown in Figure 5.3a where the initial Gaussian profile (blue solid line) transforms into an eigenfunction and starts to grow exponentially in time. After some time, when $n \sim n_0$ the nonlinear effects start to slow down the linear growth. Eventually, the new stationary equilibrium is reached as

75

shown in the time evolution plot of total density Figure 5.3b. The blue dashed line shows the initial density profile, and the red dotted line represents the evolution of the density during the nonlinear regime which is a combination of large density perturbation and equilibrium density. After about $t\omega_{LH} \sim 105$, the new equilibrium profile is formed and it stays constant for the rest of the simulation $105 < t\omega_{LH} < 500$, as shown by the green and purple solid lines for times $t\omega_{LH} = 105$ and $t\omega_{LH} = 500$ respectively which coincide.

It is interesting to note that, the new density equilibrium forms a prominent peak in the beginning of the acceleration region due to the form of unstable density eigen function shown in Figure 5.3a. Therefore, the continuity equation

$$(n_0 + n)(v_0 + v) = const,$$

implies that the total velocity will have the deceleration region in the new equilibrium as shown in Figure 5.3c. The perturbation of electrostatic potential corresponding to the described density and velocity profiles is shown in Figure 5.3d. The perturbation is plotted rather than a full value of electrostatic potential, as the perturbation is still relatively small in comparison to the equilibrium value, which is

$$\frac{2e\phi_0}{Mv_{00}^2} = \left(1 - \left(\frac{v_{0d}}{v_{00}}\right)^2\right)\frac{x}{L}. \tag{5.12}$$

5.6.2 The oscillatory instability zone

In the oscillatory zone, the situation is similar, but the growth rate is smaller than in the preceding aperiodic zone, so the linear phase is longer $t\omega_{LH} < 350$. At the linear phase, the eigenfunction grows exponentially in time and additionally oscillates as shown in Figure 5.4. Every figure in this subsection is branched into two sub-figures for the first and second half of the oscillation period. In the nonlinear regime, the new stationary equilibrium is replaced with a standing wave. Figures 5.5 is a standing density wave which is similar to aperiodic solution shown in Figure 5.3b, but oscillates in time. Similar standing waves can be observed for velocity in Figures 5.6 and electrostatic potential perturbation in Figures 5.7.

(a) Density perturbation

(b) Full density

(c) Full ion velocity

(d) Electrostatic potential perturbation
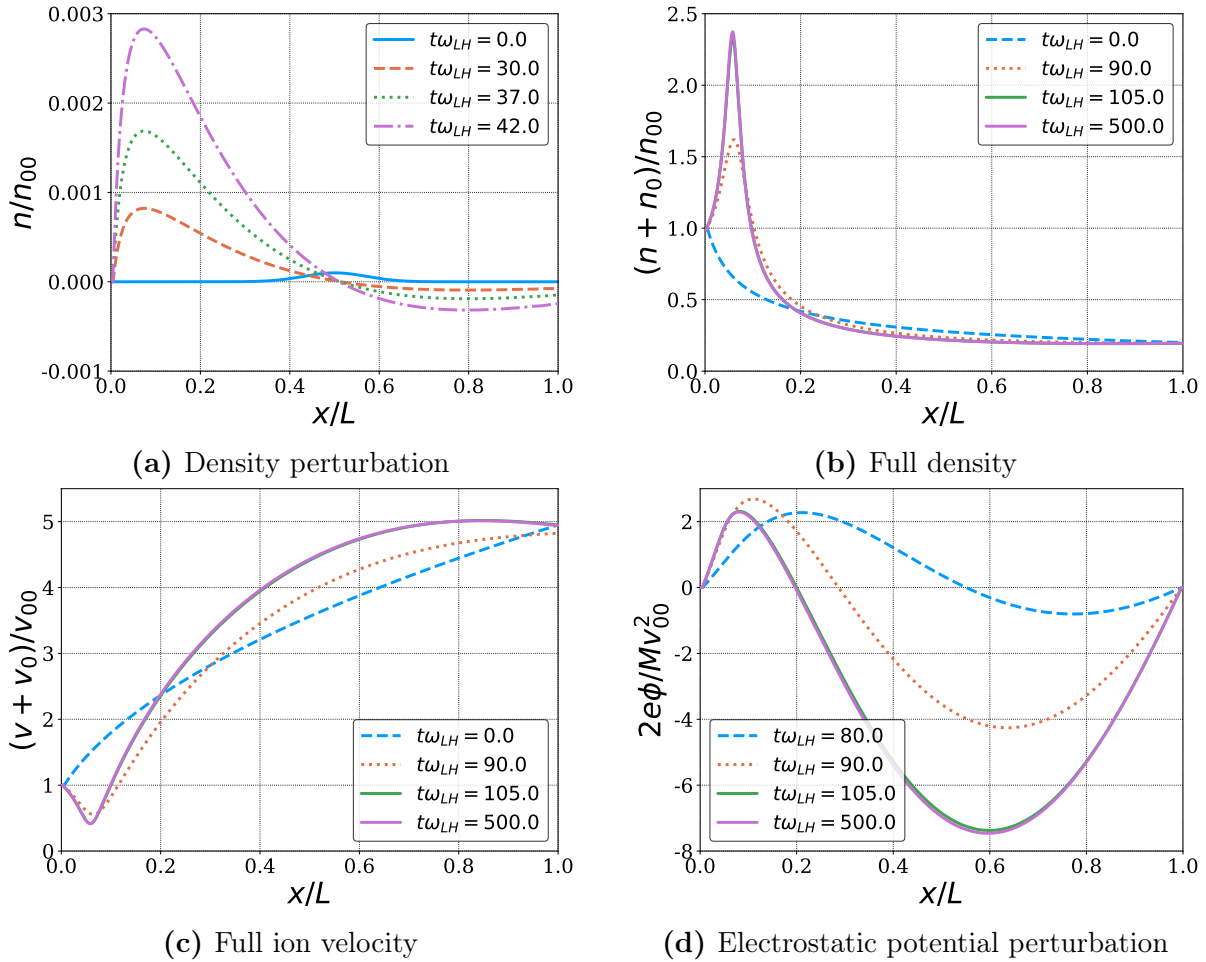
Figure 5.3: The time evolution of ion density, ion velocity, and electrostatic potential spatial profiles in aperiodic Pierce zone for $\alpha = 1.05\pi$ and initial ion velocity $v_{00} = 0.2v_{0d}$.

5.7 Finite Larmor radius effects

As was mentioned earlier, the Pierce zone number defines the number of zeros of the unstable eigenfunction. For example, the unstable eigenfunction in the first Pierce zone has one zero in the interior region (excluding boundary points) as shown in Figure 5.3a, while the second Pierce zone has two as shown in Figure 5.4. Therefore, the effective wavelength is decreasing with bigger zone number. In this situation, one needs to include effects relevant to smaller scales. The next order term is finite Larmor radius effect [115]. In order to include it, the

77

(a) First half period of oscillation

(b) Second half period of oscillation
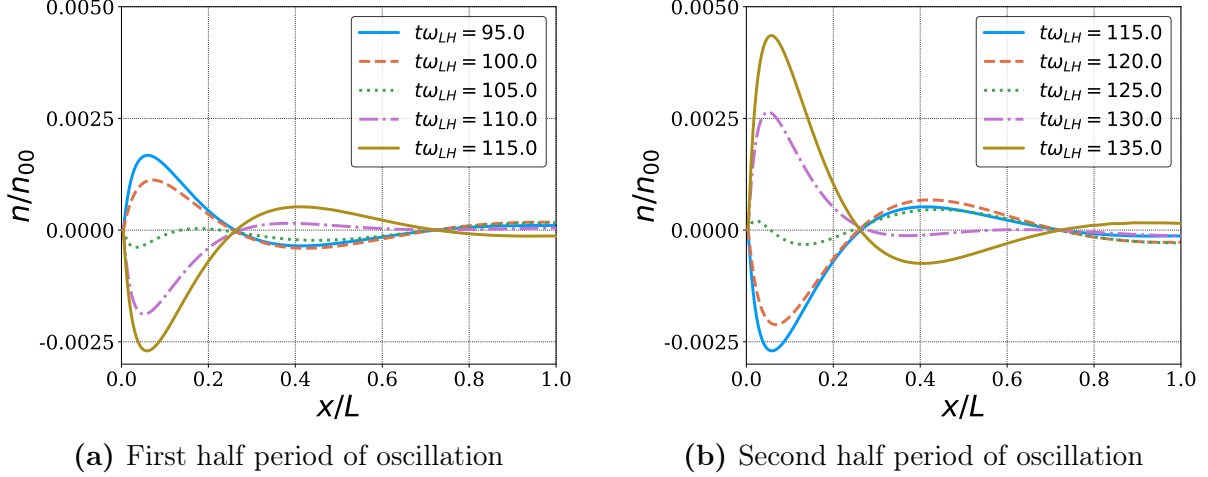
Figure 5.4: Linear growth of unstable eigenfunction in oscillatory Pierce zone for $\alpha = 1.55\pi$ and initial ion velocity $v_{00} = 0.2v_{0d}$.

electron equation (5.6) is modified into

$$\partial_x^2\phi + \frac{1}{n_0}\partial_x n_0 \partial_x\phi + \frac{m\omega_{ce}^2}{en_0}\left(n - \rho_e^2\partial_x^2 n\right) = 0, \tag{5.13}$$

where ρ_e is a electron Larmor radius.

The new free parameter in equation (5.13), namely, the electron Larmor radius, is chosen to be $\rho_e = 0.05L$ in dimensionless units, which corresponds to typical Hall truster acceleration region length $L \sim 1cm$, electron temperature $T_e = 15eV$ and magnetic field $B = 160G$.

Numerical simulation results for linear growth rates with FLR effects are shown in Figure 5.8a. One can see that FLR effects stabilize higher order zones while the first zone stays almost without modifications. If one investigate the parameter space further, higher Pierce zones may be stabilized partially as it is shown in Figure 5.8b where $v_{00}/v_{0d} = 0.4$ parameter was used. Nonlinear simulations reveal that dynamics is not significantly modified by FLR effects.

5.8   Conclusions

The linear theory of the instability first described in Ref. [71] has been confirmed here with numerical simulations providing the necessary linear benchmark for our nonlinear studies. The instability growth rate and the form of the unstable eigenfunction which depend on the

(a) First half period of oscillation

(b) Second half period of oscillation

Figure 5.5: Oscillating quasi-stationary profile of ion density in oscillatory Pierce zone for $\alpha = 1.55\pi$ and initial ion velocity $v_{00} = 0.2v_{0d}$.

Pierce parameter α are shown in Figure 5.1 where one can see distinct Pierce zones. The effective wave number of the eigenfunction grows with zone number. We find a significant modification of previous linear results [71] with the addition of FLR effects which are significant in the case of short wavelengths. As shown in Figure 5.8, the first Pierce zone stays relatively unchanged, while higher order zones are stabilized.

After the linear growth phase, the aperiodically unstable mode saturates into a new nonlinear equilibrium which is shown in Figure 5.3. The interesting feature of this equilibrium is the presence of deceleration zone as shown in Figure 5.3c. It is interesting to note that this feature can be attributed to the shape of the unstable density eigenfunction which has a maximum (the unstable velocity eigenfunction has a minimum at the same location). It is of interest to note that non-monotonous electric field profiles (that include deceleration regions) were observed in experiments [123, 124]. In the oscillatory zone, the oscillatory eigenfunction in nonlinear regime becomes a standing wave with similar deceleration regions (but oscillating in time).

The classical Pierce problem (in our case $v_{00} = v_{0d}$) has similar solutions, i.e., stationary and oscillating nonlinear equilibria, as was investigated by many authors, most notably see Ref. by Godfrey [56]. Previous works have identified the regimes when oscillating solutions bifurcate (at some values of Pierce parameter α) into the combination of oscillating modes leading to the chaotic oscillations [56, 92, 80]. We did not find such bifurcations or chaotic

79

(a) First half period of oscillation

(b) Second half period of oscillation

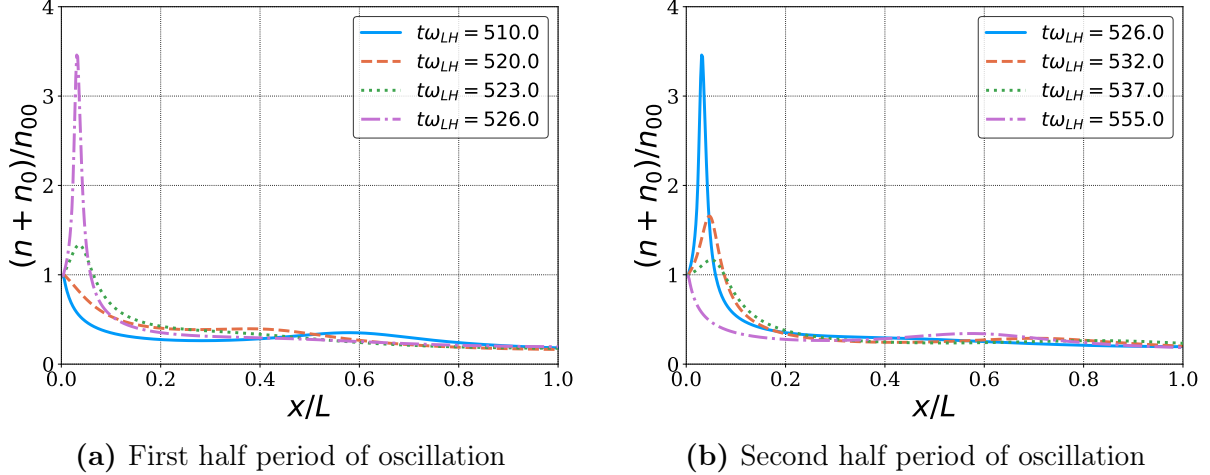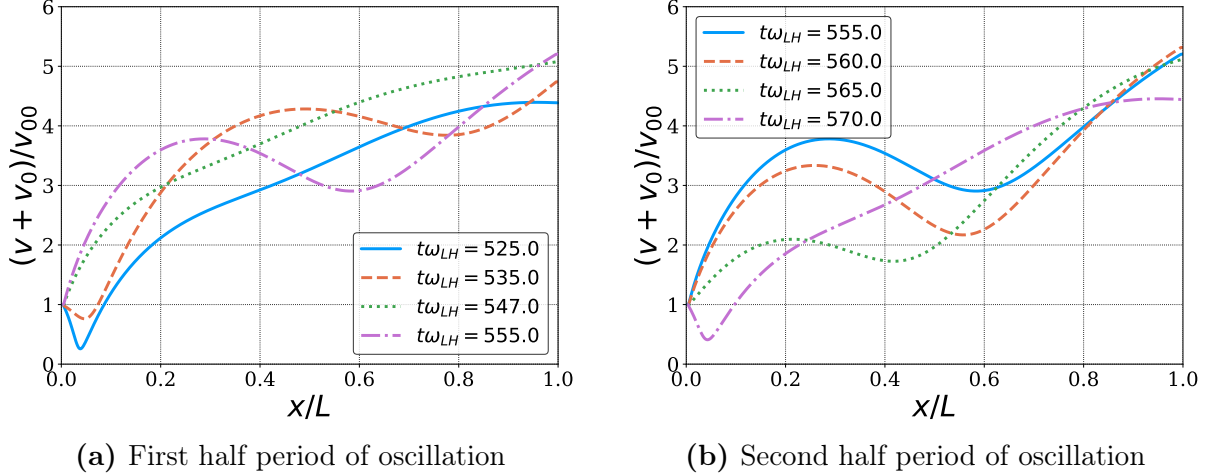**Figure 5.6:** Oscillating quasi-stationary profile of ion velocity in oscillatory Pierce zone for $\alpha = 1.55\pi$ and initial ion velocity $v_{00} = 0.2v_{0d}$.

solutions in the second Pierce zone in our case. An important difference between the standard Pierce modes as in Ref. [104] and our case is that our profile of the ion velocity is nonuniform resulting in partial suppression of the instability for higher zones. We conjecture that partial mode stabilization and the shift of Pierce zones for non-uniform profiles relative to the Pierce instability is the reason for the absence of chaotic regimes. Further parametric studies with respect to α, v_{00}/v_{0d} parameters and initial conditions to support this claim are left for future work.

In this paper, we neglected all resistive effects, so the instability discussed in Ref. [78] does not occur here. For some typical plasma parameters though, the growth rates of both instabilities can be of the same order, $\gamma \sim 0.1\omega_{LH}$. We note here that the nonlinear stages for the resistive mode of Ref. [78] and for the nonlocal (Pierce like) mode studied here are different. In the first case, where instability is driven by resistive electron cross-field current, the instability is local. In this case, local nonlinear interactions due to ion trapping [35] are the saturation mechanism which results in wave sharpening and breaking leading to cnoidal type waves. For the Pierce like instability induced by boundary effects, only selected mode(s) continue to grow seemingly excluding the growth (generation) of the shorter wavelengths. The nonlinear effects saturate the mode by modifying the instability source — the velocity flow profile, thus resulting in velocity profile which has a local minimum.

Plasma density gradients and collisions can also destabilize the azimuthal lower-hybrid
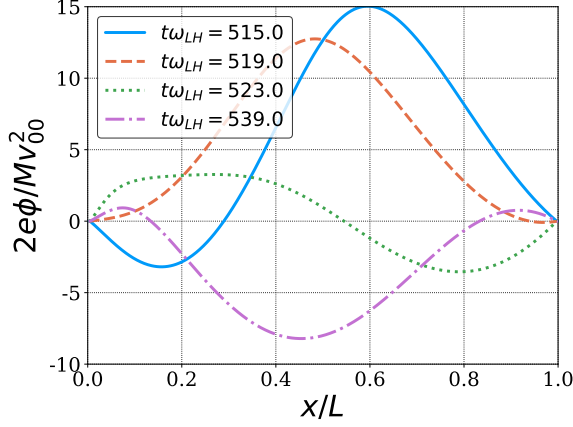
(a) First half period of oscillation
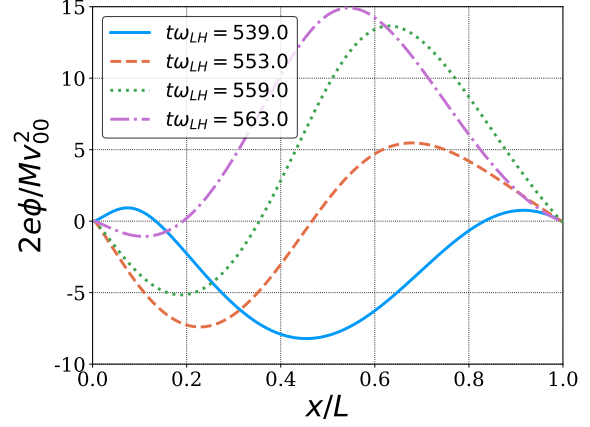
(b) Second half period of oscillation

Figure 5.7: Oscillating quasi-stationary profile of electrostatic potential perturbation in oscillatory Pierce zone for $\alpha = 1.55\pi$ initial ion velocity $v_{00} = 0.2v_{0d}$.
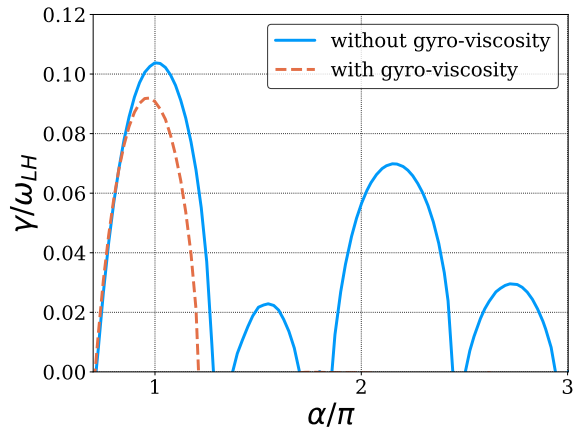
(a) $v_{00} = 0.2v_{0d}$ (Instability was absent for $\alpha > 1.21\pi$)
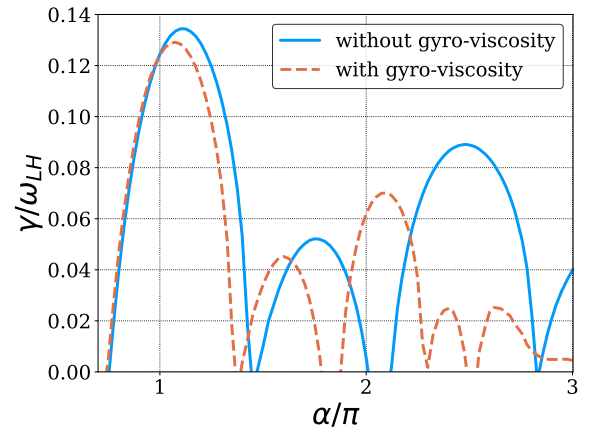
(b) $v_{00} = 0.4v_{0d}$

Figure 5.8: Effect of FLR on linear growth rate, for $L/\rho_e = 20$.

mode [115, 87], which becomes Simon-Hoh instability in the low-frequency limit. Interaction of the azimuthal (resulting in anomalous current), and axial modes due to resistive and boundary effects such as studied here will have to be investigated within a unified framework which is left for future studies.

Acknowledgments

CHAPTER 6

EFFECT OF ANOMALOUS RESISTIVITY ON AXIAL MODES

6.1 Introduction

It was shown, in Chapter 4, that in partially magnetized plasmas with perpendicular electric and magnetic fields (e.g., Hall thruster shown in Figure 1.2) the equilibrium ion flow v_0 along the electric field $\mathbf{E}_0 = E_0 \hat{\mathbf{x}}$ excites large amplitude axial waves. The instability occurs due to the phase shift between ballistic ion current (4.7) and electron current $j_e = \sigma E_0$ where the conductivity mechanism is not significant; in other words, it can be classical $\sigma = \sigma_\nu$ or anomalous $\sigma = \sigma_a$. At the same time, in Chapter 3, it was shown that the turbulence, driven by the density gradient and the equilibrium electron flow $u_0 = cE_0/B_0$ (ExB drift), produces an anomalous current

$$j_e = \frac{ce}{B_0} \left\langle \widetilde{n} \widetilde{E_y} \right\rangle, \tag{6.1}$$

which is at least two orders of magnitude higher than collisional current ($j_\nu = \sigma_\nu E_0$). Anomalous conductivity is then defined as

$$\sigma_a = \frac{j_e}{E_0} \gg \sigma_\nu \sim \nu \omega_{pe}^2/\omega_{ce}. \tag{6.2}$$

Here, $\widetilde{n}$ and $\widetilde{E_y}$ are turbulent fluctuations of the plasma density and azimuthal electric field respectively (the slab geometry perpendicular to the magnetic field and notations introduced in Chapter 3 are used in this chapter). Therefore, one can expect an anomalous current, caused by the Hall drift wave turbulence, to be the main driver of axial mode instability. Hence, the focus of this chapter is to investigate the nonlinear interaction of these modes, so, we consider the full system (3.1)-(3.4) with equilibrium ion flow ($v_0 \neq 0$) which was neglected in Chapter 3.

The saturation mechanism of Hall drift waves is the polarization drift due to ExB Lagrangian advection; in other words, the Poisson bracket term in equation (3.3). It produces coherent large-scale nonlinear structures (shear flows and vortices) and is responsible for the inverse energy cascade. The axial mode saturation occurs due to nonlinear terms in the ion equations (3.1), (3.2). Therefore, the characteristic time scale and amplitude for the axial instability is different from the gradient driven modes. In particular, simulations in Chapter 4 revealed that the axial mode saturation time and amplitude are higher. Therefore, the dynamics of Hall drift wave turbulence in the presence of an equilibrium ion flow occurs in the following order: (i) the most unstable gradient driven waves are excited and grow exponentially; (ii) they form a turbulence with properties described in Chapter 3, thus enhancing axial electron conductivity; (iii) axial modes grow due to resistive instability and anomalous conductivity; (iv) axial mode saturates into a high amplitude cnoidal-like wave traveling in the axial direction.

6.2   Results of nonlinear simulations

Similar to Chapter 3, nonlinear simulations of system (3.1)-(3.4) is performed with fluid simulation framework BOUT++. First, we measured the evolution of energy-like quantities (3.6) and anomalous current (6.1) in the nonlinear simulation similar to the one discussed in Chapter 3, but with an equilibrium ion flow $v_0 \neq 0$ (still without electron-neutral collisions $\nu = 0$). The results are shown in Figures 6.1, 6.2. We can see the linear phase $t\omega_{LH} < 2.5$ where gradient driven waves are growing exponentially and anomalous current is absent. At later times $t\omega_{LH} > 2.5$, the nonlinear interactions of Hall drift waves become important and exponential growth slows down. It leads to the enhancement of axial electron current which then drives axial instability. Therefore, Hall drift wave growth transits into the axial mode growth which has larger saturation time. Notice that energy-like functional E_n corresponding to ion density perturbation at time $t\omega_{LH} = 10$ is ten times bigger in the presence of the equilibrium ion flow as confirmed by Figures 3.3, 6.1.

Now, we perform the simulation where the nonlinear terms in the ion equations (3.1), (3.2) are artificially turned off to remove the effect of axial mode saturation. In this case, axial

Figure 6.1: Time evolution of (3.6) with parameters $\nu = 0$, $v_0 = 3.72c_s$, $L_n = 48.8\rho_e$, $\sqrt{m_i/m_e} = 427$, $u_0 = 241.8c_s$.
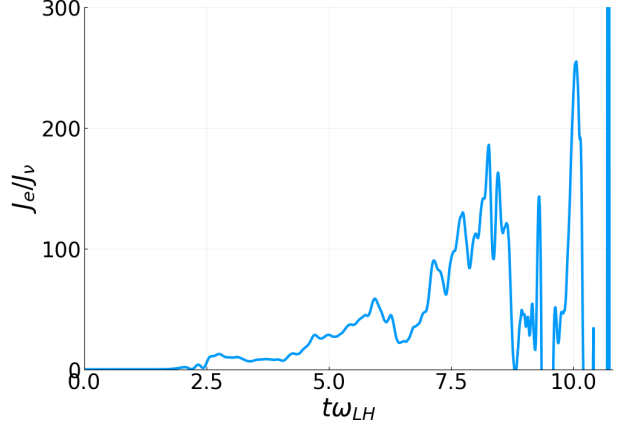
Figure 6.2: Anomalous axial current in units of classical collisional current. The current was smoothed with window function of order 25. Parameters used $\nu = 0$, $v_0 = 3.72c_s$, $L_n = 48.8\rho_e$, $\sqrt{m_i/m_e} = 427$, $u_0 = 241.8c_s$.

modes grow exponentially and at some point start to dominate the spatial density profile, so we can confirm the nonlinear driving of axial modes from Hall drift wave turbulence. We also change boundary conditions for axial direction from periodic to Dirichlet in the left end and Neumann in the right end, to correspond to the boundary conditions used in Chapters 4, 5 where axial instabilities were studied. The spatial profiles of plasma density for late time $t\omega_{LH} = 30$ for this simulation are shown in Figures 6.3. Figure 6.3a shows that, at this time, axial modes completely dominate the profile ($k_y \approx 0$). Axial modes are "linear" and do not have cnoidal form as shown in one dimensional slice Figure 6.3b. The structure of energy-like quantities (3.6) also confirms exponential growth of axial modes as shown in Figure 6.4. Notice that in the absence of electron-neutral collisions, axial modes ($k_y = 0$) do not modify the generalized vorticity $\partial_t \eta = 0$, as follows from the equation (3.3). Hence, the generalized vorticity is saturated, while plasma density is growing indefinitely. Thus, electron-neutral collisions are important feedback mechanism from axial modes to Hall drift waves and codependent large-scale structures (shear flows and vortices).

Finally, we consider the full system (3.1)-(3.4) with electron-neutral collisions and non-linear ion equations. Thus, saturation mechanisms for Hall drift waves and axial modes are present, as well as linear feedback on Hall drift waves from axial modes. The Hall drift wave

(a) Two dimensional profile

(b) One dimensional slice
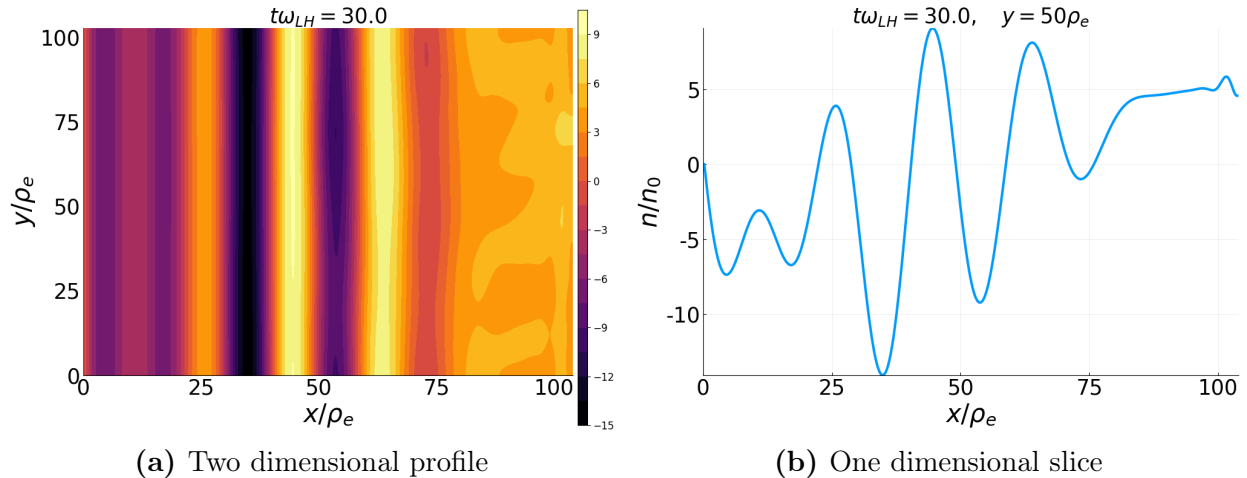
Figure 6.3: Normalized density n/n_0 spatial profiles in the simulation without ion nonlinearities. Parameters used $\nu = 0$, $v_0 = 3.72c_s$, $L_n = 48.8\rho_e$, $\sqrt{m_i/m_e} = 427$, $u_0 = 241.8c_s$.

turbulence tend to form large-scale structures with small wave numbers (i.e., strong shear azimuthal flows and vortices). At the same time, nonlinear dynamics of the axial instability tend to form cnoidal waves with large wave numbers. Therefore, the dynamics of the full system is complicated due to intrinsic scale separation. Thus, we increased the resolution (and axial system length) in the following simulation and switched back to fully periodic boundary conditions. The evolution of energy like functionals (3.6) in full system is shown in Figure 6.5 where the clear linear growth phase transitions into nonlinear saturation. In the full system, electron-neutral collisions provide the main order feedback from axial modes electric field on Hall drift waves. Thus, the axial modes are responsible for further enhancement of axial current as shown in Figure 6.6. Now, we illustrate the time evolution of spatial profiles of generalized vorticity η/n_0 with consequent snapshots in Figures 6.7, 6.8, with corresponding times $t\omega_{LH} = 3.0, 14.22, 22.1, 35.41, 70.86$. Each figure has a two dimensional profile to illustrate whole structure of turbulence and one dimensional slice to highlight large axial variations (presence of axial modes). Similar to results in Chapter 3, the most unstable modes (Hall drift waves) grow exponentially in time and then when nonlinear interaction start to play a dominant role, shear azimuthal flows are formed as shown in Figure 6.7a. At an early time, the axial modes are not yet developed and large amplitude axial variations are absent, as shown in Figure 6.7b. At later time, axial modes appear with large amplitudes and
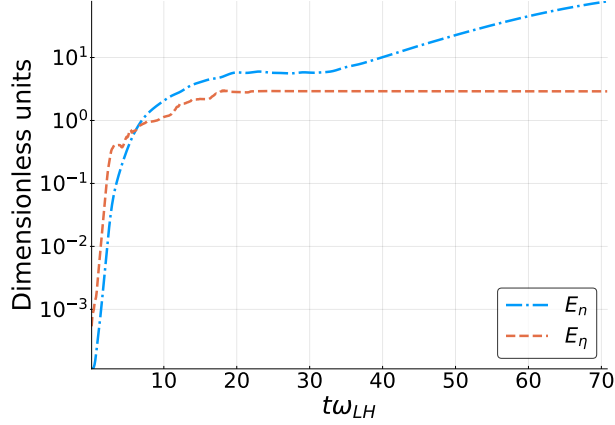
Figure 6.4: Time evolution of (3.6) with linear ion equations and parameters $\nu = 0$, $v_0 = 3.72c_s$, $L_n = 48.8\rho_e$, $\sqrt{m_i/m_e} = 427$, $u_0 = 241.8c_s$.
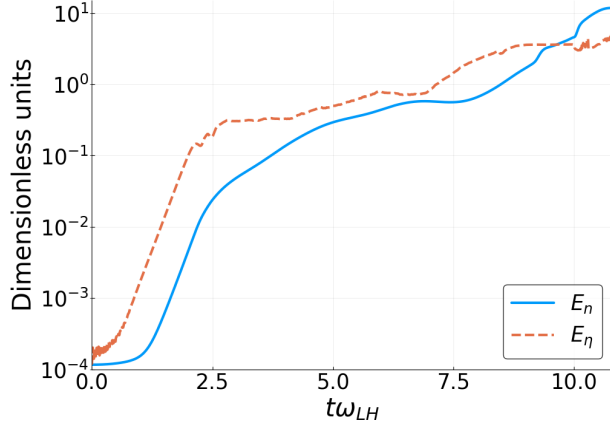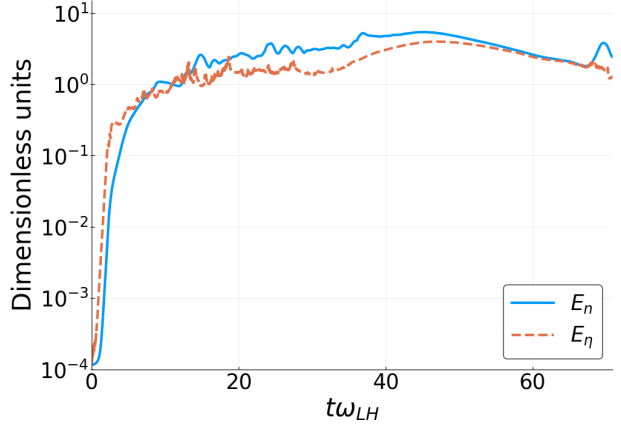
Figure 6.5: Time evolution of (3.6) with parameters $\nu = 0.28\omega_{LH}$, $v_0 = 3.72c_s$, $L_n = 48.8\rho_e$, $\sqrt{m_i/m_e} = 427$, $u_0 = 241.8c_s$.

coexist with shear azimuthal flows and vortices as shown in Figure 6.7c. Notice that axial modes have sharp cnoidal-like peaks as can be seen in Figure 6.7d. The full dynamics is complicated and do not always include vortices, shear flow and axial modes at the same instant. As shown in Figures 6.8a-6.8f, prominent axial modes can disappear (Figures 6.8a, 6.8b), or completely dominate the spatial profile (Figures 6.8c, 6.8d), or coexist with shear flows (Figures 6.8e, 6.8f).
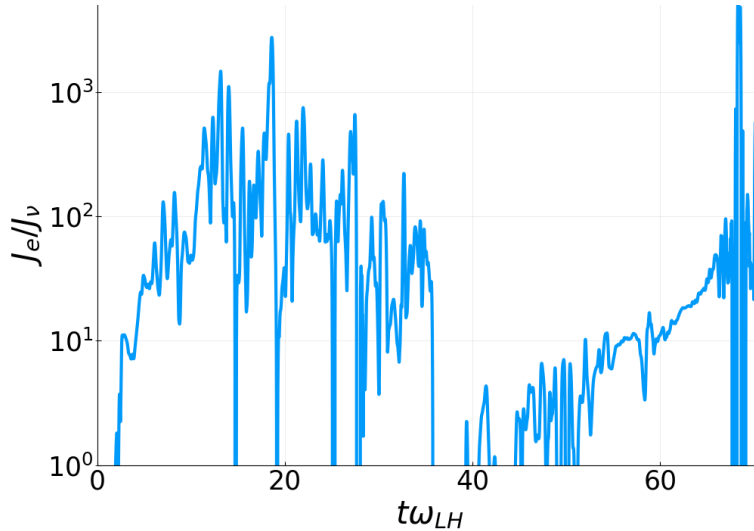
Figure 6.6: Anomalous axial electron current in units of classical collisional current with parameters $\nu = 0.28\omega_{LH}$, $v_0 = 3.72c_s$, $L_n = 48.8\rho_e$, $\sqrt{m_i/m_e} = 427$, $u_0 = 241.8c_s$. The current was smoothed with window function of order 30.

86

(a) Two dimensional profile

(b) One dimensional slice

(c) Two dimensional profile

(d) One dimensional slice

Figure 6.7: Normalized generalized vorticity η/n_0 spatial profiles at times $t\omega_{LH} = 3.0, 14.22$. Parameters used $\nu = 0.28\omega_{LH}$, $v_0 = 3.72c_s$, $L_n = 48.8\rho_e$, $\sqrt{m_i/m_e} = 427$, $u_0 = 241.8c_s$.

6.2.1 Streamers

An analogy with fully magnetized plasmas, we study the inverse energy cascade in a partially magnetized plasma which leads to the formation of large-scale shear flows (c.f., zonal flows). In fully magnetized plasmas, zonal flows usually occur together with streamers [11, 25, 90]. Streamers are coherent nonlinear structures, usually observed in drift wave turbulence which are localized in the azimuthal direction (poloidal direction in tokamaks) and extended in the axial direction (radial direction in tokamaks). Here, we report the formation of stable streamers in partially magnetized plasmas which can exist for long periods of time $t\omega_{LH} \sim 5$ as shown in Figures 6.9.

6.3 Summary

A density gradient in partially magnetized plasmas produces small scale turbulence, Hall drift waves. The turbulence tends to cascade energy into larger scales, forming coherent nonlinear structures (i.e., shear flows and vortices). This process is accompanied by significant enhancement of axial electron current. High electron current triggers an axial instability which is destabilized by the phase shift between electron current and the ion current Doppler shifted due to equilibrium ion flow. The axial instability saturates, forming coherent nonlinear structures resembling cnoidal waves. This nonlinear dynamics of partially magnetized plasma was studied with the reduced fluid model proposed in [115] and fluid simulation framework BOUT++ for typical Hall thruster parameters ($\nu = 0.28\omega_{LH}$, $v_0 = 3.72c_s$, $L_n = 48.8\rho_e$, $\sqrt{m_i/m_e} = 427$, $u_0 = 241.8c_s$). It was established that the dynamics starts with the strongest instability exciting Hall drift waves. The nonlinear interactions of Hall drift waves enhances electron current and excites the axial instability even when axial modes are linearly stable (i.e., in the absence of electron-neutral collisions). The main saturation mechanism of axial modes is then nonlinear terms in the ion continuity and Euler equations, and the feedback mechanism to Hall drift waves is with electron-neutral collisions. This was confirmed by a simulation where those effects were artificially turned off. It was demonstrated that the full dynamics of Hall drift and axial modes have large coherent nonlinear structures such as shear flows, vortices, cnoidal waves, and streamers.

(a) Two dimensional profile

(b) One dimensional slice

(c) Two dimensional profile

(d) One dimensional slice

(e) Two dimensional profile
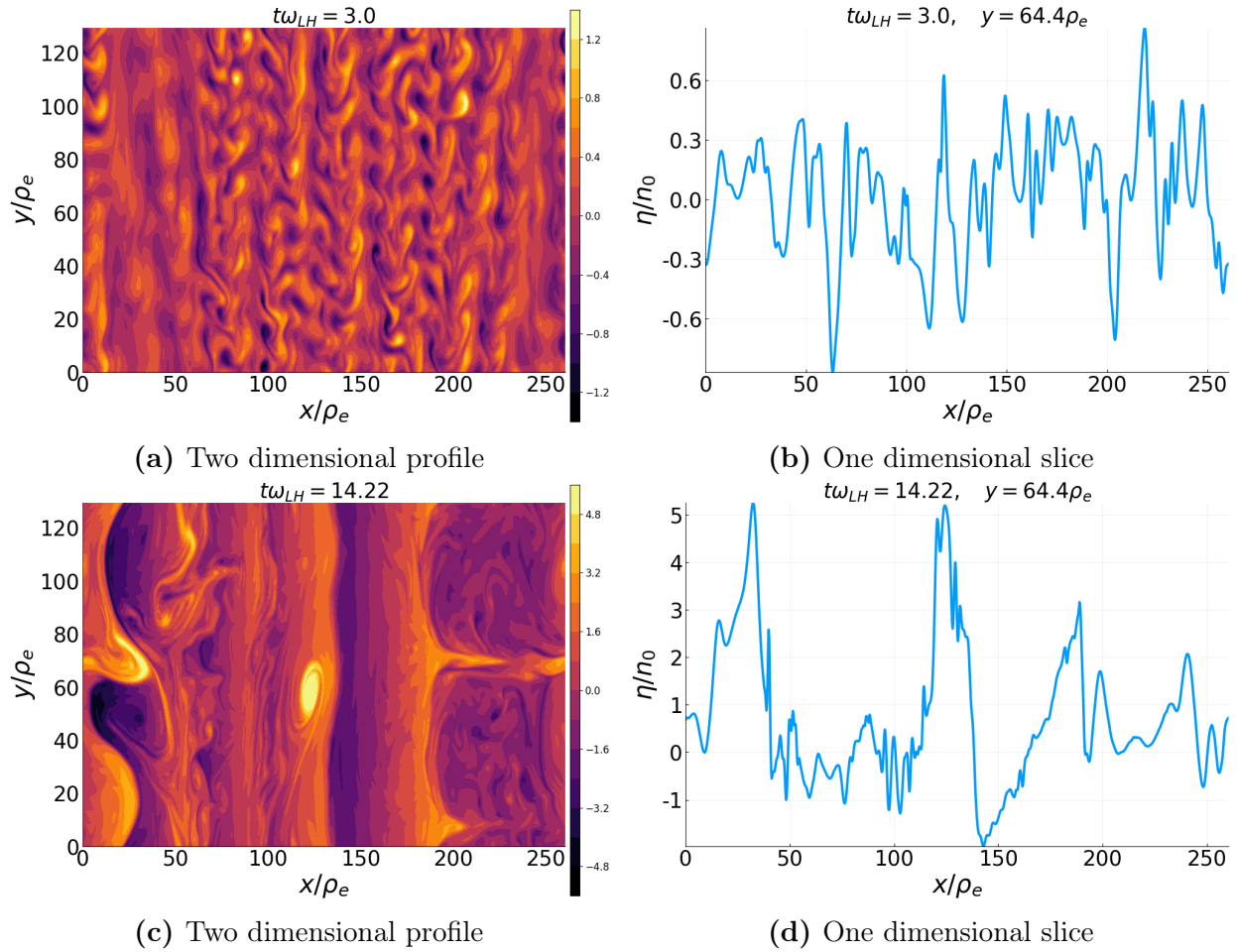
(f) One dimensional slice
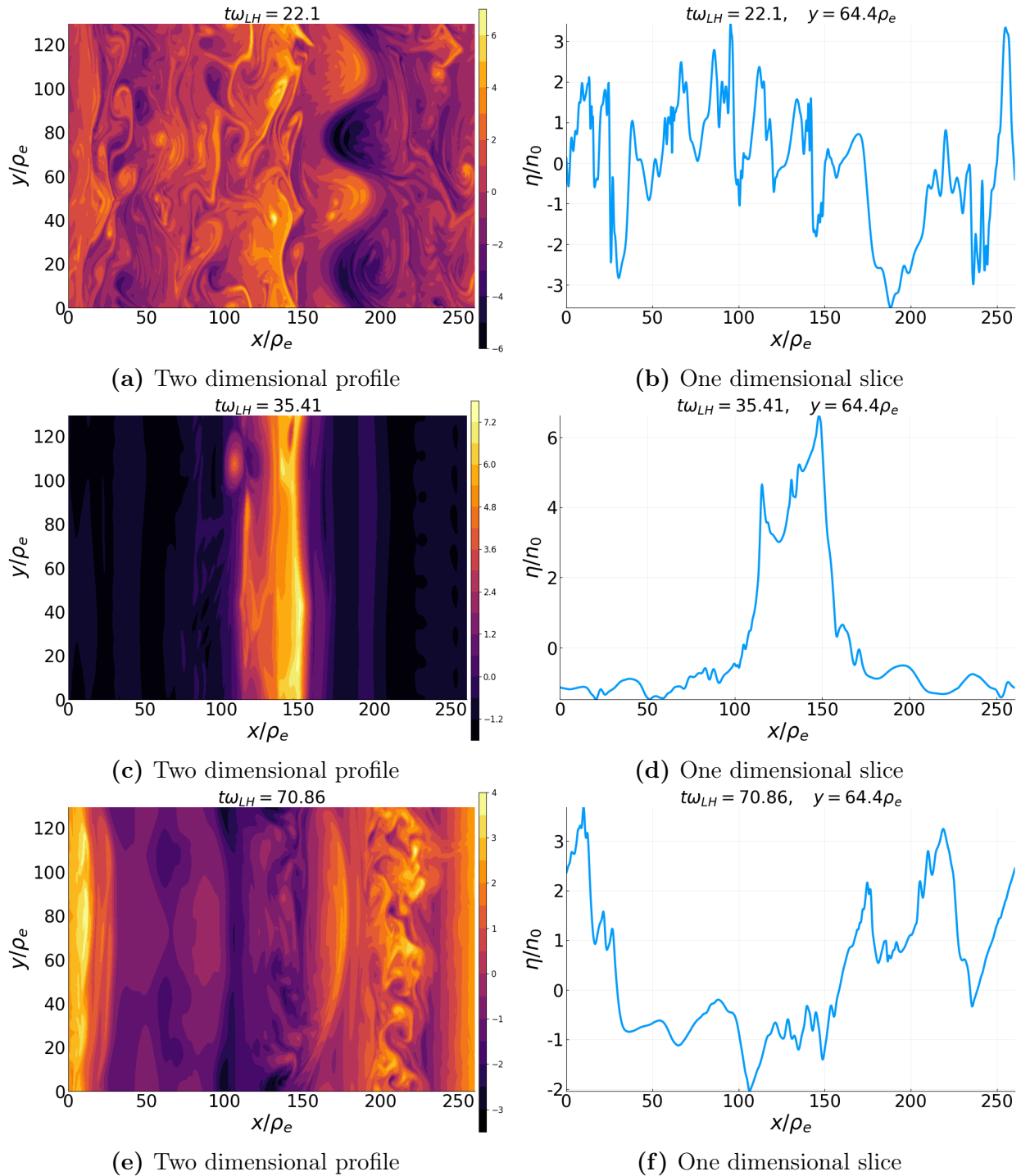
Figure 6.8: Normalized generalized vorticity η/n_0 spatial profiles at times $t\omega_{LH} = 22.1, 35.41, 70.86$. Parameters used $\nu = 0.28\omega_{LH}$, $v_0 = 3.72c_s$, $L_n = 48.8\rho_e$, $\sqrt{m_i/m_e} = 427$, $u_0 = 241.8c_s$.
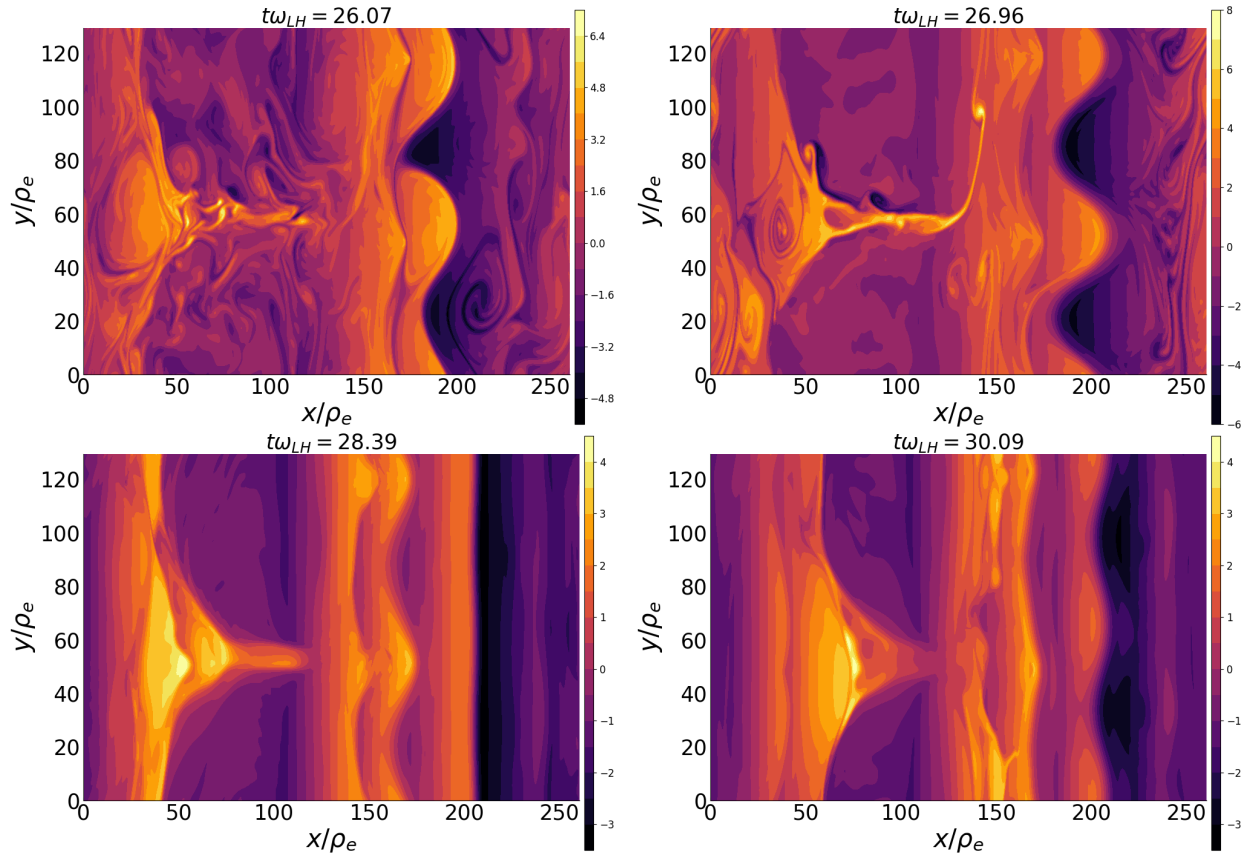
Figure 6.9: Normalized generalized vorticity η/n_0 spatial profiles for streamer formation. Parameters used $\nu = 0.28\omega_{LH}$, $v_0 = 3.72c_s$, $L_n = 48.8\rho_e$, $\sqrt{m_i/m_e} = 427$, $u_0 = 241.8c_s$.

Chapter 7

Coupling of PIC and Vlasov spectral solver in velocity space

7.1 Preface

Kinetic plasma dynamics involve a phenomena on a wide range of scales in velocity space. Such phenomena are difficult to resolve simultaneously within a single algorithm; e.g., with PIC method. Moreover, complicated turbulent plasma dynamics is very difficult to solve with standard PIC method because of high particle noise. In this chapter, I propose a novel approach which overcomes this problem by combining the PIC method with an accurate spectral method. This hybrid method allows efficient high fidelity simulations of nonlinear dynamics in systems with large-scale separation; e.g., a weak beam-plasma systems. The material in this chapter is based on the paper published in Los Alamos Space Weather Summer School Research Reports [75].

7.2 Abstract

A new method for the solution of the kinetic equations for a collisionless plasma has been developed. It treats part of the distribution function with a spectral (moment-based) expansion based on Hermite polynomials, while the remaining part of the distribution function is described with macro-particles as in the Particle-In-Cell (PIC) approach. The goal is to combine the high accuracy of spectral methods with the flexibility of PIC in dealing with complex distribution functions that might otherwise require a large number of moments for convergence. The application of the new method is studied on the example problem of the

91

interaction of a weak beam with the background plasma. This problem is challenging for both conventional PIC and spectral methods due to the low density of the beam and the complex, quickly evolving, shape of the distribution function. The potential of the new method is demonstrated and its efficiency and accuracy are characterized.

7.3   Introduction

The Vlasov-Maxwell system describes the kinetic evolution of a collisionless magnetized plasma, which is very difficult for analytical and numerical methods. First of all, it is a time dependent system of partial differential equations which describes the evolution of six-dimensional phase space. This fact implies that high computational resources are required to resolve the system. The kinetic equation is also highly nonlinear meaning that it can lead to turbulence and chaos. Such solutions usually need high resolution. Moreover, a collisionless magnetized plasma is characterized by a large number of very different time and space scales making the system of equations very stiff. For example, light electrons respond to perturbations much faster than heavy ions. In the presence of a strong magnetic field, it is common to have large anisotropy along and across the magnetic field which also makes the problem stiff.

There are a lot of different numerical methods to solve Vlasov-Maxwell system. One of the main distinctions between them is the approach to treat phase space. Probably the most popular method is particle-in-cell (PIC) method [12] where phase space is discretized with macro-particles. The PIC method is very robust and it can be efficiently parallelized. Another common approach is Eulerian Vlasov [30, 118, 50], where phase space is discretized with a stationary computational grid. The third method is spectral [6, 110, 64, 108]. Spectral methods handle phase space by expanding the distribution function with basis functions. The proper choice of functions can dramatically improve the efficiency of the method.

The numerical methods discussed above have another important distinction — time discretization. Explicit methods are the simplest ones. Unfortunately, they suffer from various numerical stability constraints. Recently, fully implicit methods are gaining in popularity in kinetic simulations due to their unconditional stability and ability to exactly satisfy physical

conservation laws. For example, see recent papers for conservative implicit PIC [85, 28] or spectral methods [41, 126, 91, 23].

The main goal of this work is to construct and investigate a new hybrid method which is based on combining PIC and spectral methods. The main idea is to divide the distribution function in phase space into two regions and resolve one part with macro-particles and another with a basis function expansion. The PIC noise decreases as $\sim 1/\sqrt{N_p}$ where N_p is a number of macro-particles, thus it becomes computationally expensive to obtain high accuracy. So one of the targeted results is to improve the accuracy of PIC by resolving the part of a distribution function with the spectral approach. On the other hand, the spectral method may require a high number of expansion functions (and computational time) to handle the complex part of the distribution function, therefore treating complex part with macro-particles may boost the performance. To the best of the author knowledge, PIC and spectral coupling was never done before. Thus, it is important to investigate the properties and merits of the new method.

The paper is organized as follows: Section 7.4 introduces the main equations and a mathematical formulation of the new method. A Landau damping benchmark is shown in Section 7.5. The comparison of the new numerical method against the pure spectral approach is conducted in Section 7.6. Finally, Section 7.7 summarizes the results.

7.4   Method description

We will demonstrate the hybrid method with the example of one-dimensional electrostatic unmagnetized plasma. Thus the Vlasov-Maxwell system takes the form,

$$\partial_t f^s + v\partial_x f^s + \frac{q^s}{m^s}E\partial_v f^s = 0, \tag{7.1}$$

$$\partial_x E = \sum_s q^s \int_{-\infty}^{+\infty} f^s dv, \tag{7.2}$$

where s superscript denotes a species (e.g. electrons, ions, etc.); t, x, v are time, space and velocity variables respectively; $f^s = f^s(t, x, v)$ is the distribution function; q^s, m^s are charge and mass; E is the electric field. All variables are dimensionless and the normalization units

defined as

$$t = t^d \omega_{pe}, \qquad x = \frac{x^d}{\lambda_D}, \qquad E = \frac{e\lambda_D}{T_e}E^d, \qquad f = \left(\frac{T_e}{m_e}\right)^{3/2}\frac{f^d}{n_0}, \qquad q = \frac{q^d}{e}, \qquad m = \frac{m^d}{m_e},$$
(7.3)

with periodic boundary conditions

$$f^s(t, 0, v) = f^s(t, L, v), \quad E(t, 0) = E(t, L), \quad f^s(t, x, \pm\infty) = 0,$$
(7.4)

where d superscript denotes dimensional variables; ω_{pe} is the plasma frequency; λ_D is the Debye length; n_0 is the plasma density; L is the domain length; e, m_e, T_e are electron charge, mass and temperature, respectively.

To begin the formulation of the hybrid method, we write the distribution function f^s for each species s in the form

$$f^s = f^s_{spectral} + f^s_{particle},$$
(7.5)

meaning that we solve two instances of Eq. (7.1) separately for $f^s_{spectral}$ and $f^s_{particle}$ with the common electric field which depends on the sum of all distribution functions. We solve one instance with the spectral method and another with the PIC method. To simplify notations, we will move the separation (7.5) into the species superscript. This means that we are solving the system (7.1)-(7.2) for $s =$ spectral electrons, particle electrons, spectral ions, particle ions, etc. We also introduce superscripts for spectral and PIC part only: ss and ps respectively.

Note that nonlinear partial differential equations (PDE) generally do not permit the separation (7.5) because a sum of two PDE solutions may not be a solution. In our case, this separation is possible if we keep a common electric field.

7.4.1 PIC

In the particle-in-cell method, we solve the Eq. (7.1) in the Lagrangian reference frame by following the characteristics of the macro-particles. In this frame, the distribution function is always constant. Thus we only need to follow the frame evolution. Following [12], for

electrostatic momentum conserving explicit PIC we have the following equations

$$\frac{dx_i^{ps}}{dt} = v_i^{ps} \tag{7.6}$$

$$\frac{dv_i^{ps}}{dt} = \frac{q^{ps}}{m^{ps}} E^{local}(x_i^{ps}) \tag{7.7}$$

$$E^{local}(x_i^{ps}) = \sum_{j=0}^{N_x-1} E_j S(x_j - x_i^{ps}) \tag{7.8}$$

where $i = (1, \ldots, N_p)$ and N_p is the number of macro-particles; x_i^{ps}, v_i^{ps} are position and velocity of a macro-particle i; q^{ps}, m^{ps} are charge and mass of a species ps; $E_j, E^{local}(x_i^{ps})$ are the electric field at the grid point x_j and particle position x_i^{ps} respectively; S is the interpolation function; N_x is the number of grid points.

To compute the electric field at the grid point we would need the charge density which is

$$\rho_j = \sum_{ps} \sum_{i=1}^{N_p} q^{ps} S(x_j - x_i^{ps}). \tag{7.9}$$

7.4.2 Spectral method

There are a lot of different spectral methods [57] some of which are specifically designed to solve kinetic equation [6, 110, 64, 108]. Here we closely follow the approach taken by [41]. Therefore, to solve Eq. (7.1), we approximate the distribution function and the electric field with the expansion

$$f^{ss}(t, x, v) = \sum_{n=0}^{N_v-1} \sum_{k=-N_k}^{N_k} C_{n,k}^{ss}(t) \Psi_n(\xi^{ss}) \exp\left(2\pi i \frac{kx}{L}\right), \tag{7.10}$$

$$E(x) = \sum_{k=-N_k}^{N_k} E_k \exp\left(2\pi i \frac{kx}{L}\right), \tag{7.11}$$

where N_k is the number of spatial Fourier modes defined to satisfy $N_x = 2N_k + 1$; N_v is the number of Hermite modes; $\xi^{ss} = (v - u^{ss})/\alpha^{ss}$ with free parameters u^{ss}, α^{ss} which affect convergence of the spectral method. The expansion functions in velocity space are defined as

$$\Psi_n(\xi) = \Psi^n(\xi) = \frac{\pi^{-1/4}}{\sqrt{2^n n!}} H_n(\xi) \exp\left(-\frac{\xi^2}{2}\right), \tag{7.12}$$

where $H_n(\xi)$ is a Hermite polynomial of degree n in ξ with the definition

$$H_0(\xi) = 1, \quad H_1(\xi) = 2\xi, \quad \xi H_n(\xi) = \frac{1}{2} H_{n+1}(\xi) + n H_{n-1}(\xi). \tag{7.13}$$

The final step is to use the orthogonality of Hermite and Fourier basis

$$\int_{-\infty}^{+\infty} \Psi_n(\xi)\Psi^m(\xi)d\xi = \delta_{n,m}, \tag{7.14}$$

$$\int_0^L \exp\left(2\pi i x \frac{n-m}{L}\right) dx = \delta_{n,m}. \tag{7.15}$$

The orthogonality gives us a final system of equations

$$\frac{dC_{n,k}^{ss}}{dt} = -\alpha^{ss}\frac{2\pi i k}{L}\left(\sqrt{\frac{n}{2}}C_{n-1,k}^{ss} + \frac{u^{ss}}{\alpha^{ss}}C_{n,k}^{ss} + \sqrt{\frac{n+1}{2}}C_{n+1,k}^{ss}\right) + \tag{7.16}$$

$$+\frac{q^{ss}}{m^{ss}\alpha^{ss}}\left[E_* * \left(-\sqrt{\frac{n}{2}}C_{n-1,*}^{ss} + \sqrt{\frac{n+1}{2}}C_{n+1,*}^{ss}\right)\right]_k, \tag{7.17}$$

where $n = (0,\dots,N_v - 1)$; $k = (-N_k,\dots,N_k)$ and the convolution is defined as

$$[A_* * B_*]_k = \sum_{k'=-N_k}^{N_k} A_{k-k'}B_{k'}. \tag{7.18}$$

7.4.3 Hybrid

Finally, the hybrid method comprises the PIC and spectral parts, coupled by the solution of Poisson's equation (7.2) including all contributions to the plasma density. The field equation is also solved with spectral method using the expansion (7.11) and the orthogonality condition (7.15), therefore

$$E(x_j) = \sum_{k=-N_k}^{N_k} E_k \exp\left(2\pi i \frac{kx_j}{L}\right), \tag{7.19}$$

$$E_k = \frac{L}{2\pi i k}\left(\sum_{ss} q^{ss}\alpha^{ss}\sum_{n=0}^{N_v-1} h_n C_{n,k}^{ss} + \rho_k\right), \tag{7.20}$$

$$\rho_k = \frac{1}{N_x}\sum_{j=0}^{N_x-1} \rho_j \exp\left(-2\pi i \frac{kx_j}{L}\right), \tag{7.21}$$

where

$$h_n = 0, \qquad\qquad\qquad \text{for odd n}, \tag{7.22}$$

$$h_n = \frac{\sqrt{2\pi}}{\pi^{1/4}}\left(\frac{1}{(n/2)!}\sqrt{\frac{n!}{2^n}}\right), \qquad\qquad \text{for even n}. \tag{7.23}$$

Thus the system of equations (7.6), (7.7), (7.17) with binding equations (7.8), (7.9), (7.20), (7.19), (7.21) is a system of time dependent ordinary differential equations which can be integrated, for example, with a family of Runge-Kutta methods.

7.5 Landau damping benchmark

To investigate the properties of the new hybrid method a numerical code was developed. However, before proceeding with this study, the correctness of the code must be verified. In this section, the ability of the code to reproduce Landau damping is demonstrated.

Landau damping is a collisionless/entropy conserving damping of electrostatic waves in the plasma. It is derived from the dispersion equation [82]

$$1 + k^2 + \frac{\omega}{2k} Z\left(\frac{\omega}{2k}\right) = 0. \tag{7.24}$$

where the normalization corresponds to (7.3); ω is the frequency; k is the wave vector; $Z(z) = \pi^{-1/2} \int_{-\infty}^{+\infty} e^{t^2} dt/(t - z)$ is the dispersion plasma function.

To benchmark the numerical code we measure the damping rate of an electrostatic wave in the simplest scenario: quasineutral plasma of two species — electrons and hydrogen ions with temperature of T_e and T_i respectively. In order to compare numerical and theoretical damping rates, a particular mode is excited to observe its evolution. We choose $k = 0.5$. The analytical solution of Eq. (7.24) for this k is $\Re(\omega) = 1.414$ and $\Im(\omega) = 0.154$. The numerical resolution is chosen to resolve smallest physical time and length scales and to reproduce Landau damping, i.e., time discretization $\Delta t = 10^{-2}$, system length $L = 4\pi$, number of spatial points $N_x = 128$, number of particles $N_p = 10^5$, and number of Hermite polynomials $N_v = 51$.

The Landau damping occurs on the time scales where the ion dynamics is negligible in comparison to the electron dynamics. Thus, to check the PIC and the spectral part of the code separately, we conduct two separate tests: (a) electrons are resolved with the spectral part of the code and ions with the PIC part; (b) electrons are resolved with the PIC part of the code and ions with the spectral part. The results of the simulations are shown in Figure 7.1 where we can clearly see that the electrostatic wave damps according to the

theoretical prediction. We also can see that the spectral part of the code Figure 7.1a is more precise than the PIC part Figure 7.1b for the relatively similar resolution (the computation time is similar).

(a) electrons — spectral, ions — PIC   **(b)** electrons —PIC, ions — spectral
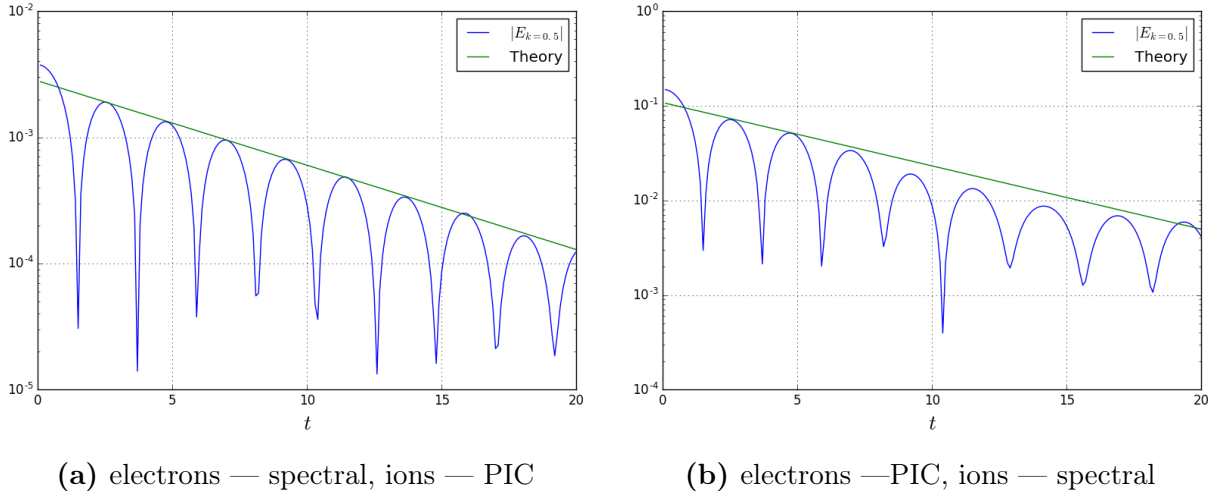
Figure 7.1: Landau damping benchmark

7.6   Weak beam-plasma interaction problem

In this section the capabilities of the new hybrid method are demonstrated on a classical problem — the interaction of a weak electron beam with plasma. This problem is very challenging for the pure PIC method [106] because the required resolution and characteristic evolution time are increasing with the weaker beam density. During the beam-plasma interaction, the electron distribution function forms a plateau in velocity space. Therefore, a pure spectral method requires a high number of expansion functions to capture the correct dynamics. In order to improve performance, the hybrid method treats the bulk plasma with the spectral method and the beam with macro-particles.

The following simulation parameters with normalization (7.3) are used:

- 3 species — ions (with mass 1836), background electrons and beam electrons

- Domain length is 2048 with periodic boundary conditions

- Electron beam mean velocity is 10

- Electron bulk and beam thermal velocities are 1

- Ion thermal velocity is $1/\sqrt{10 \cdot 1836}$

- Beam density is 10^{-2}

The hybrid and spectral codes use the same

- initial condition shown in Figure 7.2

- time discretization (Runge-Kutta 4)

- spectral discretization of plasma bulk with 51 Hermite polynomials

At the same time, they resolve the electron beam differently

- Hybrid code uses macro-particles with different number of particle per cell (ppc)

- Spectral code uses the expansion with different number of Hermite polynomials N_v

After some time the electron distribution function flattens to form a plateau which is shown in Figure 7.3. One can see that spectral and hybrid codes converge to the same solution. To quantify the accuracy, we define an error

$$\epsilon(t) = \frac{\int |f(t,x,v) - f_{ref}(t,x,v)| \, dxdv}{\int |f_{ref}(t,x,v)|dxdv} \cdot 100\% \tag{7.25}$$

where f_{ref} is the reference solution which is obtained by a spectral method solution with high number of Hermite polynomials $N_v = 1601$ for the beam and $N_v = 51$ for the bulk. Results are listed in Tables 7.1,7.2.

Ppc	Simulation time (s)	$\epsilon(100)$ (%)	$\epsilon(200)$ (%)
10^1	1207	0.232	0.308
10^2	1459	0.226	0.327
10^3	3906	0.119	0.416
10^4	31425	0.123	0.128

Table 7.1: Hybrid method performance

N_v	Simulation time (s)	$\epsilon(100)$ (%)	$\epsilon(200)$ (%)
51	1794	0.501	2.674
101	2364	0.072	0.347
201	3703	0.013	0.043
401	5987	0.004	0.017

Table 7.2: Spectral method performance
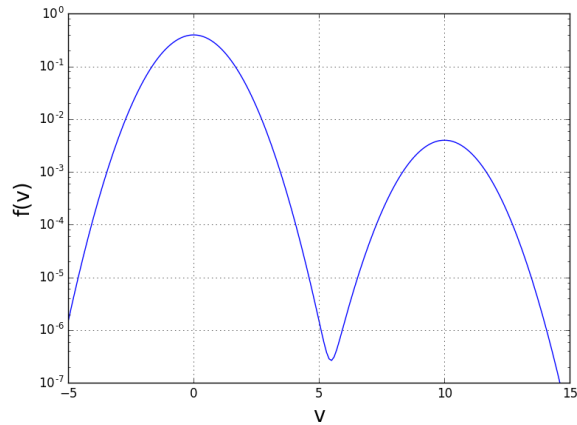
Figure 7.2: Initial condition for electron distribution function averaged over spatial variable x for the beam-plasma problem.

7.7 Discussion and conclusion

In this letter, the new hybrid method to solve Vlasov-Maxwell system was described. The new key concept is to resolve one part of the velocity space with macro-particles and another with the spectral expansion. This approach gives more flexibility to balance between accuracy and computational load in comparison to pure PIC and spectral methods.

The numerical method was implemented and benchmarked with Landau damping problem. The benchmark revealed that the code can reproduce the correct damping rate either with the PIC or with the spectral part.

Next, the new method was applied to the problem of weak electron-beam plasma interaction. This problem combines phenomena with different time scales. The essential part of the beam instability is Landau resonance which is responsible for production and absorption of Langmuir waves. Therefore, the plasma frequency, electron time scales, should be resolved.

On the other hand, to capture the correct dynamics, one needs to consider a nonlinear wave interaction between Langmuir waves and the ion sound which happens on ion time scales. Thereby, the combination of different time scales makes this problem challenging for computational physics.

The results (Tables 7.1,7.2) show that sufficiently small error could be obtained by discretizing the electron beam with a small number of macro-particles ($10-100$ particle per cell (ppc)). To obtain similar error with the pure spectral method, one needs to use ~ 100 polynomials which is computationally more expensive. The difference in performance may be more prominent in 3-dimensional case.

It is important to note that a comparison of numerical methods is an extremely difficult task. For instance, the error definition (7.25) uses the pure spectral method as a reference solution. This fact makes it difficult to reason about hybrid method convergence. Thus, one needs to investigate further the correct measure of the error.
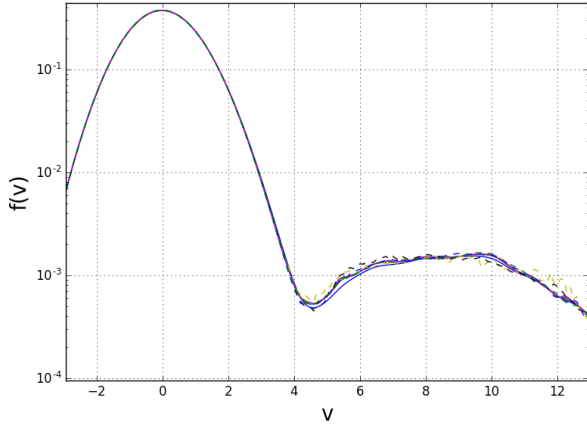
(a) time 100
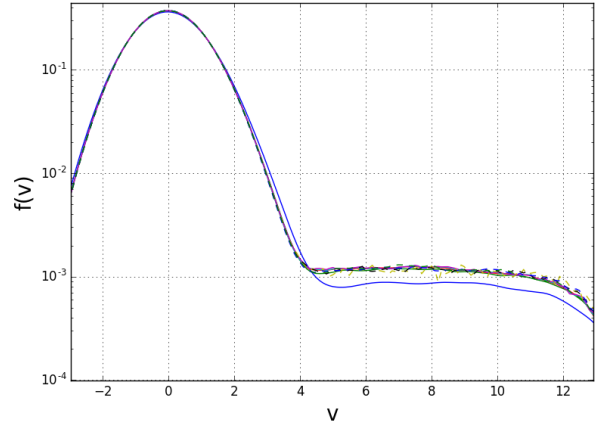
(b) time 200
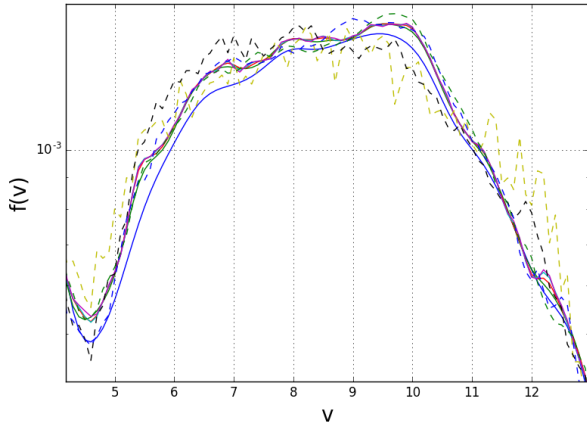
(c) zoom-in of Figure 7.3a
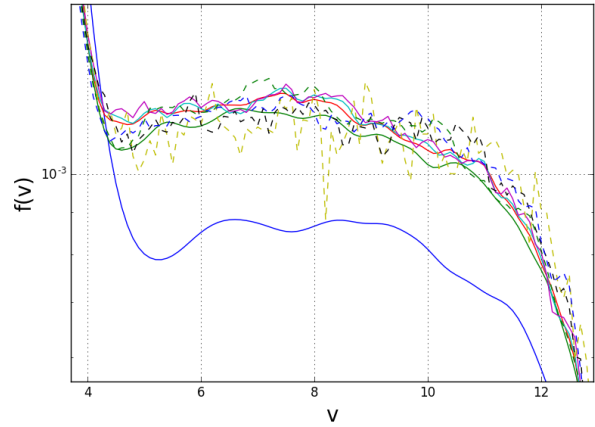
(d) zoom-in of Figure 7.3b

spectral Nv = 51	hybrid ppc = 10
spectral Nv = 101	hybrid ppc = 100
spectral Nv = 201	hybrid ppc = 1000
spectral Nv = 401	hybrid ppc = 10000
Reference solution	

(e) Common legend

Figure 7.3: Electron distribution function averaged over spatial variable x for hybrid and spectral methods at $t = 100, 200$.

Chapter 8

Discussion and conclusion

Plasma physics is a mature science discipline addressing the behavior of ionized gases with a large number of collective nonlinear phenomena in the form of waves, fluctuations, and self-organized structures born out of fluctuations. A large portion of this work is devoted to the study of partially magnetized plasmas in crossed electric and magnetic fields and with plasma density gradients using a reduced fluid model introduced in Ref. [115]. Such plasmas are of interest for a number of applications in plasma material processing, electric propulsion, and space physics. In many such applications, the effect of the magnetic field on ions is small and can be neglected, while electrons are strongly magnetized and their mobility across the magnetic field is significantly reduced. This asymmetry and external electric field result in large equilibrium flows for electrons and ions leading to various instabilities studied in this thesis. Electrons with large $\mathbf{E} \times \mathbf{B}$ drift (in the direction perpendicular to the electric and magnetic fields) together with plasma density gradients excite Hall drift waves (or anti-drift waves). At the same time, ions are accelerated in the direction of the applied electric field and their motion excites axial modes. The nonlinear regimes of these instabilities and ensuing wave turbulence are studied in this thesis.

In Chapter 3, we have shown that the wave turbulence excited in partially magnetized plasma with the electron drift and density gradients exhibits inverse energy cascade; in other words, energy is transfered into large-scale structures from small-scale (most unstable) Hall drift waves. The nonlinear dynamics produces large-scale flows in the azimuthal direction (along $\mathbf{E} \times \mathbf{B}$ drift) with strong shear in the axial direction (direction of the equilibrium electric field). These types of zonal flows have been observed in other plasma systems in laboratory. For example, these are seen in tokamaks and in isomorphically similar geophysical systems, such as shallow water dynamics in the atmosphere and oceans on Earth and other

planets (e.g., zonal flows and the Great Red Spot on Jupiter). Our study shows that at a later stage, the shear flows become unstable and form vortices similar to those found in the Kelvin–Helmholtz instability. The vortices can stay quasi-stationary for a long time (in comparison with the linear growth rate). It was shown that the wave turbulence in this system produces highly intermittent anomalous electron axial transport for at least two orders of magnitude above classical collisional values. It has been suggested that this mechanism is responsible for the anomalous current and spoke formation in Hall effect thrusters [113].

A picture of the inverse cascade, zonal flows generation, secondary instability of the zonal flow similar to Kelvin–Helmholtz mechanism, demonstrated in this thesis for partially magnetized plasmas, is similar to the zonal flow dynamics in fully magnetized plasmas (e.g., tokamaks). In strongly magnetized plasmas, small-scale standard drift wave instabilities nonlinearly cascade energy into large-scale coherent nonlinear structures such as zonal flows (poloidal flows with strong shear in the radial direction) and streamers (structures localized in the poloidal direction and extended in the radial direction).

Zonal flow dynamics (in the framework of the Hasegawa-Mima equation) was studied analytically in Chapter 2 where saturation mechanism of zonal flow energy was established due to the nonlinear self-interaction. We have shown that this mechanism could be more important compared to other standard mechanisms of zonal flow saturation, namely due to the drain of drift wave energy reservoir into the zonal flows.

The equilibrium ion and electron currents in the axial direction excite another type of instability whose nonlinear regime was studied in Chapter 4. This instability occurs due to the phase shift between the electron current (can be classical or anomalous) and the ion current which is Doppler shifted because of the equilibrium ion flow. It was shown that the finite electron inertia and Larmor radius effects are necessary for the cutoff of the instability growth rates at high wave numbers ($k\rho_e \sim 1$) and thus are important for nonlinear simulations providing required physics based cut-off at the highest grid resolution length scale (without artificial damping at high k). We have shown, through nonlinear fluid simulations, that the axial instability saturates due to ion trapping at large wave amplitudes and results in coherent structures resembling cnoidal waves. We conjecture that this mechanism may be responsible for breathing mode oscillations in Hall effect thrusters [78].

As was previously shown [71], the axial instability of lower hybrid waves can be excited by boundary effects without collisional or anomalous electron axial current. This mechanism for linear lower-hybrid waves is formally (mathematically) similar to the Pierce instability. In Chapter 5, we showed that the finite Larmor radius effect stabilizes this instability for high Pierce zone numbers (slow ion flows). The nonlinear simulations have revealed that, for Pierce parameters corresponding to aperiodic instability (odd Pierce zones), the instability saturates in a new nonlinear stationary equilibrium state. For an oscillatory instability (even Pierce zones), the instability saturates to a stationary (oscillating) standing wave.

Azimuthal flows emerging in Hall drift wave turbulence studied in Chapter 3 are non-linear modes with strong shear in the axial direction. At the same time, the resistive axial modes studied in Chapter 4 are the linear eigenmodes with strong axial variations. There-fore, the strong coupling and interactions are expected when both modes are present and complex multi-scale nonlinear dynamics emerge due to both electron and ion equilibrium flows [66, 129, 53, 109]. This dynamics was studied in Chapter 6 where it was shown that the wave turbulence develops from the most unstable (small-scale) Hall drift waves which, via the inverse energy cascade, form large-scale azimuthal flows and significantly increase electron axial transport. The high anomalous current triggers an axial instability which pro-duces cnoidal axial waves. This mechanism is similar to the linear resistive mode instability mechanism where the role of the resistive linear current is replaced by the anomalous current due to small-scale fluctuations. On the other hand, the strong electric field produced by the axial modes play the role of the equilibrium electric field (in the axial direction) which affects the Hall drift waves stability providing a nonlinear feedback mechanism. The full dynamics is the result of complex interaction of nonlinearly generated azimuthal shear flows (zonal flows), vortices and large amplitude axial modes. The existence of another type of nonlinear mode, streamers, was shown in Chapter 6. These are nonlinear structures localized in the azimuthal direction and extended in the axial direction. They were also reported to appear together with zonal flows in fully magnetized plasmas resulting in intermittent axial transport [11, 25, 90].

In Chapter 7, a new flexible hybrid numerical method for the comprehensive kinetic Maxwell-Vlasov problem was proposed. The method aims to effectively resolve plasma tur-

bulence which has an intrinsic scale separation. It combines a standard method for the Vlasov equation, the PIC method, and a high-accuracy spectral method. The standard PIC method is difficult to use for turbulence problems because particle noise error scales poorly with resolution. A good solution is the spectral method; however, in collisionless plasmas the particle distribution function (PDF) may have complex shape causing poor convergence. The idea of this new hybrid method is to treat the small, complex part of the PDF as particles and describe its evolution using PIC while the "well-behaved" (Maxwellian) part of the PDF is described and evolves according to the spectral method. Thus, it allows to decrease particle noise and improve the convergence of the spectral method. This new method was implemented and tested with the classical example of Landau damping and electron beam/plasma interaction problems producing Langmuir wave turbulence. It was shown that the proposed method is more efficient than pure spectral and PIC method for moderate resolution and it is expected that improvements will be more significant for larger scale separation (e.g., weaker beam density).

References

[1] J. C. Adam, J. P. Boeuf, N. Dubuit, M. Dudeck, L. Garrigues, D. Gresillon, A. Heron, G. J. M. Hagelaar, V. Kulaev, N. Lemoine, S. Mazouffre, J. P. Luna, V. Pisarev, and S. Tsikata. Physics, simulation and diagnostics of Hall effect thrusters. *Plasma Physics and Controlled Fusion*, 50:124041, 2008.

[2] J. C. Adam, A. Heron, and G. Laval. Study of stationary plasma thrusters using two-dimensional fully kinetic simulations. *Physics of Plasmas*, 11:295, 2004.

[3] E. Ahedo, J. M. Gallardo, and M. Martinez-Sanchez. Effects of the radial plasma-wall interaction on the Hall thruster discharge. *Physics of Plasmas*, 10:3397, 2003.

[4] J. Anderson and Y. Kishimoto. Comparison of multiscale analysis models applied to zonal flow generation in ion-temperature-gradient mode turbulence. *Physics of Plasmas*, 14:012308, 2007.

[5] J. Anderson, J. Li, Y. Kishimoto, and E. J. Kim. Quasilinear analysis of the zonal flow back-reaction on ion-temperature-gradient mode turbulence. *Physics Letters A*, 372:5987, 2008.

[6] T. P. Armstrong, R. C. Harding, G. Knorr, and D. Montgomery. Solution of Vlasov's equation by transform methods. *Methods in Computational Physics*, 9:29, 1970.

[7] J. Bareilles, G. J. M. Hagelaar, L. Garrigues, C. Boniface, J. P. Boeuf, and N. Gascon. Critical assessment of a two-dimensional hybrid Hall thruster model: Comparisons with experiments. *Physics of Plasmas*, 11:3035, 2004.

[8] S. Barral and E. Ahedo. Low-frequency model of breathing oscillations in Hall discharges. *Physical Review E*, 79:046401, 2009.

[9] S. Barral, K. Makowski, Z. Peradzynski, and M. Dudeck. Transit-time instability in Hall thrusters. *Physics of Plasmas*, 12:073504, 2005.

[10] S. Barral, K. Makowski, Z. Peradzynski, N. Gascon, and M. Dudeck. Wall material effects in stationary plasma thrusters. II. Near-wall and in-wall conductivity. *Physics of Plasmas*, 10:4137, 2003.

[11] S. Benkadda, P. Beyer, N. Bian, C. F. Figarella, X. Garbet, O. Garcia, and I. Voitsekhovitch. The physics of E×B shear, zonal flows and streamers in tokamak edge turbulence. *Contributions to Plasma Physics*, 42:362, 2002.

[12] C. K. Birdsall and A. B. Langdon. *Plasma Physics via Computer Simulation*. CRC Press, 2004.

[13] J. P. Boeuf and L. Garrigues. Low frequency oscillations in a stationary plasma thruster. *Journal of Applied Physics*, 84:3541, 1998.

[14] D. Bohm. *The characteristics of electrical discharges in magnetic fields*. McGraw-Hill, 1949.

[15] J. P. Boyd. *Chebyshev and Fourier spectral methods*. Courier Corporation, 2001.

[16] S. I. Braginskii. *Reviews of plasma physics, Volume 1*. Consultants Bureau, New York, 1965.

[17] A. I. Bugrova, A. I. Morozov, and V. K. Kharchevnikov. Experimental investigation of near wall conductivity. *Sov. J. Plasma Phys*, 16:849, 1990.

[18] O. Buneman. Instability, turbulence, and conductivity in current-carrying plasma. *Physical Review Letters*, 1:8, 1958.

[19] O. Buneman. Dissipation of currents in ionized media. *Physical Review*, 115:503, 1959.

[20] O. Buneman. Excitation of Field Aligned Sound Waves by Electron Streams. *Physical Review Letters*, 10:285, 1963.

[21] M. J. Burin, G. R. Tynan, G. Y. Antar, N. A. Crocker, and C. Holland. On the transition to drift turbulence in a magnetized plasma column. *Physics of Plasmas*, 12:052320, 2005.

[22] K. H. Burrell. Effects of ExB velocity shear and magnetic shear on turbulence and transport in magnetic confinement devices. *Physics of Plasmas*, 4:1499, 1997.

[23] E. Camporeale, G. L. Delzanno, B. K. Bergen, and J. D. Moulton. On the velocity space discretization for the Vlasov–Poisson system: Comparison between implicit Hermite spectral and Particle-in-Cell methods. *Computer Physics Communications*, 198:47, 2016.

[24] S. Chable and F. Rogier. Numerical investigation and modeling of stationary plasma thruster low frequency oscillations. *Physics of Plasmas*, 12:033504, 2005.

[25] S. Champeaux and P. H. Diamond. Streamer and zonal flow generation from envelope modulations in drift wave turbulence. *Physics Letters A*, 288:214, 2001.

[26] J. G. Charney. On the scale of atmospheric motions. *Geofysiske Publikasjoner*, 17:3, 1948.

[27] G. Chen, L. Chacón, and D. C. Barnes. An efficient mixed-precision, hybrid cpu–gpu implementation of a nonlinearly implicit one-dimensional particle-in-cell algorithm. *Journal of Computational Physics*, 231:5374, 2012.

[28] G. Chen, L. Chacón, and D. C. Barnes. An energy- and charge-conserving, implicit, electrostatic particle-in-cell algorithm. *Journal of Computational Physics*, 230:7018, 2011.

[29] L. Chen, Z. H. Lin, and R. White. Excitation of zonal flow by drift waves in toroidal plasmas. *Physics of Plasmas*, 7:3129, 2000.

[30] C. Z. Cheng and G. Knorr. The integration of the Vlasov equation in configuration space. *Journal of Computational Physics*, 22:330, 1976.

[31] E. Chesta, C. M. Lam, N. B. Meezan, D. P. Schmidt, and M. A. Cappelli. A characterization of plasma fluctuations within a Hall discharge. *IEEE Transactions on Plasma Science*, 29:582, 2001.

[32] C. D. Child. Discharge from hot CaO. *Phys. Rev. (Series I)*, 32:492, 1911.

[33] E. Y. Choueiri. Plasma oscillations in Hall thrusters. *Physics of Plasmas*, 8:1411, 2001.

[34] C. P. Connaughton, B. T. Nadiga, S. V. Nazarenko, and B. E. Quinn. Modulational instability of Rossby and drift waves and generation of zonal jets. *Journal of Fluid Mechanics*, 654:207, 2010.

[35] R. C. Davidson. *Methods in Nonlinear Plasma Theory*. Academic Press, New York, 2012.

[36] R. C. Davidson and N. T. Gladd. Anomalous transport properties associated with lower-hybrid-drift instability. *Physics of Fluids*, 18:1327, 1975.

[37] J. Dawson. One-dimensional plasma model. *The Physics of Fluids*, 5:445, 1962.

[38] J. M. Dawson. Thermal relaxation in a one-species, one-dimensional plasma. *The Physics of Fluids*, 7:419, 1964.

[39] V. K. Decyk and T. V. Singh. Adaptable particle-in-cell algorithms for graphical processing units. *Computer Physics Communications*, 182:641, 2011.

[40] V. K. Decyk and T. V. Singh. Particle-in-cell algorithms for emerging computer architectures. *Computer Physics Communications*, 185:708, 2014.

[41] G. L. Delzanno. Multi-dimensional, fully-implicit, spectral method for the vlasov–maxwell equations with exact conservation laws in discrete form. *Journal of Computational Physics*, 301:338, 2015.

[42] B. Di Martino, S. Briguglio, G. Vlad, and P. Sguazzero. Parallel PIC plasma simulation through particle decomposition techniques. *Parallel Computing*, 27:295, 2001.

[43] P. H. Diamond, S-I. Itoh, K. Itoh, and T. S. Hahm. Zonal flows in plasma–a review. *Plasma Physics and Controlled Fusion*, 47:R35, 2005.

[44] A. M. Dimits, G. Bateman, M. A. Beer, B. I. Cohen, W. Dorland, G. W. Hammett, C. Kim, J. E. Kinsey, M. Kotschenreuther, A. H. Kritz, et al. Comparisons and physics basis of tokamak transport models and turbulence simulations. *Physics of Plasmas*, 7:969, 2000.

[45] B. D. Dudson, M. V. Umansky, X. Q. Xu, P. B. Snyder, and H. R. Wilson. BOUT++: A framework for parallel plasma fluid simulations. *Computer Physics Communications*, 180:1467, 2009.

[46] C. L. Ellison, Y. Raitses, and N. J. Fisch. Cross-field electron transport induced by a rotating spoke in a cylindrical Hall thruster. *Physics of Plasmas*, 19:013503, 2012.

[47] Y. B. Esipchuk, A. I. Morozov, G. N. Tilinin, and A. V. Trofimov. Plasma oscillations in closed-drift accelerators with an extended acceleration zone. *Soviet Physics Technical Physics*, 18:928, 1974.

[48] D. T. Farley. A plasma instability resulting in field-aligned irregularities in ionosphere. *Journal of Geophysical Research*, 68:6083, 1963.

[49] E. Fernandez, M. K. Scharfe, C. A. Thomas, N. Gascon, and M. A. Cappelli. Growth of resistive instabilities in E×B plasma discharge simulations. *Physics of Plasmas*, 15:012102, 2008.

[50] F. Filbet, E. Sonnendrücker, and P. Bertrand. Conservative Numerical Schemes for the Vlasov Equation. *Journal of Computational Physics*, 172:166, 2001.

[51] W. Frias, A. I. Smolyakov, I. D. Kaganovich, and Y. Raitses. Long wavelength gradient drift instability in Hall plasma devices. I. fluid theory. *Physics of Plasmas*, 19:072112, 2012.

[52] A. M. Fridman. On the phenomena of the critical magnetic field and anomalous diffusion in weakly ionized plasma. *Soviet Physics Doklady*, 9:75, 1964.

[53] G. Fuhr, S. Benkadda, P. Beyer, X. Garbet, P. Ghendrih, and Y. Sarazin. Role of E×B Shear Flow in Transport Barrier Oscillations. *Contributions to Plasma Physics*, 46:586, 2006.

[54] A. A. Galeev and R. Z. Sagdeev. Current instabilities and anomalous resistivity of plasma. In *Basic Plasma Physics: Selected Chapters, Handbook of Plasma Physics, Volume 1*, page 271, 1984.

[55] S. Gallagher, B. Hnat, C. Connaughton, S. Nazarenko, and G. Rowlands. The modulational instability in the extended Hasegawa-Mima equation with a finite Larmor radius. *Physics of Plasmas*, 19:122115, 2012.

[56] B. B. Godfrey. Oscillatory nonlinear electron flow in a pierce diode. *The Physics of fluids*, 30(5):1553–1560, 1987.

[57] D. Gottlieb and S. A. Orszag. *Numerical Analysis of Spectral Methods : Theory and Applications*. SIAM, 1977.

[58] P. N. Guzdar, R. G. Kleva, and L. Chen. Shear flow generation by drift waves revisited. *Physics of Plasmas*, 8:459, 2001.

[59] G. J. M. Hagelaar, J. Bareilles, L. Garrigues, and J. P. Boeuf. Modelling of stationary plasma thrusters. *Contributions to Plasma Physics*, 44:529, 2004.

[60] F. H. Harlow and M. W. Evans. A machine calculation method for hydrodynamic problems. *LAMS-1956*, 1955.

[61] A. Hasegawa and K. Mima. Pseudo-three-dimensional turbulence in magnetized nonuniform plasma. *Physics of Fluids*, 21:87, 1978.

[62] R. W. Hockney and J. W. Eastwood. *Computer simulation using particles*. CRC Press, 1988.

[63] F. C. Hoh. Instability of penning-type discharges. *The Physics of Fluids*, 6:1184, 1963.

[64] J. P. Holloway. Spectral velocity discretizations for the Vlasov-Maxwell equations. *Transport theory and statistical physics*, 25:1, 1996.

[65] W. Horton. Drift waves and transport. *Reviews of Modern Physics*, 71:735, 1999.

[66] Z. Q. Hu, Z. X. Wang, L. Wei, J. Q. Li, and Y. Kishimoto. Dual roles of shear flow in nonlinear multi-scale interactions. *Nuclear Fusion*, 56:016012, 2015.

[67] T. Ito, C. V. Young, and M. A. Cappelli. Self-organization in planar magnetron microdischarge plasmas. *Applied Physics Letters*, 106(25):254104, 2015.

[68] K. Itoh, S-I. Itoh, P. H. Diamond, T. S. Hahm, A. Fujisawa, G. R. Tynan, M. Yagi, and Y. Nagashima. Physics of zonal flowsa). *Physics of Plasmas*, 13:055502, 2006.

[69] G. S. Janes and R. S. Lowder. Anomalous electron diffusion and ion acceleration in a low-density plasma. *Physics of Fluids*, 9:1115, 1966.

[70] B. B. Kadomtsev. Plasma turbulence. *New York: Academic Press*, 1965.

[71] A. Kapulkin and E. Behar. Ion beam instability in Hall thrusters. *IEEE Transactions on Plasma Science*, 43:64, 2015.

[72] M. Keidar and I. I. Beilis. Electron transport phenomena in plasma devices with E×B drift. *IEEE Transactions on Plasma Science*, 34:804, 2006.

[73] M. Keidar, I. D. Boyd, and I. I. Beilis. Plasma flow and plasma-wall transition in Hall thruster channel. *Physics of Plasmas*, 8:5315, 2001.

[74] T. Klinger, F. Greiner, A. Rohde, A. Piel, and M. E. Koepke. Van der Pol behavior of relaxation oscillations in a periodically driven thermionic discharge. *Physical Review E*, 51:4316–4327, 1995.

[75] O. Koshkarov, G. L. Delzanno, G. Manzini, and V. Roytershteyn. Coupling of PIC and Vlasov spectral solver in velocity space. *Los Alamos Space Weather Summer School Research Reports*, page 27, 2016.

[76] O. Koshkarov, A. I. Smolyakov, I. D. Kaganovich, and V. I. Ilgisonis. Ion sound instability driven by the ion flows. *Physics of Plasmas*, 22:052113, 2015.

[77] O. Koshkarov, A. I. Smolyakov, and J. T. Mendonca. Nonlinear damping of zonal flows. *Plasma Physics Reports*, 42:769, 2016.

[78] O. Koshkarov, A. I. Smolyakov, I. V. Romadanov, O. Chapurin, M. V. Umansky, Y. Raitses, and I. D. Kaganovich. Current flow instability and nonlinear structures in dissipative two-fluid plasmas. *Physics of Plasmas*, 25:011604, 2018.

[79] R. Kubo. The fluctuation-dissipation theorem. *Reports on Progress in Physics*, 29:255, 1966.

[80] S. Kuhn. The physics of bounded plasma systems (BPS's): Simulation and interpretation. *Contributions to Plasma Physics*, 34(4):495–538, 1994.

[81] V. I. Kuznetzov and A. Y. Ender. Stability theory of Knudsen plasma diodes. *Plasma Physics Reports*, 41:905–917, 2015.

[82] L. D. Landau. On the vibrations of the electronic plasma. *J. Phys. (USSR)*, 10:96, 1946.

[83] L. D. Landau and E. M. Lifshitz. *Fluid Mechanics*, volume 6. Pergamon Press, Oxford, 1987.

[84] A. B. Langdon. Kinetic theory for fluctuations and noise in computer simulation of plasma. *The Physics of Fluids*, 22:163, 1979.

[85] G. Lapenta, S. Markidis, A. Divin, M. Goldman, and D. Newman. Scales of guide field reconnection at the hydrogen mass ratio. *Physics of Plasmas*, 17:082106, 2010.

[86] P. C. Liewer and V. K. Decyk. A general concurrent algorithm for plasma particle-in-cell simulation codes. *Journal of Computational Physics*, 85:302, 1989.

[87] A. A. Litvak and N. J. Fisch. Resistive instabilities in Hall current plasma discharge. *Physics of Plasmas*, 8:648, 2001.

[88] E. N. Lorenz. Deterministic nonperiodic flow. *Journal of the atmospheric sciences*, 20:130, 1963.

[89] M. A. Malkov, P. H. Diamond, and A. Smolyakov. On the stability of drift wave spectra with respect to zonal flow excitation. *Physics of Plasmas*, 8:1553, 2001.

[90] G. Manfredi, C. M. Roach, and R. O. Dendy. Zonal flow and streamer generation in drift turbulence. *Plasma Physics and Controlled Fusion*, 43:825, 2001.

[91] G. Manzini, G. L. Delzanno, J. Vencels, and S. Markidis. A Legendre–Fourier spectral method with exact conservation laws for the Vlasov–Poisson system. *Journal of Computational Physics*, 317:82, 2016.

[92] H. Matsumoto, H. Yokoyama, and D. Summers. Computer simulations of the chaotic dynamics of the pierce beam–plasma system. *Physics of Plasmas*, 3(1):177–191, 1996.

[93] N. B. Meezan, W. A. Hargus, and M. A. Cappelli. Anomalous electron mobility in a coaxial Hall discharge plasma. *Physical Review E*, 63:026410, 2001.

[94] J. T. Mendonca, R. M. O. Galvao, and A. I. Smolyakov. Nonlinear evolution of a single coherent mode in a turbulent plasma. *Plasma Physics and Controlled Fusion*, 56:055004, 2014.

[95] A. B. Mikhailovskii. *Theory of Plasma Instabilities*, volume 1: Instabilities of a homogeneous plasma. Springer, New York, 1974.

[96] N. Miyato, Y. Kishimoto, and J. Li. Global structure of zonal flow and electromagnetic ion temperature gradient driven turbulence in tokamak plasmas. *Physics of Plasmas*, 11:5557, 2004.

[97] A. I. Morozov. The conceptual development of stationary plasma thrusters. *Plasma Physics Reports*, 29:235, 2003.

[98] A. I. Morozov and V. V. Savelyev. One-dimensional hydrodynamic model of the atom and ion dynamics in a stationary plasma thruster. *Plasma Physics Reports*, 26:219, 2000.

[99] A. I. Morozov and V. V. Savelyev. *Reviews of Plasma Physics*, chapter Fundamentals of Stationary Plasma Thruster Theory, page 203. Springer US, Boston, MA, 2000.

[100] A. I. Morozov and V.V Savelyev. Numerical simulation of plasma flow dynamics in SPT. *IEPC*, 95:1115, 1995.

[101] A. I. Morozov and A. P. Shubin. Kinetics of electrons in the regime of near-wall conductivity. *Pisma v Zhurnal Tekhnicheskoi Fiziki*, 10:28, 1984.

[102] H. M. Mott-Smith. History of "plasmas". *Nature*, 233:219, 1971.

[103] J. B. Parker, Y. Raitses, and N. J. Fisch. Transition in electron transport in a cylindrical Hall thruster. *Applied Physics Letters*, 97:091501, 2010.

[104] J. R. Pierce. Limiting stable current in electron beams in the presence of ions. *Journal of Applied Physics*, 15:721, 1944.

[105] C. Rapson, O. Grulke, K. Matyash, and T. Klinger. The effects of boundaries on the ion acoustic beam-plasma instability in experiment and simulations. *Physics of Plasmas*, 21:052103, 2014.

[106] H. Ratcliffe, C. S. Brady, M. B. Che Rozenan, and V. M. Nakariakov. A comparison of weak-turbulence and particle-in-cell simulations of weak electron-beam plasma interaction. *Physics of Plasmas*, 21:122104, 2014.

[107] Y. Sakawa, C. Joshi, P. K. Kaw, F. F. Chen, and V. K. Jain. Excitation of the modified Simon-Hoh instability in an electron-beam produced plasma. *Physics of Fluids B-Plasma Physics*, 5:1681, 1993.

[108] J. W. Schumer and J. P. Holloway. Vlasov Simulations Using Velocity-Scaled Hermite Representations. *Journal of Computational Physics*, 144:626, 1998.

[109] B. D. Scott. Edge turbulence and its interaction with the equilibrium. *Contributions to Plasma Physics*, 46:714, 2006.

[110] M. Shoucri and R. R. J. Gagne. Numerical solution of the Vlasov equation by transform methods. *Journal of Computational Physics*, 21:238, 1976.

[111] A. Simon. Instability of a partially ionized plasma in crossed electric and magnetic fields. *The physics of fluids*, 6:382, 1963.

[112] A. A. Skovoroda. *Magnetic traps for plasma confinement / Magnitnye lovushki dlya uderzhaniya plazmy (Russian)*. Fizmatlit, Moscow, 2009.

[113] A. Smirnov, Y. Raitses, and N. J. Fisch. Electron cross-field transport in a low power cylindrical Hall thruster. *Physics of Plasmas*, 11:4922, 2004.

[114] A. Smirnov, Y. Raitses, and N. J. Fisch. Experimental and theoretical studies of cylindrical Hall thrusters. *Physics of Plasmas*, 14(5):057106, 2007.

[115] A. I. Smolyakov, O. Chapurin, W. Frias, O. Koshkarov, I. Romadanov, T. Tang, M. Umansky, Y. Raitses, I. D. Kaganovich, and V. P. Lakhin. Fluid theory and simulations of instabilities, turbulent transport and coherent structures in partially-magnetized plasmas of E x B discharges. *Plasma Physics and Controlled Fusion*, 59:13, 2017.

[116] A. I. Smolyakov, P. H. Diamond, and M. Malkov. Coherent structure phenomena in drift wave–zonal flow turbulence. *Phys. Rev. Lett.*, 84:491, 2000.

[117] A. I. Smolyakov, P. H. Diamond, and V. I. Shevchenko. Zonal flow generation by parametric instability in magnetized plasmas and geostrophic fluids. *Physics of Plasmas*, 7:1349, 2000.

[118] E. Sonnendrücker, J. Roche, P. Bertrand, and A. Ghizzo. The Semi-Lagrangian Method for the Numerical Resolution of the Vlasov Equation. *Journal of Computational Physics*, 149:201, 1999.

[119] T. H. Stix. *Waves in plasmas*. Springer Science & Business Media, 1992.

[120] L. Tonks. The birth of "plasmas". *American Journal of Physics*, 35:857, 1967.

[121] L. Tonks and I. Langmuir. Oscillations in ionized gases. *Phys. Rev.*, 33:195, 1929.

[122] K. Uzawa, Y. Kishimoto, and J. Li. Effect of wave-type mean flow on the modulational process of zonal flow instability. *Journal of the Physical Society of Japan*, 77:034501, 2008.

[123] J. Vaudolon, B. Khiar, and S. Mazouffre. Time evolution of the electric field in a Hall thruster. *Plasma Sources Science Technology*, 23:022002, 2014.

[124] J. Vaudolon and S. Mazouffre. Observation of high-frequency ion instabilities in a cross-field plasma. *Plasma Sources Science and Technology*, 24:032003, 2015.

[125] A. A. Vedenov. Theory of weakly turbulent plasma. *Reviews of plasma physics*, 3:229, 1967.

[126] J. Vencels, G. L. Delzanno, A. Johnson, I. B. Peng, E. Laure, and S. Markidis. Spectral Solver for Multi-scale Plasma Physics Simulations with Dynamically Adaptive Number of Moments. *Procedia Computer Science*, 51:1148, 2015.

[127] J. P. Verboncoeur. Particle simulation of plasmas: review and advances. *Plasma Physics and Controlled Fusion*, 47:A231, 2005.

[128] A. A. Vlasov. On the kinetic theory of an assembly of particles with collective interaction. *J. Phys.(USSR)*, 9:25, 1945.

[129] M. Yagi, S-I. Itoh, K. Itoh, and P. H. Diamond. Disparate scale nonlinear interactions in edge turbulence. *Contributions to Plasma Physics*, 48:13, 2008.